Abstract

LI, ANDY ON YAU. NE213 Scintillator Characterization using n/γ Digital Pulse Shape Discrimination. (Under the direction of Ayman I. Hawari.)

NE213 scintillation detectors are excellent tools for use in a mixed gamma and neutron field due to its established pulse shape discrimination ability. With proper pulse shape discrimination, gamma or neutron responses may be obtained in a mixed radiation field. The neutron response needs to be deconvolved from the detector response function to obtain an energy spectrum. To perform unfolding of neutron spectra, mono-energetic responses are needed and the responses may be obtained via experiment or simulation of the NE213 detector.

In this work, response functions were tested with the unfolding of a Cf252 spectrum. Particularly, experiments were performed at the Los Alamos National Laboratory where Cf252 spectra were obtained. During the experiment, different pre-amplifier set-ups were tested. Namely, the pulse shape discrimination ability of the system using 50 ohm, 500 ohm, and 1000 ohm termination resistors were compared. However, linear system responses were not observed with the different settings. Thus, the Amoeba Simplex fitting routine was used to augment the fall time pulse shape discrimination technique to separate the neutron and the gamma signals. Furthermore, a new figure of merit scheme was explored to quantify the pulse shape discrimination ability of the said non-linear system. Alongside the Cf252 spectra experimental measurements, the program Scinful was used to generate mono-energetic neutron responses needed for unfolding. Consequently, both the Cf252 neutron spectra and the Scinful responses were used with the program FERD-PC for unfolding.

Among the different termination resistors compared with the new figure of merit scheme, the 50 ohm resistor setting was observed to be superior. The resultant unfolded spectrum using the 50 ohm termination resistor shows excellent agreement between 2-10 MeV. However, even with the Amoeba Simplex method, results below 2 MeV are not accurate due to the poor pulse shape discrimination limit of the system used. Results above 10 MeV were not obtained due to the energy range of the used Cf252 source.

NE213 Scintillator Characterization using n/γ Digital Pulse Shape Discrimination

By

Andy On Yau Li

A thesis submitted to the Graduate Faculty of
North Carolina State University
in partial fulfillment of the
requirements for the Degree
of Master of Science

Nuclear Engineering

Raleigh, North Carolina

2007

Approved by:

Man-Sung Yim	Wenbin Lu
Mark Nelson	Ayman I. Hawari Chair of Advisory Committee

Dedication

This work is dedicated to Gap Tai and Loi Yau Li,

my grandmother and grandfather.

Biography

Andy Li was born On Yau Li to Wai Lun Li and Wai Ling Wu in the morning of June 14th 1984 in Hong Kong, China. He grew up in the small town of Taipo with his parents and extended family. On Yau showed interests in math, science and literature in school and was an avid player of Chinese flute and Chinese chess when out of class. On November 1996, after his graduation from primary school at age 12, On Yau moved with his parents to the United States.

On his move to the United States, On Yau changed his name for the more Americanized name Andy. Andy and his family first moved to the small town of Morehead City, NC, where his family owned and operated a Chinese restaurant. The restaurant business did not last, however, and they soon moved to the North Carolina capital, Raleigh, on January 1999. It was in Raleigh that Andy graduated from Leesville Road High School in 2002 and proceeded to enter North Carolina State University. Andy majored in Nuclear Engineering while in North Carolina State University. At the suggestion of his adviser, Dr. Ayman Hawari, Andy spent a summer interning out at Los Alamos National Laboratory. While at LANL, Andy began to work on scintillation detector related project under Dr. Mark Nelson. Andy graduated from Nuclear Engineering at North Carolina State University in 2005. He then entered the Master's degree program at North Carolina State University working on a joint project with Dr. Mark Nelson. Andy Plans to pursue his Ph. D. in North Carolina State University after he completes his Master's degree.

Acknowledgements

First and foremost, I would like to express my most sincere gratitude to Dr. Ayman Hawari for his guidance and direction throughout the years. I am grateful for the opportunities he had presented to me, and I appreciate all of the efforts he had spent on my behalf on this project. I look forward to our continued relationship for years to come.

I am grateful for the Advance Nuclear Technology group at Los Alamos National Laboratory for hosting me. I would also like to thank Dr. Mark Nelson for working with me in this project. Furthermore, I would like to thank Scott Gardner and Ken Butterfield for directing my attention to Amoeba and answering my many questions about data fitting. I am also grateful for the many others who had worked with me at LANL.

I would also like to thank Dr. Man-Sung Yim and Dr. Wenbin Lu for serving on my thesis committee.

Finally, I am grateful for my family and my friends for their support and encouragement throughout the years.

Table of Contents

List of Tables

List of Figures

Introduction

1.1 Scintillation Detectors Overview

Scintillation detectors are among the first types of detectors used for radiation detection and measurement. Scintillation detectors detect radiation types and strength through light emissions (scintillation) inside the detector, which is then detected and amplified by a photomultiplier for subsequent signal processing. There are many different types of scintillation detectors available, and each detector type possesses different characteristics making it suitable for different purposes.

Inorganic scintillation detectors are typically crystals of alkali metals, such as NaI(Tl), LiI(Eu), CsI(Tl) and CaI(Na), where the elements in parentheses are impurities introduced into the crystal lattice deliberately to act as activators for scintillation. Inorganic scintillation detectors are typically used for gamma detection due to their high counting efficiency, which is due primarily to their high density in comparison to other gaseous detectors. When radiation enters the detector, electrons are excited from the valence band to the conduction band in the crystal lattice. As electrons are excited to conduction band, holes are formed in valence band. Both electrons and holes then, commonly called electron-hole pairs, may move around freely in the crystal lattice in the corresponding band. The amount of electron-hole pairs are proportional to the energy deposited by the incoming radiation. The holes drift and ionize the activator atoms, followed by the deionization of an election capture forming a neutral configuration that may corresponds to an excited energy state of the activator atom. The new excited state is of a lower energy than the initial conduction band and thus preventing self-absorption by the crystal lattice. The excited activator atoms

then de-excite by emitting a photon, the photon is then amplified through the photo-multiplying tube and a signal is generated.

In comparison to inorganic scintillation detectors which depend on the crystal lattice's energy bands for light generation, organic scintillation detectors depend on the energy transition in the energy levels of a single molecule. Many organic scintillation detectors are either liquid or plastic and are made up of mostly hydrogen and carbon, with the most commonly used organic scintillation detectors being NE213 and NE110. As radiation enters the detector, it interacts and excites electrons of a molecule to an excited singlet state (denote by S_1, S_2, S_3 where the ground state is S_0). If the electron possesses energy corresponding to a level between two states, the electron will de-excite to the lower energy state through vibration and energy transfers to nearby electrons. Then, the electron would further de-excite itself by scintillation (Figure 0-1). The amount of energy lost by the electron, however, is generally less than the excitation energy to one of the energy states. As the electron would normally de-excite to one of the sub-levels (levels between S_0 and S_1) of ground state, thus preventing self-absorption, and lose the rest of its energy through vibrations. Besides excitation to the singlet ground state where electron de-excitation through scintillation is relatively fast, the electrons may also be excited to a triplet state, where scintillation de-excitation is delayed. The de-excitation time for a singlet electron is in the order of nanoseconds, where as the de-excitation time for a triplet electron is in the order of milliseconds. Thus, excitation to the triplet state may contribute to the uncertainty in fast measurements using an organic scintillation detector. Impurities in the scintillation may cause quenching effect, where the de-excitation scintillation is not proportional to the energy

of the radiation detected due to other mechanisms of energy loss such as heat. As in the case of an inorganic scintillation detector, the light is then collected and amplified in the photo-multiplying tube and a signal is then generated.

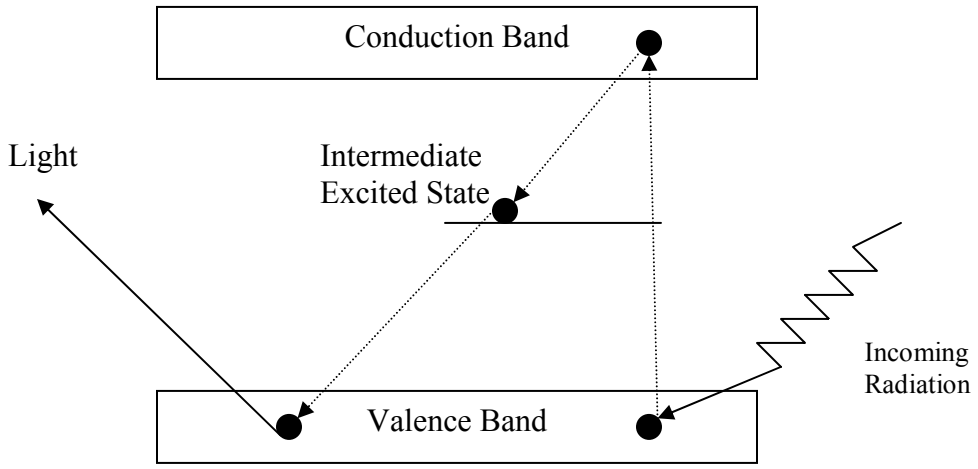

Figure 0-1-Simplified electron excitation schematics.

Both inorganic and organic scintillators rely on electron excitation and de-excitation to generate a photon, however, each type is used in different situations. Inorganic scintillators are typically denser than organic scintillation detectors, making their counting efficiency higher. Also, inorganic scintillators excel at gamma detection through the photoelectric effect due to the high Z number (atomic number) of the crystal. However, because of their high Z number, inorganic scintillators are insensitive to high energy neutrons as elastic neutron scattering events with high Z nuclei do not deposit much energy. Inorganic scintillation detectors may detect thermal neutrons through nuclear reactions, such as the ^{6}Li(n,alpha) reaction in the LiI(Eu) detector. For certain crystal types, the growth and manufacturing of a large crystal often prove difficult, which effectively limits the usage of certain detector types to small scale laboratory applications. Organic scintillation detectors are generally less dense, making their efficiency less than desirable. Due to the their low Z

number, organic scintillation detectors are also not sensitive to gamma radiation except through Compton scattering, where the gamma radiation does not deposit all of its energy in the detector and only a continuum with energies lower than the gamma ray's full energy is typically observed in a gamma ray spectrum. Organic scintillators may, in comparison to inorganic detector, detect and measure neutron energies. Since neutrons generate recoiling nuclei in the detector with energy, depending on target mass, from zero up to potentially the incoming energy, deducing the measured neutron spectrum requires unfolding using known response functions. Also, with energy higher than fission neutrons (> 10 MeV), competing carbon reactions may skew the energy spectrum and causes complications in unfolding. Gamma ray radiations are generally present with a neutron source and may further complicate the unfolding process. With pulse shape discrimination, the gamma rays may be differentiated from neutrons and removed from the neutron pulse height spectrum prior to unfolding. Compared to inorganic scintillators, organic scintillators are much easier to manufacture. Many sizes and shapes may be made, which makes organic scintillators very attractive for large scale neutron detection projects.

Depending on the purpose of the experiment, different types of scintillators may be used. Inorganic scintillators are mostly used for gamma ray measurements while organic scintillators are mostly used for neutron measurements, though organic scintillators also require prior measured response functions to unfold the measured energy spectrum. ([1], [2], [3])

1.2 Pulse Shape Discrimination Overview

As stated, organic scintillators can detect both neutrons and gamma rays. Depending

on the measurement desired, however, some of the incoming radiation should be rejected. Pulse shape discrimination (PSD) techniques are used to separate two or more types of radiation and one of the main strengths of an organic liquid scintillator is its ability to perform PSD in a mixed radiation environment. Traditionally PSD performed on scintillators is based on several principles. First, it is well known that different particles have a different associated stopping power in a medium and tt follows then that different particles interact differently in a medium. Mainly the heavier particles (such as alphas), which have a high stopping power, are observed to produce a quenching effect, resulting in less light being produced per particle's incoming energy. Quenching causes the excited electrons to de-excite via radiationless processes, such as phonen and heat. Conversely the lighter particles (such as electrons) quench less, resulting in effectively a higher amount of light being produced in comparison with a heavy particle of equivalent energy. Some PSD techniques, such as the rise time technique which is common in gas detectors, are based off of the direct consequence of the clustering of charges on heavier particles (Also called quenching in gas detectors), while other PSD techniques are based upon the decay fluorescence of the scintillator. As stated, heavier particles tend to quench the detector volume resulting in a less light being procuded overall in comparison with lighter particles. Heavier particles also generate more triplet electrons than lighter particles. Normally electrons excite to a singlet excitation state, but more triplet states can be observed with heavy incoming particles. Triplet states have a longer de-excitation time than singlet states, thus resulting in longer decay fluorescence time for the scintillator. Some PSD techniques, such as the fall time and the charge integration techniques are based upon the decay fluorescence difference of the particle types. ([1], [2], [4])

Over the years, the aforementioned techniques were explored and used with success, and they will be described in details a later section. With the advent of computers and data analysis tools, the recent efforts in developing PSD had shifted from hardware focused approaches (such as the Forte method and other analog methods ([5], [6]), which will be described) to data analysis approaches (such as statistical estimates and template matching technique ([7], [8], [9])). Specifically, the later approach performs PSD on mixed particle-type data post data collection rather than performing PSD during data collection. This approach allows for flexibility in the development and the implementation of the PSD technique to the data obtained. However, this approach is also often more time consuming and requires more data storage space than concurrent data collection PSD. In this work, a post data collection PSD technique using the amoeba simplex regression is explored and tested on a non-linear system using NE213 liquid scintillator.

Chapter 2 Liquid Scintillator Detection Principles

2.1 Proton Recoil Mechanisms

In an organic scintillator, proton recoil occurs when an incoming neutron collides elastically with a proton. The proton then ionizes surrounding electrons in its track for subsequent detection. Since a neutron has the approximately the same mass as a proton, the neutron may transfer all of its energy to a proton in one collision depending on the angle of collision. Therefore, a precise response function of the detector must be known to unfold the resulting proton continuum. Besides proton collisions, a neutron may also collide with carbon atoms in the detector, causing a skew in the resulting spectrum.

Assuming stationary proton in the laboratory system, neutrons and protons with non-relativistic energy (E<<939 MeV) have energies E_n^c and E_P^c in the center of mass system where

$$E_n^{\,c} = \left(\frac{m_P}{m_n + m_P}\right)^2 E_n \qquad 2.1$$

$$E_P^{\,c} = \frac{m_n m_P}{(m_n + m_P)^2} E_n \qquad 2.2$$

E_n is neutron energy in the laboratory system; m_n and m_P are mass of the neutron and proton respectively. With Q=0 in neutron scattering, the products E_n^{c}' and E_P^{c}' have the same total energy as the reactant. Also, in atomic mass units, neutron has a weight of 1 and proton has a weight of A and thus Equation (2.1) and (2.2) maybe rewritten as

$$E_n^{\,c}{}' = E_n^{\,c} = \left(\frac{A}{1+A}\right)^2 E_n \qquad 2.3$$

$$E_P{}^{c\prime} = E_P{}^{c} = \frac{A}{(1+A)^2} E_n \qquad 2.4$$

Upon conversion from the center of mass system into the laboratory system, the recoiled proton energy E_P becomes

$$E_P = \frac{4A}{(1+A)^2}(1-\cos\alpha)E_n \qquad 2.5$$

where α is the neutron scattering angle in the center of mass frame. Upon transformation of α to ϑ, where ϑ is the recoil angle measured from the incoming neutron's initial path in the laboratory frame, Equation (2.5) becomes

$$E_P = \frac{4A}{(1+A)^2}(\cos^2\vartheta)E_n \qquad 2.6$$

Since A and E_n are constant for a given interaction, the maximum and minimum of the recoil proton's energy then depends on the scattering angle. The minimum energy is zero and it occurs when the recoiled proton scattered perpendicularly from the neutron. The maximum energy of the recoiled proton is

$$E_P = \frac{4A}{(1+A)^2} E_n \qquad 2.7$$

which occurs when the proton is forwardly scattered.

Since a continuum from zero energy up to energy shown in Equation (2.7) is expected, the probability of interaction for each scattering angle must be examined to estimate the shape of the ideal spectrum. Let $P(\alpha)d\alpha$ be the probability that a neutron will be scattered into an angle $d\alpha$ about α, then

$$P(\alpha)d\alpha = 2\pi \sin\alpha d\alpha \frac{\sigma(\alpha)}{\sigma_s} \qquad 2.8$$

where $2\pi \sin\alpha d\alpha$ is the differential slice of an angle $d\alpha$ about α to all space, and $\frac{\sigma(\alpha)}{\sigma_s}$ is the fraction of neutrons scattering into the angle α. If $P(E_P)dE_P$ is defined as the probability of a neutron that will be scattered into an energy dE_P about E_P, where the recoiled energy E_P is caused by scattering angle α, then

$$P(\alpha)d\alpha = P(E_P)dE_P \qquad 2.9$$

and

$$P(E_P) = P(\alpha)\frac{d\alpha}{dE_P} = 2\pi \sin\alpha \frac{d\alpha}{dE_P}\frac{\sigma(\alpha)}{\sigma_s} \qquad 2.10$$

Using Equation (2.5) to substitute the relationship $\frac{d\alpha}{dE_P}$, Equation (2.10) becomes

$$P(E_P) = P(\alpha)\frac{d\alpha}{dE_P} = \frac{(1+A)^2}{A}\frac{\sigma(\alpha)}{\sigma_s}\frac{\pi}{E_n} \qquad 2.11$$

In the case of a hydrogen atom, neutron hydrogen scattering is isotropic up to about 14 MeV. Thus, substituting $\sigma(\alpha) = \frac{\sigma_s}{4\pi}$ into Equation (2.11) and A=1 for hydrogen, it becomes

$$P(E_P) = \frac{1}{E_n} \qquad 2.12$$

As can be seen with Equation (2.12), for an ideal hydrogen scattering detector, the ideal energy spectrum is simply a uniformly distributed continuum between zero energy and initial neutron energy E_n (Figure 2-1).

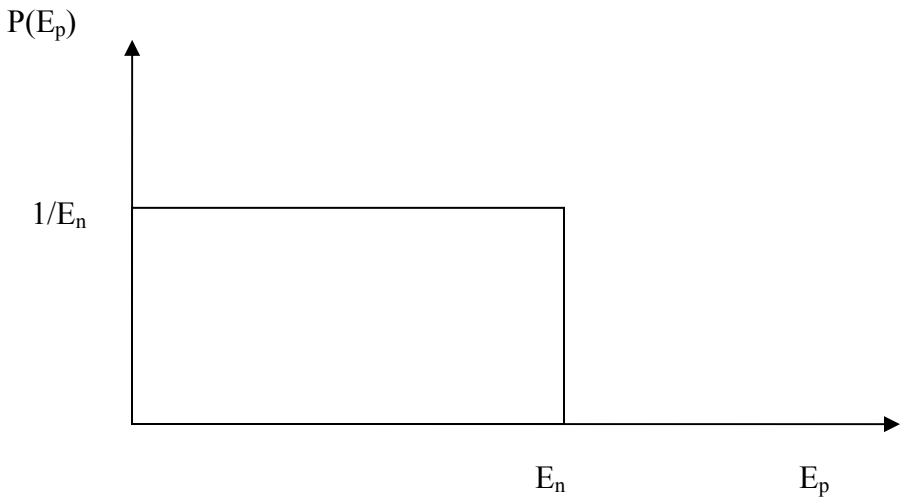

Figure 2-1-Ideal hydrogen nucleus recoil energy spectrum

In Figure 2-1 above, an ideal hydrogen nucleus recoil energy spectrum is shown, where the probability for a neutron interacting in the detector volume is equal for all energies. In a real detector, however, many different factors contribute to the formation of the measured spectrum. The many factors which contribute into a real spectrum will be now discussed ([1], [2], [3]).

2.2 Spectrum Distortions

2.2.1 Carbon Scattering

All organic scintillation detectors contain carbon. From Equation (2.7) it can be seen that the maximum amount of energy transfer from a neutron to a carbon in a single collision is 28% of its initial energy. Combined with the low light output from heavy particles (Non-linearity of light output will be explained in a later section), scattering from carbon alone only contribute to low energy events and will cause a skew in the spectrum favoring low energy events (Figure 2-2).

Furthermore, the carbon scattered neutron may scatter again with another proton in the detector volume. Since the neutron will have lower energy after initial scattering with the carbon nucleus, the neutron may at most deposit 72% of its initial energy in its second scattering (assuming with a hydrogen atom). Therefore, fewer events will be recorded in the resulting energy spectrum corresponded to energy between 72% to 100% of the maximum neutron energy due to carbon scattering ([1], [2]).

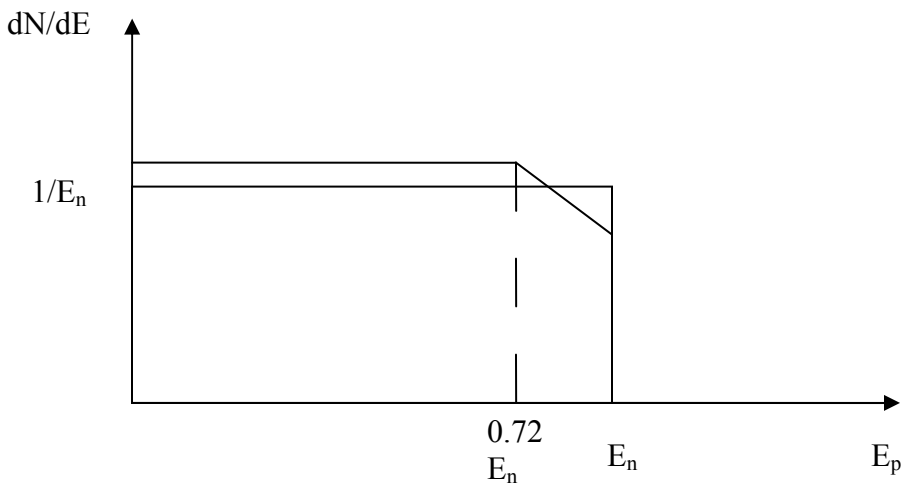

Figure 2-2-Effect of carbon scattering in an organic scintillation detector

2.2.2 Nonlinear Light Output

Depending on the energy and the particle type incoming or recoiling in case of neutron detection, the light output of an organic scintillation detector may not be linearly proportional to the incoming radiation's energy. The reason for the nonlinearity of light outcome is unknown, but is suspected to be the result of nonlinear specific energy loss by heavy charge particles inside the detector. Specifically, gamma rays and electrons exhibit linear responses, while protons and neutrons exhibit nonlinear light output ([1], [2],[10]).

For example, Figure 2-3 illustrates the characteristic light output of a NE213 detector as a function of particle energy.

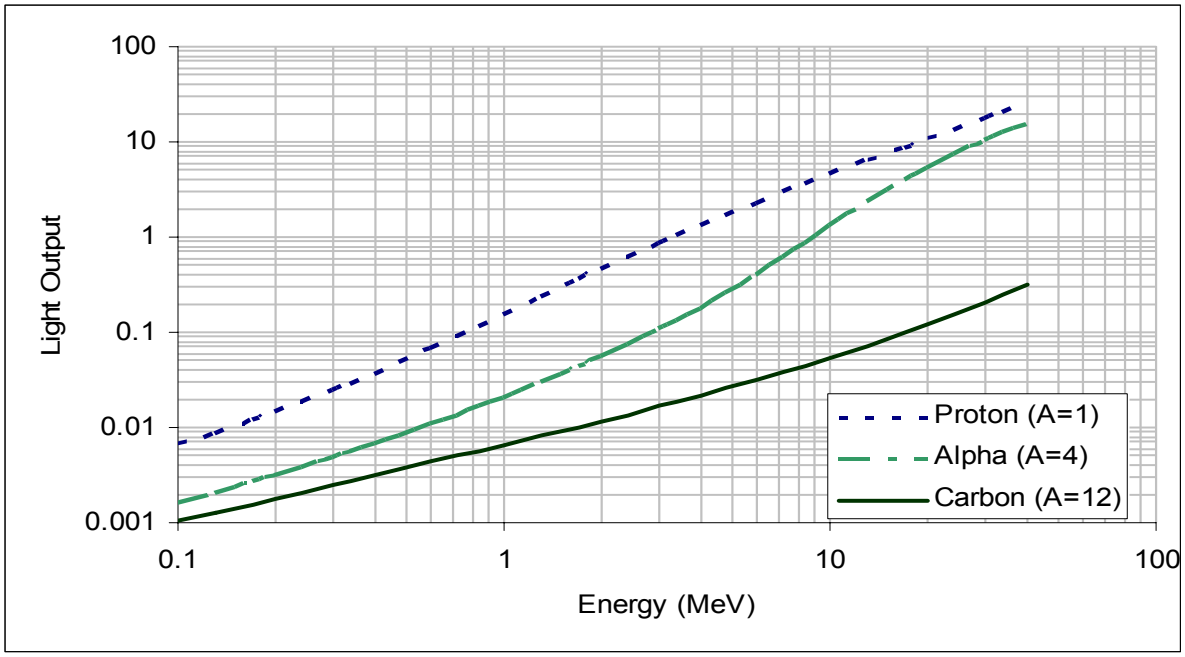

Figure 2-3-Light output vs. particle type and energy by Verbinski et al ([10]). The proton light output is related to energy by $L = 1.13E_R^{1.4318}$.

For hydrogen atoms, the light output L from proton recoil is approximately related to energy E_R by

$$L = kE_R^{\frac{3}{2}} \qquad 2.13$$

where k is a proportionality constant.

Spectra obtained from an organic scintillation detector are typically calibrated to give the quantity $\frac{dN}{dL}$, or number of counts in a bin with width dL. To obtain the energy spectrum $\frac{dN}{dE}$, the light spectrum must be transformed with the quantity $\frac{dL}{dE}$ such that

$$\frac{dN}{dE} = \frac{dN}{dL}\frac{dL}{dE} \tag{2.14}$$

where $\frac{dL}{dE}$ may be obtained from Equation (2.13)

$$\frac{dL}{dE} = \frac{3}{2}kE_R^{\frac{1}{2}} \tag{2.15}$$

Moreover, with Equation (2.13), (2.14) and (2.15), it can be shown that the shape of the light spectrum $\frac{dN}{dL}$ obtained is skewed by the quantity $\frac{dL}{dE}$ (Figure 2-4, [1]), where

$$\frac{dN}{dL} = \frac{\frac{dN}{dE}}{\frac{dL}{dE}} = \frac{\text{Constant}}{\frac{3}{2}kE_R^{\frac{1}{2}}} = k'L^{-\frac{1}{3}} \tag{2.16}$$

where k' is simply a proportionality constant.

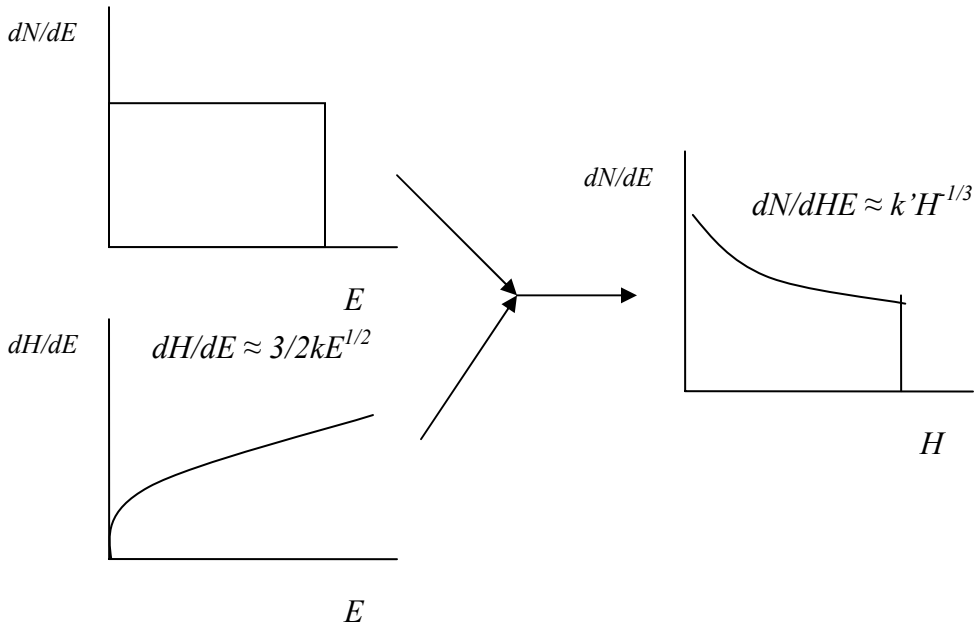

Figure 2-4- Effect of nonlinear light output on an ideal spectrum deconvolved from an ideal proton scattering energy spectrum and a differential light curve.

Also as can be seen in Equation (2.14), the quantity $\frac{dL}{dE}$ must be known accurately to determine the energy spectrum. Since the energy spectrum $\frac{dN}{dE}$ must be unfolded to obtain the source spectrum, an error in $\frac{dL}{dE}$ would be compounded in the final source spectrum. For the purpose of obtaining the energy spectrum, the curves presented by Verbinski et al. (Figure 2-3, [10]) will be used.

2.2.3 Light Calibration

Since a NE213 detector does not output in energy or light unit directly, a light calibration must be made. One light unit in a detector for a given gain setting is defined as 1.13 times the half height of the Na22 1275 keV energy peak ([6]). Thus, any spectrum taken with the NE213 detector should be taken with a Na22 spectrum as well to calibrate the results to light or energy scale.

2.2.4 Edge Effect

If the incoming neutrons have sufficient energy such that the recoiled proton's mean free path is not small in comparison with the detector dimensions, then edge effect will be observed in the detector output. Edge effect is caused by incomplete energy deposition by the recoiled protons. The protons, after recoil, will deposition some of their energy through electron ionization then escape the detector volume. Thus, the resulting energy spectrum of the detector would have more low energy response due to edge effect (Figure 2-5, [1]).

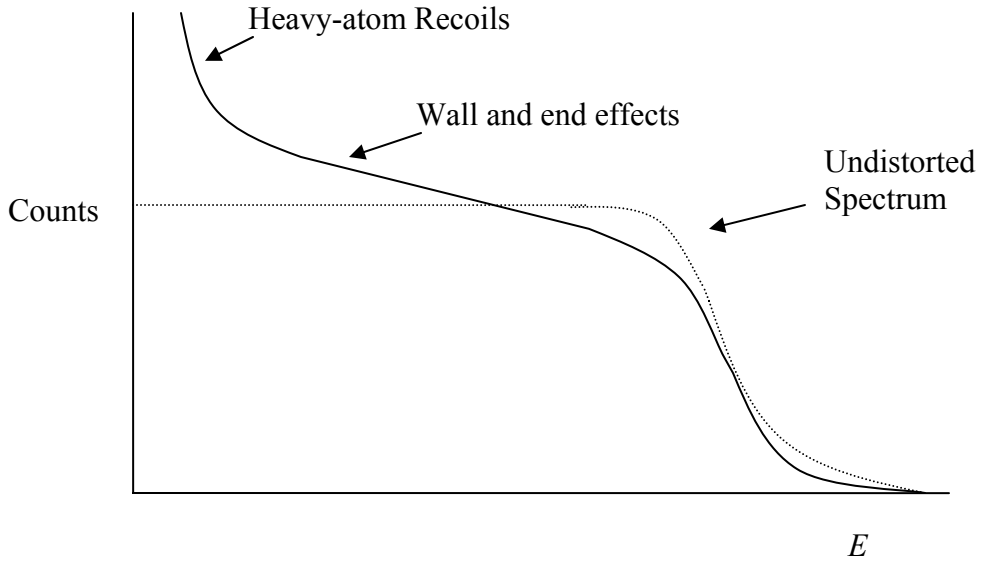

Figure 2-5-The effect of carbon recoil and edge effect on an energy spectrum.

2.2.5 Multiple Hydrogen Scattering

For large detectors, it is possible for neutrons to undergo multiple scattering before stopping or escaping from the detector volume. If a neutron undergoes multiple carbon scatterings, then the resulting spectrum would be similar to that resulting from a single carbon event, where more low energy events will be observed. On the other hand, if the neutron undergoes multiple hydrogen scatterings, the effect could be significant in the resulting spectrum. All events from a single neutron, even from multiple scatterings, happen within a short period of time and will be recorded as one even in the final spectrum. Since the average energy lost in a single neutron hydrogen collision is half of the neutron's initial energy, multiple scatterings with hydrogen increases the energy transferred to the detector and causes more high energy events to be observed.

2.2.6 Finite Detector Resolution

Since no detector possesses perfect resolution, the energy spectrum obtained will always be smeared in comparison with the ideal spectrum (Figure 2-1). In essence, electronic noises, non-uniform light collection (Due to the difference in the location of interaction), and the statistical nature of detection techniques all contribute to the finite resolution of the detector as shown in Figure 2-6 ([1]).

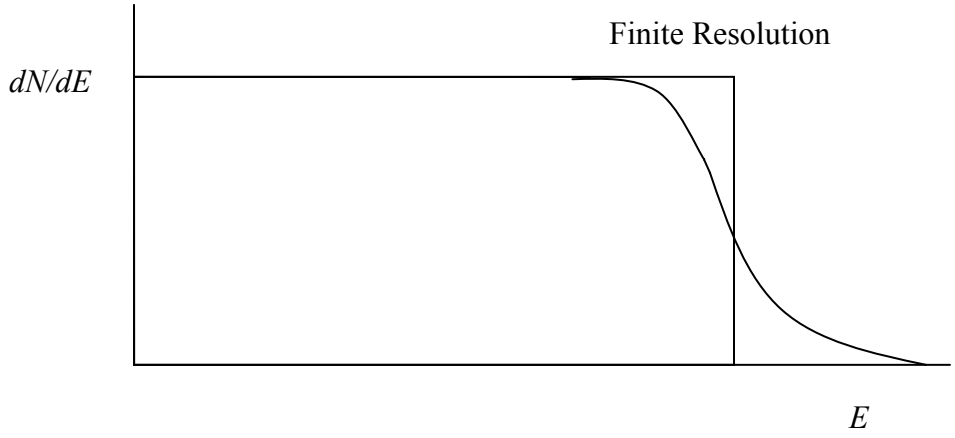

Figure 2-6-Effect of finite resolution on an ideal spectrum.

2.2.7 Pulse Shape Discrimination Capability

Liquid scintillators are capable of detecting both neutron and gamma pulses. Neutrons mostly react through isotropic proton recoil as described. Gamma rays, due to the low-z (atomic number) content of the scintillator, generally react through Compton scattering as oppose to photoelectric events in other gamma detectors. Furthermore, different particle type causes electron excitation through different excitation mechanisms. Since neutrons react mainly through proton recoil, the ionization density along the recoiled proton's track is high enough to produce triplet state electrons and thus producing high decay fluorescence. In

contrast, gamma ray reactions mainly produce singlet state electrons and lower decay fluorescence. Specifically, the light produced from the NE213 scintillator has three distinct components: a short 3 ns rise time, an intermediate 32 ns transient and a long 270 ns fall time which is affected by the decay fluorescence ([4]). Pulse shape discrimination (PSD) for NE213 detectors typically makes use of the 270 ns tail component to distinguish between neutrons and gammas. The PSD ability is important with measurements taken in a mixed gamma/neutron area where only one particle's response is desired, PSD can filter out the undesirable particles' responses from the detector.

2.3 Pulse Shape Discrimination Methods

The ability of the NE213 scintillator to perform PSD is extremely important as it allos for the separation of signals in a mixed field environment. For example, most neutron measurements have gamma back ground signals, with PSD, the gamma signals may be filtered. PSD techniques are used to separate two or more types of radiation. Over the years, several PSD methods were proposed and implemented for different scenarios and they each have their strengths and weaknesses. This section will give a brief introduction to some of the methods that had been used in recent years.

2.3.1 Rise Time Method

Proportional counters often use the rise time method (RT) to perform PSD in a mixed environment. In organic scintillators, different particle types cause a difference in the decay light component, whereas in gas-filled proportional counters, a difference in the rise time is observed. The difference in rise time stems from the ranges of heavy and light particles.

Heavy particles in a proportional counter typically have a much shorter range than light particles, thus the ionization track of the heavy particles is much shorter than that of the lighter particles. An example is that gamma rays induced fast electrons often will pass through the proportional counter where as a neutron recoiled proton will follow a short path and comes to rest within the detector volume. It follows that the shorter track of the heavier particles has a shorter corresponding charge collection time compared with the longer track of the lighter particles. The difference in rise time may then be exploited to perform PSD ([1]). Since liquid scintiallors de-excite through a different mechanism, the rise-time difference is not directly observed ([1], [2]). However, liquid scintillators may use a preamplifier with a time constant to integrate the fall time of the pulses, and thus imitate the rise time method. With the RT method in general, a rise time to pulse height converter (RHC) can be used to convert the rise time to a pulse. The magnitude of the resulting pulse then is indicative of the pulse's particle type. A single channel analyzer then may be used in conjunction with a coincident counting system to filter out a certain type of particles. The strength of this particular method is its accuracy: 1/500 false rejection for neutron with energy less than 500 keV and 1/50 for neutron with energy less than 60 keV ([6]). The limitation of this method is its dependency on the hardware and the restriction of gas proportional counters.

2.3.2 Forte Method

The Forte method is a PSD scheme used with a pulse shape discriminator designed by Forte. The circuitry uses signals from the anode and some of the dynodes in the photomultiplier and is able to produce a large positive pulse for neutrons and a small positive

or large negative pulse for gammas ([2]). The signals may then be gated with coincidence modules and delay lines to achieve PSD. The main strength of this method is the type of pulses created making neutron and gamma pulses easily distinguishable once the original pulse passed through the PSD circuitry. The main draw back for the Forte method is that it is extremely hardware intensive. The dynodes used must be tested with the correct gain to ensure no saturation occurred, and then modifications of the photomultiplier tube base must be done so then the dynode may output the correct signal to the pulse shape discriminator. Also, the Forte method must be used with the correct pulse shape discriminator (designed by Forte). Even though this method is not usable for those who do not possess the hardware described, its description here serves as an illustration on the variety of PSD schemes and the various in-house designed hardware which may accompany them ([5], [6])

2.3.3 Zero Crossing Method

The zero crossing method (ZC) utilizes the zero crossing point of the pulse as a reference to perform PSD. The zero crossing point is the point at which a bipolar duplication of the original pulse, made by super-imposing an inversion of the original pulse, crosses the zero bias axis. The ZC scheme first separates the signals into multiple branches (Figure 2-7). The scheme then uses either a double delay line or a *CR* circuit to help find the zero crossing point of a given pulse. The interval between the zero crossing point and the leading edge of the pulse gives an indication of the fall time of the pulse, and thus pulse shape. The time difference is fed into a time to amplitude converter and then the gamma and neutron signals are separated by the discrimination setting on a single channel analyzer down in the data processing chain. The desired particle type is then recorded using a coincidence system. The

main advantage of this method is its sensitivity to low energy pulses, which is effective down to about 30 keV neutrons with the use of a time of flight scheme concurrently. However, a constant fraction discriminator along with a time to amplitude converter must be used with this scheme. Several reports compared this method favorably with the charge integration method ([10]).

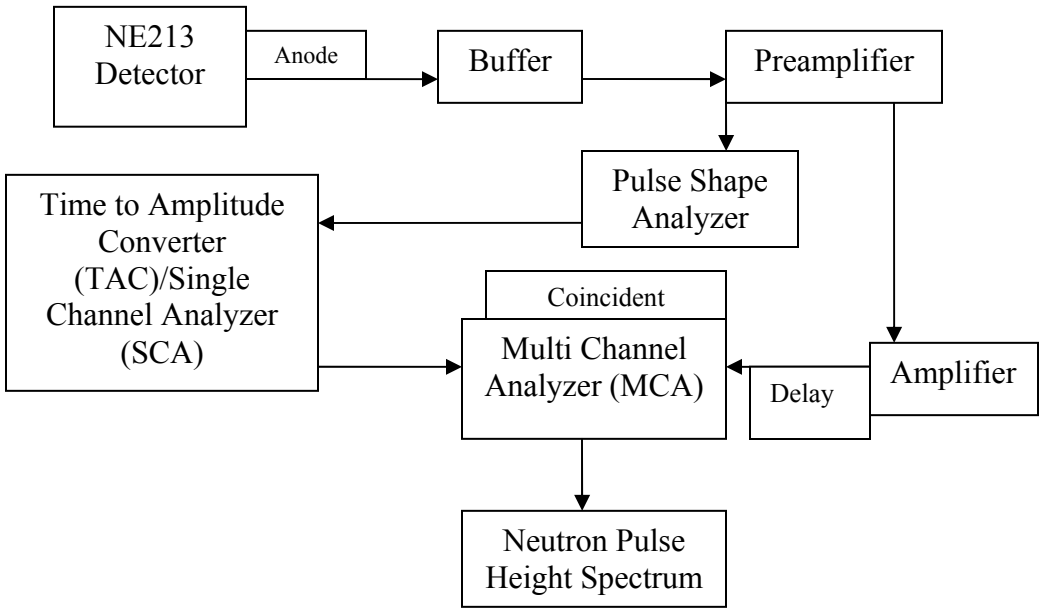

Figure 2-7-Simple experimental scheme illustrating the data branch of the zero crossing method.

2.3.4 Fall Time Method

The fall time method utilizes the same principle as the ZC method, in that the fall time of the pulses examined is indicative of the pulse shape. The difference between the two methods, however, is that the fall time method measures fall time directly, whereas the ZC method measures the fall time through a series of analog time gates. The fall time may be measured with analog equipment or with post-data collection analysis. Since neutron pulses have higher decay fluorescence, their fall time will be higher than gamma pulses. The main

advantage of this method is its flexibility in that the fall time may be measured during or after data collection. However, with some setups, the fall time is not as stable as the ZC method. The fall time reference may drift with differing pulse size, leading to non-ideal PSD spectra.

2.3.5 Charge Integration Method

The charge integration method (CI) is the least hardware intensive method out of all schemes mentioned. CI compares a short portion of the pulse's charge with its total charge, the tail-to-total ratio or the rise to total ratio, to determine the pulse shape. An example of an integrated gamma pulse is shown in Figure 2-8. The ratio used depends on the detector used; the tail ratio is normally used with liquid scintillators and the rise time ratio with gas detectors. Gammas and neutrons are separated by a tail-to-total ratio specific to the system used; the ratio may be used post data-collection to perform PSD. In principle, this method is similar to ZC, with the exception that the difference between the gamma and the neutron pulses is compared on a normalized basis. Though several papers had pointed out that with lower incoming particle energies, ZC is superior to CI. The main strength of CI, however, is that CI is relatively straight forward to implement. In principle, only the detector and a digitizer are needed to record the pulse shape. In actuality, however, the pulses may have to be shaped and conditioned before recording so a few other components such as a pre-amplifier may be desired. Even with the added components for pulse shaping, the CI system is much simpler than other PSD systems mentioned. Also since PSD maybe performed by software, more flexibility is allowed in the data collection components and implementation ([10][11], [13], [14]).

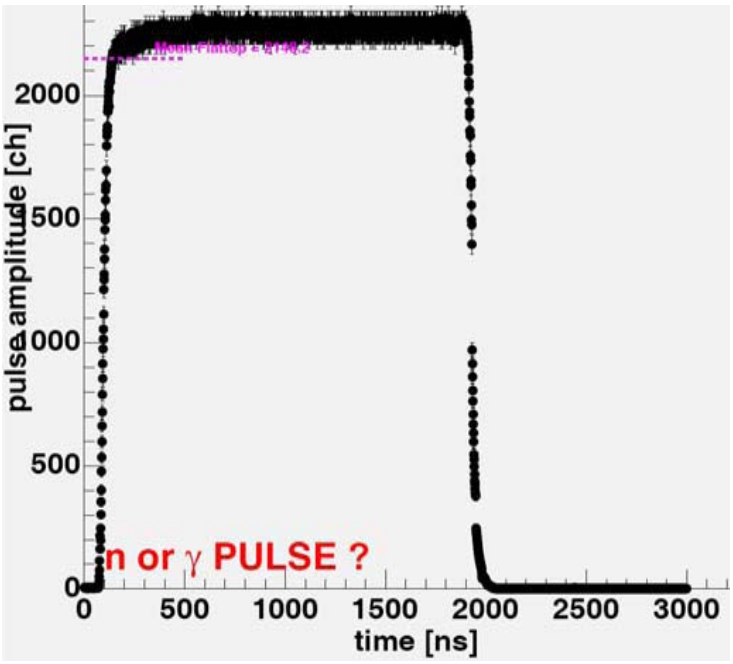

Figure 2-8-Example of a gamma ray pulse taken with the charge integrating method.

2.4 Figure of Merit

NE213 liquid scintillation detectors' ability to perform PSD enables it to be employed in a neutron/gamma mixed field. The figure of merit (FOM) is a measure of a detector system's PSD capability and may be given by

$$\text{FOM} = \frac{\Delta s}{(FWHM_{\gamma} + FWHM_{n})} \qquad 2.17$$

Where Δs is the separation between the gamma and the neutron peak, and *FWHM* is the full width at half max of the individual peaks. The peaks described are the individual particle's peak seen in the histogram of the PSD parameter (Figure 2-9). A good PSD capability is denoted by a large FOM value. As a large FOM value consists of a large peak separation distance and small spread in both the neutron and the gamma peak.

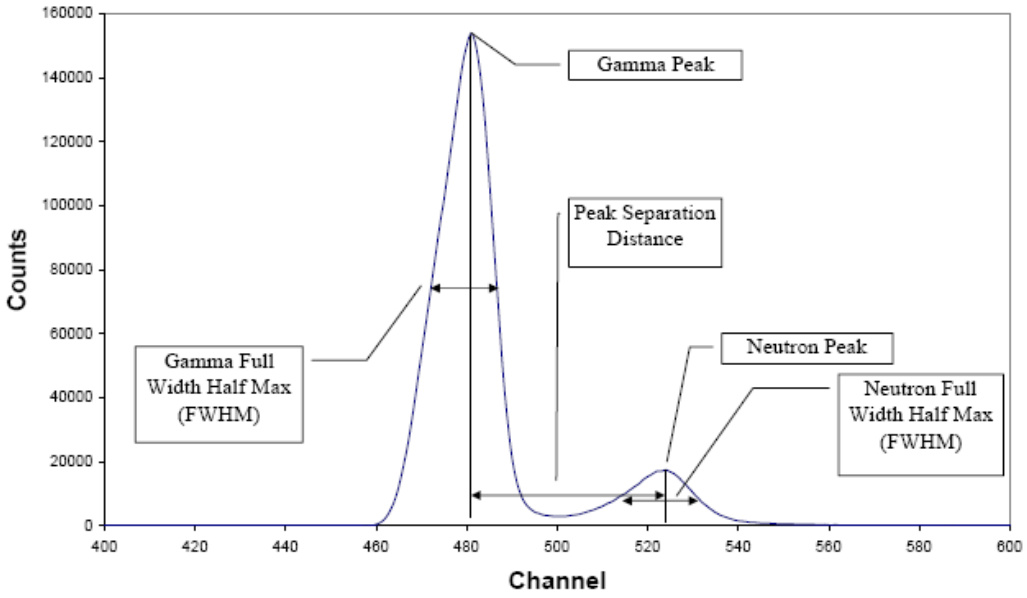

Figure 2-9-A sample PSD histogram showing the relevant parameters for FOM calculation.

Typically, PSD results are plotted in such a way that the FOM capability of the system can be easily visualized. Specifically, there are two common types of PSD plots: one with the PSD parameter plotted against a normalization parameter and one is a histogram representation of the PSD parameter. For the histogram type the PSD parameter is shown explicitly after binning ([1], [2]).

A problem with the aforementioned FOM scheme is that the scheme only takes into account a linear spectrum. If non-linearity exists in the system, then more than two peaks may be observed (Figure 2-10). In such cases, the definition of FWHM for the neutron and the gamma peaks becomes unclear, and another scheme should be used.

2.5 Modified Figure of Merit

When non-linearity exists in the system or when the traditional FOM scheme is not clearly applicable (Figure 2-10), a new scheme may be developed and used to compare the

PSD capability of the system ([15]). In the PSD histogram below, due to non-linearity of the system gain, multiple peaks exist. In such cases, the traditional FOM scheme breaks down as the definition of the peak separation and the FWHM becomes unclear.

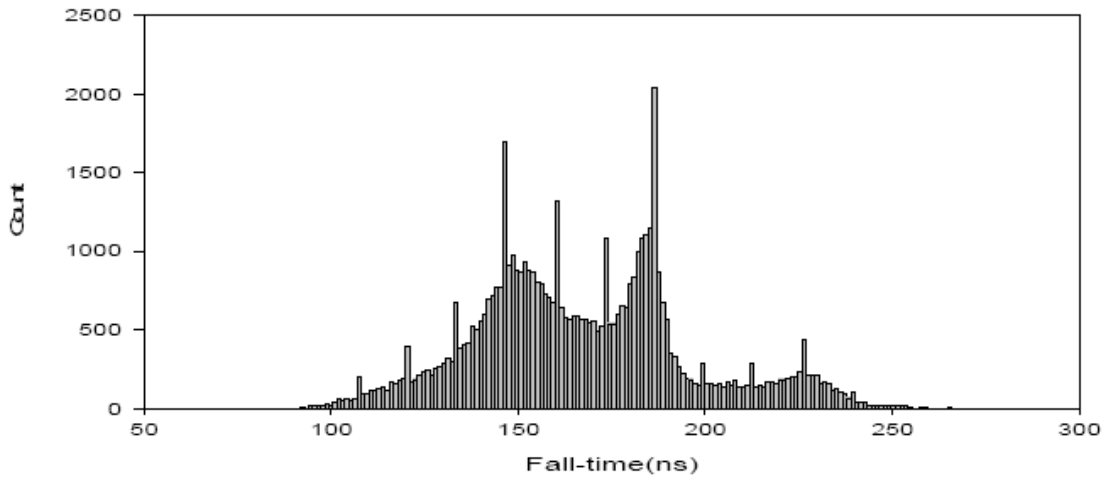

Figure 2-10-PSD histogram of a non-linear system.

The corresponding PSD scatter plot of the Figure 2-10 is below in Figure 2-11. In the scatter plot, it is clear that the fall time of the pulses does not vary linearly with the height of the pulse. Furthermore, it is clear that the peaks of Figure 2-10 are created from the curvature of the scatterplot.

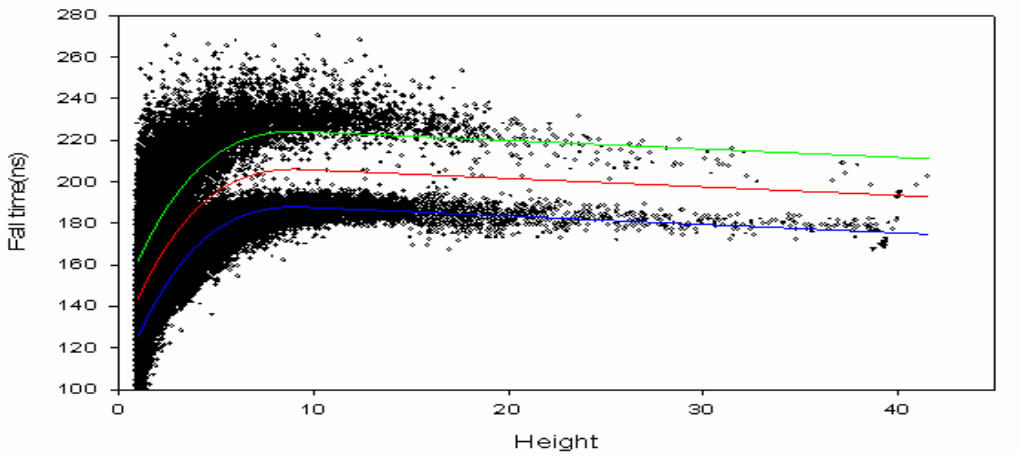

Figure 2-11-PSD plot of a non-linear system.

In Figure 2-11, a separation function (Red line), a neutron mid-line (Green line) and a gamma mid-line (Blue line) function are plotted. With the functions, a new FOM scheme (FOM*) may be derived with the following expression:

$$\text{FOM}^* = \frac{\frac{\int n(h) - \gamma(h) dh}{\int dh}}{(\sigma(\gamma) + \sigma(n))} \qquad 2.18$$

The numerator expression $\frac{\int n(h) - \gamma(h) dh}{\int dh}$ describes the neutron and gamma peak separation by normalizing the difference between a neutron and a gamma mid-line function represented by $n(h)$ and $\gamma(h)$ as shown in the PSD plot. Furthermore, the denominator term $(\sigma(\gamma) + \sigma(n))$ described the combined spread of the peaks. $\sigma(\gamma)$ is the standard deviation of the gamma peak in respect to the gamma mid-line function and $\sigma(n)$ is the standard deviation of the neutron peak. As can be seen, the new FOM scheme preserves the definition of the traditional FOM scheme by using translated expression for both the numerator and the denominator terms. Furthermore, if an appropriate fitting routine is used to calculate the separation and the mid-line functions, a more objective FOM may be obtained, as the new scheme's definitions are more clear than the old scheme's, especially when in the old FOM scheme the FWHM of the peaks are not readily clear when the peak separation is small.

2.6 FOM* Function Fitting

To fit the neutron and the gamma mid-line functions separately, an initial arbitrary separation function will need to be defined. However, all three functions may be fitted simultaneously to avoid subjective ambiguous neutron/gamma separation with the amoeba simplex routine ([15]).

The amoeba simplex fitting routine is also called the Nelder-Mead Simplex Method, and was first developed by Nelder and Mead. A simplex is a generalized triangle with (n+1) vertices in an n-dimensional plane. The method uses a sequence of simplexes to find the minimum of a given function $f(a_1, a_2, ..., a_n)$. The amoeba algorithm is intrinsically non-linear and is effective in bypassing local minima during minimization.

2.6.1 Amoeba Algorithm

The simplex method for finding the minima of a given function $f(A) = f(a_1, a_2, ..., a_n)$ will be given in this section.

1) With an n-parameter function $f(a_1, a_2, ..., a_n)$, $(n+1)$ initial points must be chosen. For example, for a 2-parameter function $f(A) = f(a_1, a_2)$, three initial guesses $f(X) = (x_1, x_2)$, $f(Y) = (y_1, y_2)$ and $f(Z) = (z_1, z_2)$ must be chosen.
2) Define $B = \{b_1, b_2, ..., b_n\}$ (B for best), where $f(B) = f(b_1, b_2, ..., b_n)$ produces the smallest function from the pool of values. Similarly, define $W = \{w_1, w_2, ..., w_n\}$ (W for worst), where $f(W) = f(w_1, w_2, ..., w_n)$ produces the largest function value. The goal now is to shrink the simplex in such a way that W improves.
3) With B and W defined, it is then possible to find the mid-point M, where M is the average of all points excluding W. With M then, a reflection R may be found. Specifically, R denotes the set of coordinates given by a projection of W along M, where $R = M + (M - W)$ (Figure 2-12).

4) If $f(R) = f(r_1, r_2, ..., r_n)$ is less than $f(W)$, an expansion point should be tested. Basically, the point E denotes an expansion of R along the mid-point M, where $E = R + (R - M)$ (Figure 2-13).

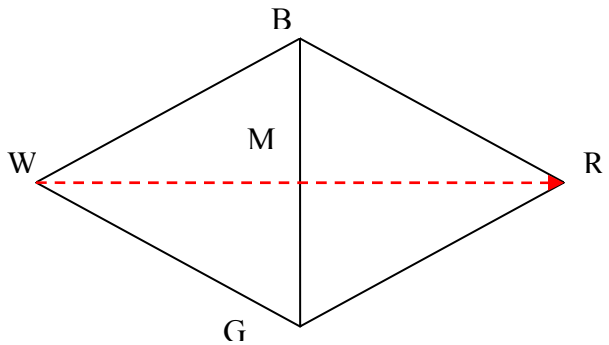

Figure 2-12-Reflection in a 2-D case.

5) If either $f(R)$ or $f(E)$ is smaller than $f(W)$, then $f(W)$ should be replaced by the smallest value of the two. After the replacement, the whole process is repeated from step 2). However, if $f(W)$ is less than $f(R)$, then two contraction points C_1 and C_2 should be considered (Figure 2-14).

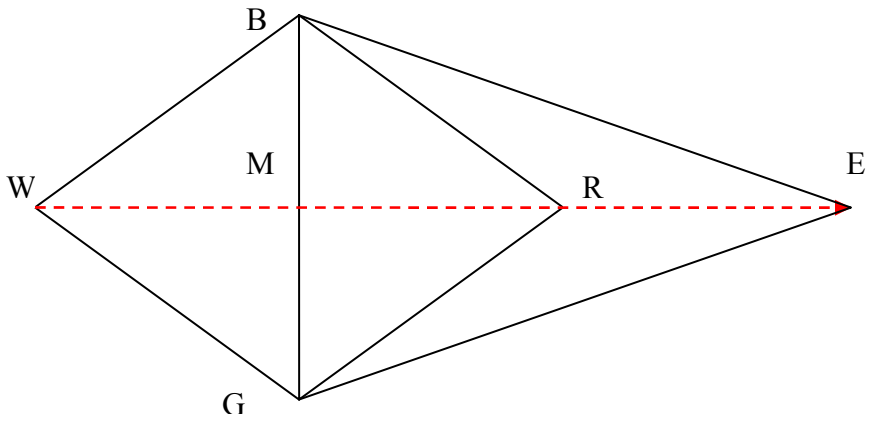

Figure 2-13-Expansion in a 2-D case.

6) The points C_1 and C_2 are defined as the mid-points between *W-M* and *M-R*, respectively. Thus $C_1 = \frac{1}{2}(W + M)$ and $C_2 = \frac{1}{2}(M + R)$. The smaller function value between $f(C_1)$ and $f(C_2)$ is then compared with $f(W)$. If either $f(C_1)$ or $f(C_2)$ is smaller than $f(W)$, then W is replaced by the point and the process is repeated from step 2).

7) If none of the function values $f(R)$, $f(E)$, $f(C_1)$ or $f(C_2)$ is smaller than $f(W)$, the simplex must shrink toward the best point B (Figure 2-15). Specifically, every vertices of the simplex $B, X, Y, ..., W$ undergoes the transformation $X^* = \frac{1}{2}(X + B)$. Afterwards, the function f is then re-evaluated at every point and the order of $B, X, Y, ..., W$ are reassigned and the process begins anew from step 2).

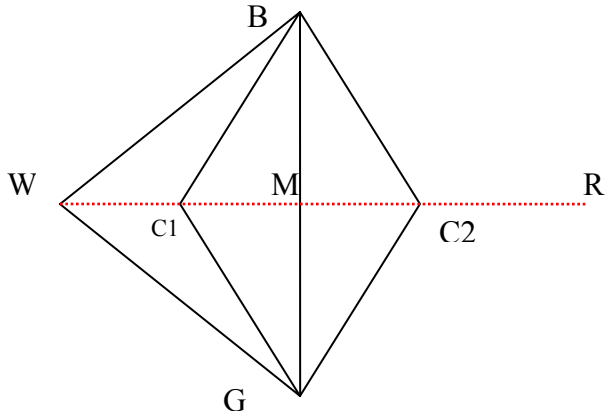

Figure 2-14-Contraction in a 2-D case.

8) The process repeats until a given tolerance is reached, typically defined by $T < \left|\left(f(B) - f(W)\right)\right|$.

For a more detailed explanation of the amoeba scheme, please refer to [16], [17].

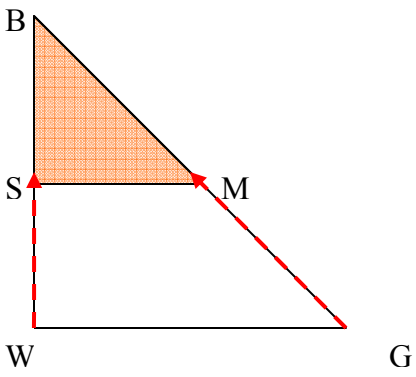

Figure 2-15-Shrinkage in a 2-D case.

2.6.2 Current Implementation

The current problem lies in fitting suitable curves to the PSD plots obtained from non-linear system, such as Figure 2-16. The curves are needed to obtain a modified figure of merit (FOM*), which is discussed in an earlier section.

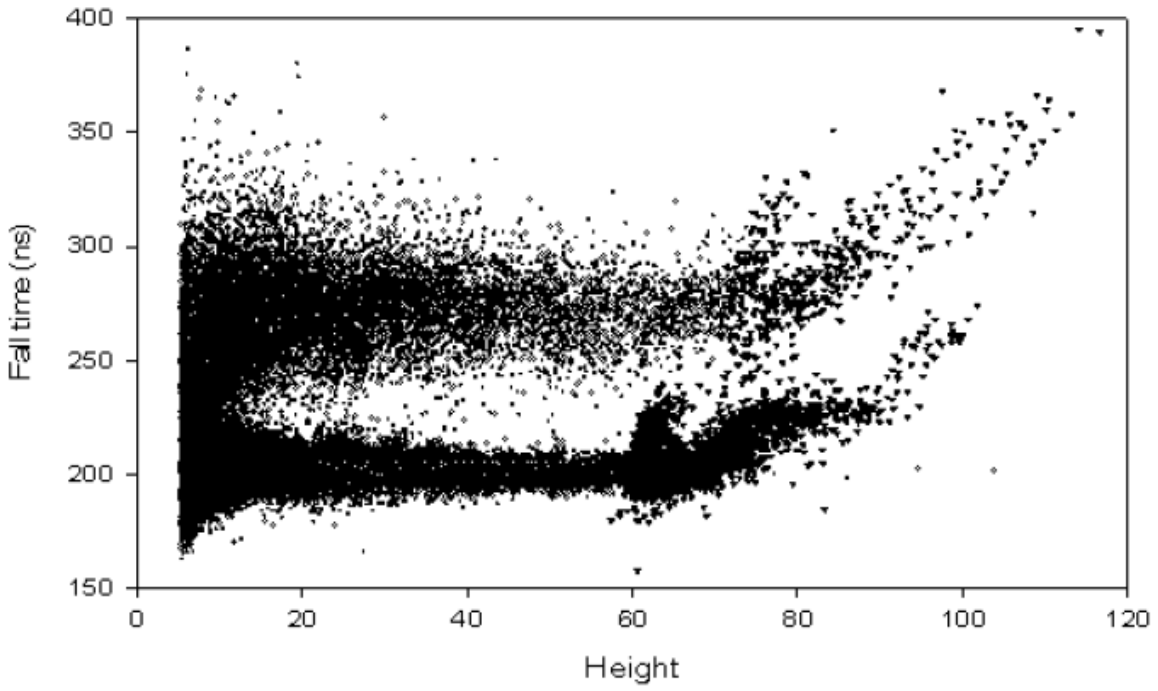

Figure 2-16-A non-linear PSD plot obtained from Acqris digitizer with a 500 ohm termination set-up.

Originally, a gamma/neutron separation curve was fitted manually to the space between the upper neutron and the lower gamma region. Then separate linear regression lines are fitted to each of the regions. Cubic regressions were used to fit the separation and the mid-line functions in this method. With this method, however, the separation function is needed, and since the curve is fitted manually (Figure 2-17), huge error may be present. Furthermore, the neutron and gamma regression lines often crossed and caused errors in subsequent calculation. Thus, the option of using the amoeba method to fit all three curves simultaneously was explored and tested (Figure 2-18).

The function that simplex minimizes in this case is the simple regression:

$$f = \sum (X_i - X(h))^2 \qquad 2.19$$

Where X_i is the individual date point and $X(h)$ is the fitted function of height (h).

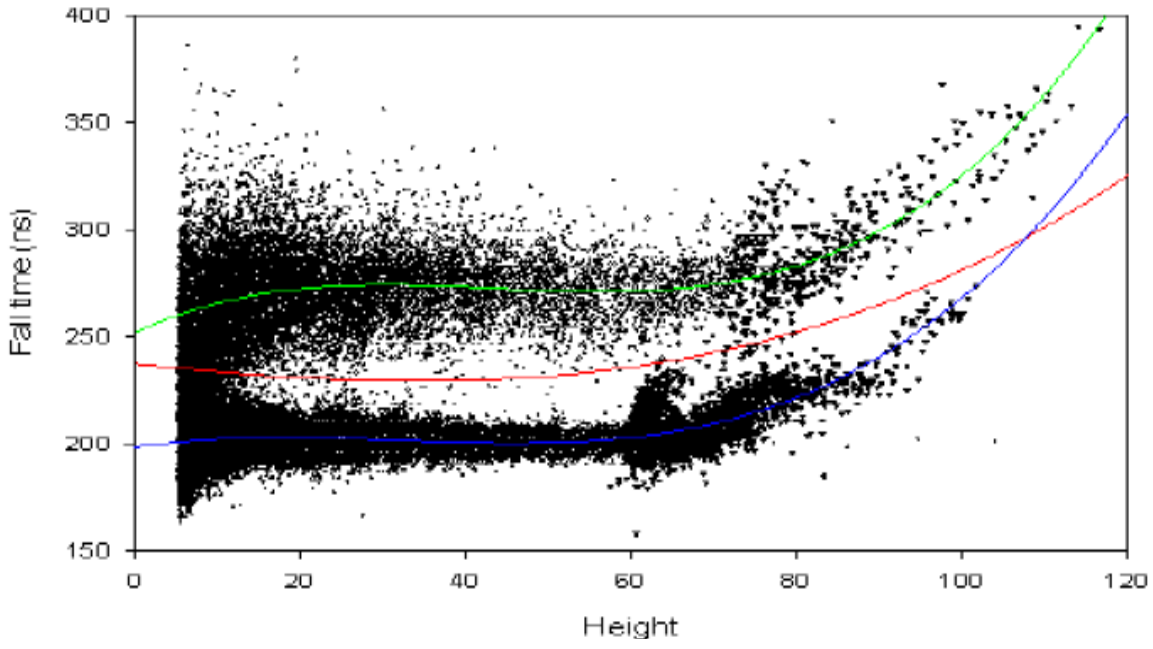

Figure 2-17-500 ohm PSD plot fitted with separate regressions for separation and mid-line functions.

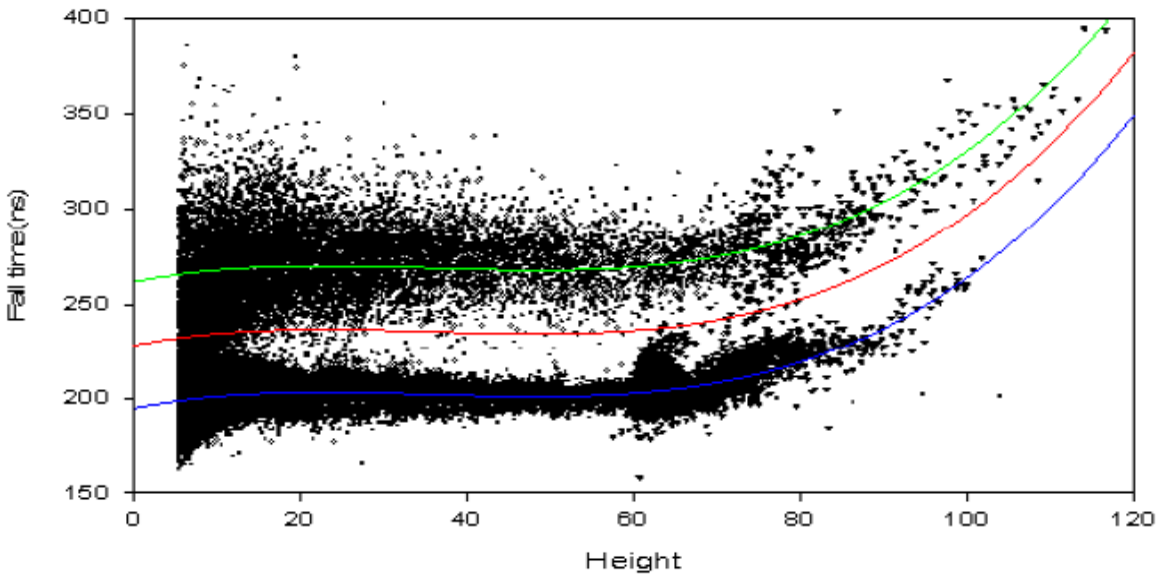

Figure 2-18-Amoeba solution to the 500 ohm PSD. Green line is the neutron mid-line function, red the separation function and blue the gamma mid-line function.

According to Figure 2-16, there are three distinct regions in the PSD plots: the upper neutron, lower gamma and the middle separation regions. As such, three cubic equations are used (Figure 2-18) and referenced in the amoeba routine, and they are as follows:

$$\gamma(h) = a_\gamma + bh + ch^2 + dh^3 \qquad 2.20$$

$$S(h) = a_\gamma + a_S + bh + ch^2 + dh^3 \qquad 2.21$$

$$N(h) = a_\gamma + a_N + bh + ch^2 + dh^3 \qquad 2.22$$

In the equations above, $a_\gamma, a_S, a_N, b, c, d$ are free parameters and amoeba is free to adjust them. A note of interest is that the three regions are assumed to be the same shape, thus the only difference between the equations is the intercept term a. Also, the presented equations may be modified depending on the shape of the PSD plot.

2.6.3 PSD Implications

As shown in Figure 2-18 above, the amoeba method may be used to separate neutron and gamma data. Even though in the current implementation, amoeba is used to obtain functions for the FOM* scheme, the amoeba method itself is a powerful method that may be used outside of the current scope. Even with the traditional FOM scheme, a need exists to separate neutron and gamma data. If the detection system is set up in such a way that allows for post data collection PSD, the amoeba method may easily be used to extract neutron data. Even in a linear concurrent PSD-data collection system, the amoeba method may still be used to find the optimum value of the PSD parameter, such as the lower level discriminator cut-off in a traditional charge integrating system. The capability of amoeba performing PSD on a non-linear post data collection PSD system will be demonstrated in the experimental section; however, its ability to perform PSD on any system should not be overlooked.

2.7 Response Function

With good PSD techniques, neutron spectra may be separated from gamma spectra in a mixed field measurement data set. If the neutron data set is obtained from a mono-energetic neutron source, then the detector's response function for that particular neutron may be determined ([18], [19]). To illustrate, consider the probability of a recoiled proton's energy is in interval dE about E where

$$P(E_P)dE = \frac{1}{E_n}dE \qquad 2.23$$

Then the ideal proton energy spectrum with bin width dE_P, defined to be $N(E_P)dE_P$, is given by

$$N(E_P)dE_P = N_H T \int_0^{E\max} \sigma(E_n)\phi(E_n)dE_n \frac{dE_P}{E_n} H(E_n - E_P) \qquad 2.24$$

where

N_H =Hydrogen atom number density

T =Time of measurement of the recoil protons

$\sigma(E_n)$ =Elastic scattering cross section of hydrogen

$\phi(E_n)dE_n$ =Neutron flux of neutrons with energy dE_n about E_n

$\frac{dE_P}{E_n}$ = probability of a recoiled proton's energy is dE_P about E_P

$H(E_n - E_P)$ =Function with value $H(E_n - E_P) = 1 \big| E_n \geq E_P$, and 0 otherwise

The measured spectrum $M(E)dE$ with all of the spectrum distortions taken into consideration is given by

$$M(E)dE = \int_0^{E\max} dER(E, E_P)N(E_P)dE_P \qquad 2.25$$

$M(E)dE$ may also be expressed in terms of the neutron source spectrum (or neutron flux) $\phi(E_n)dE_n$, where

$$M(E) = \int_0^{E\max} dE_n k(E, E_n)\phi(E_n) \qquad 2.26$$

In both Equation (2.25) and (2.26), both $R(E, E_P)$ and $k(E, E_n)$ are defined as the response function to relate the ideal neutron spectrum and the neutron flux spectrum to the measured spectrum. $k(E, E_n)$ can be related to $R(E, E_P)$ through the relationship

$$k(E, E_n) = \int_0^{E\max} dE_P R(E, E_P) N_H T \frac{\sigma(E_n)}{E_n} H(E_n - E_P) \qquad 2.27$$

To unfold the measured spectrum to obtain the source spectrum $\phi(E_n)$ then, both $M(E)dE$ and $k(E,E_n)$ must be determined. $M(E)dE$ is simply the measured spectrum, obtainable through a detector system. $k(E,E_n)$ can be determined by characterizing the detector system. As can be observed through Equation (2.26), if the neutron source is mono-energetic with energy *E*, Equation (2.26) may be rewritten as a differential spectrum with the source flux ϕ_0

$$M(E)dE = k(E,E_n)\phi_0 dE \qquad 2.28$$

With the aid of an accelerator as a source for monoenergetic neutrons or a computer simulation to simulate the source detector interaction, the response function for mono-energetic neutrons with different energy may be determined. Then, if the quantity $k(E,E_n)$ for many energy levels is known, a response surface maybe constructed for a range of energies. The response surface may then be used to unfold the measured spectrum $M(E)dE$ to obtain the source spectrum $\phi(E_n)$ (Equation (2.26)). For this project, the program Scinful (*Scin*tillation *Ful*l Response to neutron detection) is examined and used for the purpose of generating response functions $k(E,E_n)$ for neutron spectrum unfolding.

2.8 Scintillator Full Response to Neutron Detection

Scinful (Scintillator Full Response to Neutron Detection) is a Monte Carlo program which can be used to simulate NE213 or NE110 scintillation detectors. In Scinful, a cylindrical detector and a point source are modeled; each particle from the source is monitored and tracked through out the program. The final output from Scinful is a $\frac{dN}{dL}$

spectrum, where L is the light output from the detector. Besides the total spectrum, Scinful can also give the light output from each individual reaction, and if desired, Scinful can also output the spectra in terms of energy instead of light output. In the following sections, Scinful will be dissected and each process of the calculations will be discussed ([20], [21]).

2.8.1 Input File

The input file of Scinful consists of seven lines and they are given below:

1) Comment Lines
2) # of Histories, Detector Type, Attenuation Coefficient
3) Source Energy, Low Energy Bound, Distribution, Energy Cut off
4) Random Number Generator Seed
5) x, y, z of the source location
6) Detector Radius, Detector Height, Collimator Radius
7) Wbox

The interpretation of each variable:

Comment Lines- This line is designated to the description of the program, this line may be left blank

# of Histories- Number of interaction simulated in the detector

Detector Type- May be either 213 or 110, a negative sign in front of the numbers denotes pulse shape discrimination

Attenuation Coefficient- The attenuation coefficient for light transport in the detector, Scinful only performs light transport along the height of the detector.

Source Energy- The upper bound of the source energy in MeV, if the source is mono-energetic, this is the source energy. The magnitude of the source must be less than 100 MeV.

Low Energy Bound- The lower energy bound of the source energy in MeV, 0 should be inputted if the source is mono-energetic.

Distribution- The distribution of the source energy:

0 if the source is mono-energetic

<0 if the source energy is uniformly distributed

>0 if the source follows a Maxwellian distribution with temperature equals to the number inputted

Random Number Generator Seed- Seed for the random number generator

x, y, z of source location- the (x, y, z) coordinates of the source. The origin of the coordinate system is the center of the detector front face. The x, y plane is the detector front face and the negative z axis runs along perpendicular to the front face of the detector.

Detector Radius- The radius of the detector in cm.

Detector Height- The height of the detector in cm.

Collimator Radius- The radius of the front collimator in cm.

Wbox- Scinful uses Wbox to calculate the width of light bins used in the spectrum.

2.8.2 Solid Angle Determination

Scinful determines the solid angle of the source through Monte Carlo method. Scinful first estimates a solid angle which encompasses the entire detector surface. Depending on the source location in respect to the detector, the method of estimation will be different. In any case, however, Scinful attempts to find a straight line from the source to the

closest and the furthest edge on the detector surface, the angle between the two lines is Scinful's first estimate of the solid angle. If the source is positioned in such a way such that both the sides and the front face of the detector is visible to the source, Scinful calculates the front face component and the side component separately then sums the two.

After the initial estimate is chosen, Scinful then emits particles in the estimated solid angle. If a particle does not hit the detector surface, a new particle will be generated until the detector surface is hit. If the detector surface is hit, Scinful will then track the particle in the detector and perform subsequent calculations. In the end, the total number of particles emitted and the particles hitting the detector is tallied. The final true solid angle then is simply the initial solid angle times the ratio of the tracked particles.

2.8.3 Interaction

After the solid angle is determined, the energy of the particles emitted is sampled from the energy distribution specified in the input file. With the energy of the particle then, all of the cross-sections pertained to the energy are tallied. Except for hydrogen in which an experimental fit is used, all of the other cross-sections are stored in tabular form in the program. In all, eleven different types of interactions are taken into account in Scinful. Table 2-1 contains the eleven reaction types in Scinful, respective reaction threshold, and the reference for each reaction ([22]).

The hydrogen cross-section agrees extremely well with ENDF/B-V data (Figure 2-19). The carbon reaction cross-sections, on the other hand, typically agree well with ENDF/B-V data at low energy, but deviates above 15-20 MeV (Figure 2-20). The deviation typically stems from in house tweaking to compensate for the lack of actual data for some of

the reactions. Furthermore, the reactions listed above with an * in the reference are not found in ENF/B-V cross-section archive. The reliability of those cross-sections is suspicious due to the lack of data on them, as only one or two papers had published results on those reactions. Furthermore, only one major reaction with Hydrogen is listed, whereas ten different carbon reactions are listed in Scinful. This is primarily due to the fact that hydrogen elastic scattering cross-section dominates the hydrogen total cross-section for energy above 1 eV (Figure 2-21), which is the effect range of the program due to other tabulation limits (Such as proton range table used in range calculations).

Table 2-1-Scinful reaction types, reaction thresholds, and references.

Reaction Types	Threshold	Reference
(n,H) Elastic Scattering	-	ENDF/B-V
(n,C) Elastic Scattering	-	ENDF/B-V
(n,C) Inelastic Scattering	2.5 MeV	ENDF/B-V
C(n,2n)B	21.5 MeV	ENDF/B-V
C(n,α)Be	7.5 MeV	ENDF/B-V
C(n,d)B	15.25 MeV	ENDF/B-V
C(n,p)B Bounded State	13.7 MeV	ENDF/B-V
C(n,p)B Unbounded State	17.35 MeV	Datum*
C(n,n')3α	17.35 MeV	Nuclear Physics A394*
C(n,t)B	21.5 MeV	Subramamian*
C(n,3He)Be	22.0 MeV	Phys. Rev. C28*

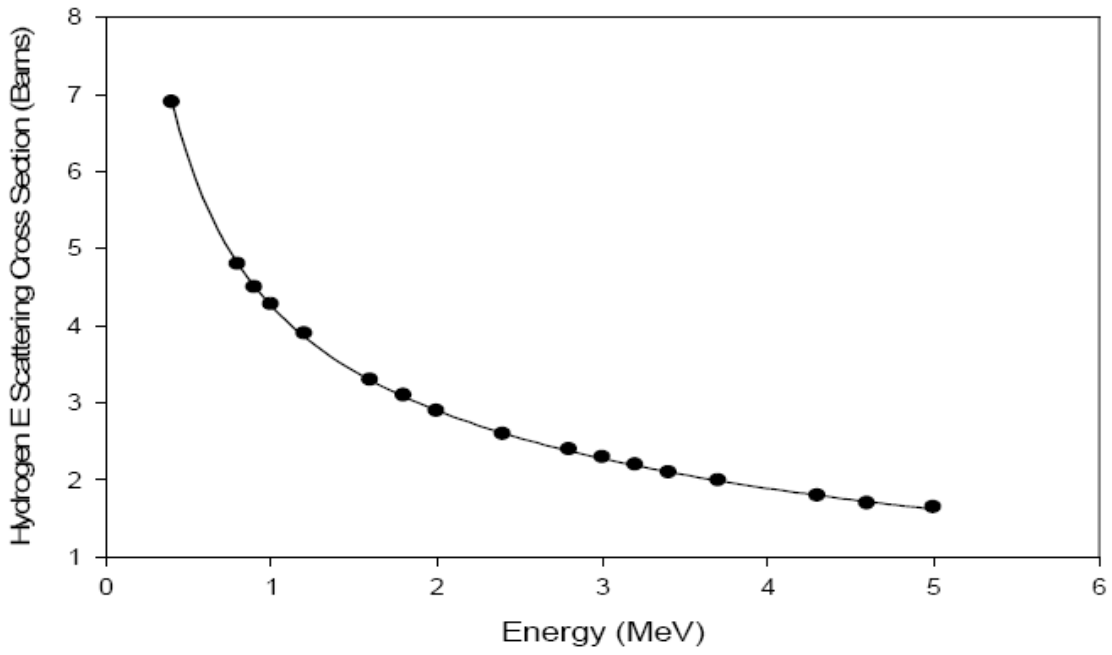

Figure 2-19-Scinful cross section comparison with ENDF data, hydrogen cross-section confirms well with ENDF data.

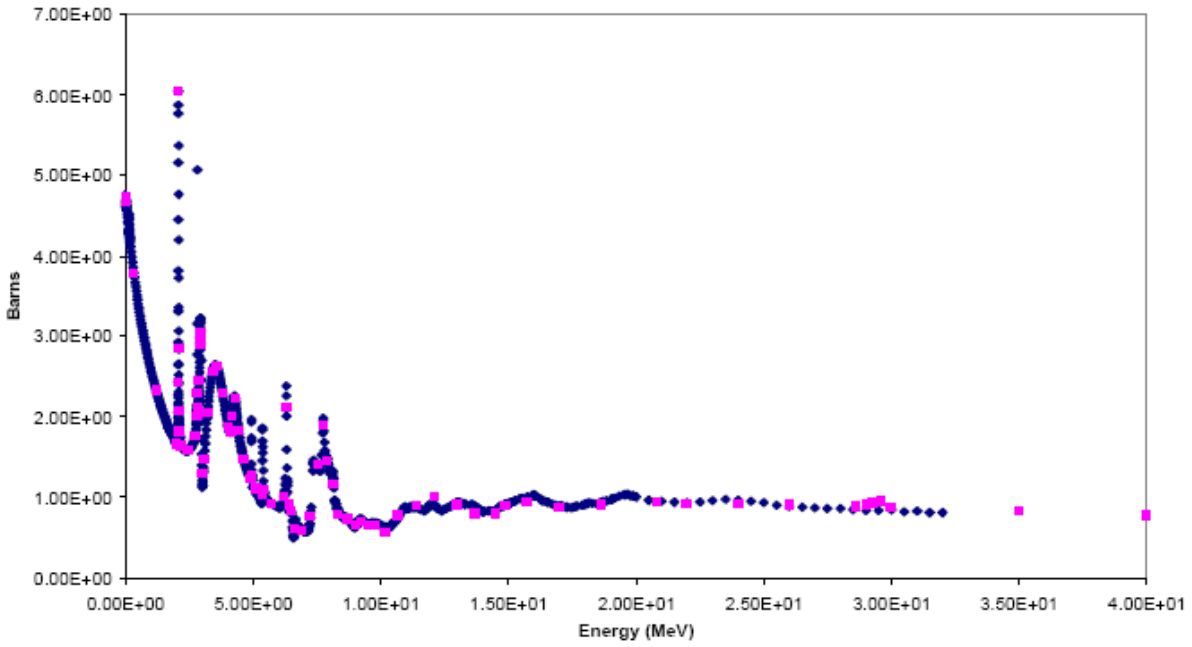

Figure 2-20-Carbon elastic cross-section confirms well with ENDF data up to around 20 MeV, then starts to deviate.

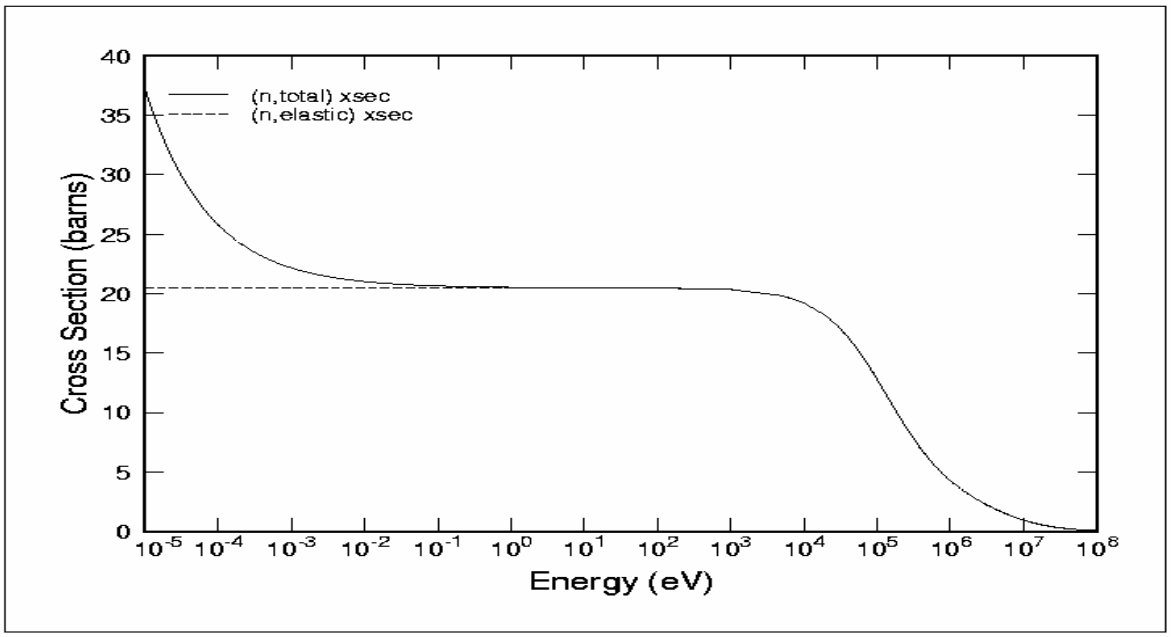

Figure 2-21-Hydrogen elastic scattering cross-section dominates total cross-section data.

After Scinful tallies all of the available cross-sections, the fraction of each cross-section to the total cross section is then found. A number generator then generates a number to compare to the hydrogen fraction. If the hydrogen fraction is greater than the random number, hydrogen elastic scattering will then occur for the particular particle. If, however, the random number is greater than the hydrogen fraction, the random number less the hydrogen fraction will then be compared with carbon elastic scattering. The process continues until a reaction is finally chosen. The order of random number-cross-section comparison does not matter if there is no intrinsic bias in the random number generator.

2.8.4 Products Light Output

After an interaction type is chosen, Scinful then calculates the reaction energy and the products' vector with the proper two body kinematics. For example, in the case of (n,H) elastic scattering, Scinful first determines the energy of the neutron to determine if the

reaction is isotropic. If the reaction is not isotropic (E>13.7 MeV), then an angular distribution function is used, and the outgoing products' energies are chosen based on the randomly chosen weighted scattering angle. If the scattering is isotropic, then the scattering angle is simply chosen randomly, and then relates to the products' energies and directional vectors. With the products' energy, in this case hydrogen atoms from scattering, the products' range are then determined from tabulated data. The data sets are mainly from well-known data and are assumed reliable. From the products' energies, their interaction cross-sections are then sampled and converted to path lengths (Or mean free paths). The path lengths and ranges are then compared. If the path length is greater than the range, then the particular product is assumed to have stayed in the detector and the full energy of the product is deposited. If the range is greater than the path length, then the product is assumed to have escaped. The difference between the range and the path length is then taken and the product is assumed to escape carrying with it energy equals to the difference (Looked up again in the range table). Depending on the interaction, the method of determining the outgoing path lengths and the energies of the products may be different, but the process of product escape determination and energy loss mechanism is the same with all reactions.

In the kinematics calculation of Scinful, the energies of the products are tracked at two points. First, the products' energies are found after the interaction. If the products are determined to have stayed in the detector, the product then deposits all of its energy in the detector. The light output at this point is simply the tabulated Verbinski light curve values based on the particular product's energy after the reaction. If a product escapes from the detector, the energy of the product deposited in the detector is then the difference between

the energy after the interaction and the energy at the point of escape (Found by the difference of range and path length). The light output from escaped product then, is equal to the difference in light output between the total output and the light corresponded to the escaped product's energy.

2.8.5 Post-Interaction Neutrons Fate

In addition to determining the fate of the reaction product, Scinful also determines the fate of the neutron after the interaction, assuming that the neutron is conserved or is a product in the reaction. The neutron's energy is first determined through the conservation of energy. The neutron energy is simply the initial energy less the energy of the products. After the determination of neutron energy, the neutron energy is immediately checked against the E-cutoff parameter set forth in the input file. If the neutron energy is less than the E-cutoff parameter, the neutron is considered 'dead,' and is not tracked in the program anymore. If the neutron energy is above the E-cutoff, then at this point, Scinful checks the interaction probability for the neutron. If the neutron does not interact in the volume, then the neutron escapes. If the neutron interacts, then the neutron simply cycles through the program again with the new proper energy. Also, if the neutron interacts more than once, all of the light output from the different interactions is summed as is observed in an actual scintillation detector.

2.8.6 Different Interaction Type Considerations

Since neutrons above E-cutoffs are allowed to interact again in the detector, it is possible for the neutron to undergo a few different reactions in its lifetime as listed in Table 2-1.

Scinful's total output sums the light output from all of the different reactions the neutron undergoes, regardless of reaction type. Besides the total light output, Scinful is also capable of outputting individual reaction lights. Scinful banks each light output and reaction type individually after each interaction. Thus in the output, the contribution of each reaction type to the total output can be seen.

2.8.7 Scinful Output

Up until this point in the program, Scinful tracks each particle with exact energy. With exact energy then, Scinful tally each particle output with exact light output (in Light Units). Then, before output, Scinful smears the light output to match the output in a real detector. Scinful smears the light by binning the light, effectively broadening each light value.

From the input file, Scinful obtains the value Wbox. With Wbox, Scinful calculates the light bin width by

$$Width_i = (I * Wbox)^2 \qquad 2.29$$

where I is the number of light bins, ranging from 1 to 475. Scinful only permits 475 light bins in the output. Furthermore, with the light bin width, the i^{th} light bin is then given by

$$Bin_i = Bin_{i-1} + (I * Wbox)^2 \qquad 2.30$$

and

$$Bin_0 = 0 \qquad 2.31$$

Then, Scinful records the event in the i^{th} light bin, as defined above, if the light output from the event is between Bin_{i-1} and Bin_i. Furthermore, all of the outputs, total or individual

components, are binned by the same light bins as defined above.

Besides output all events in light bins, Scinful can also output the results according to energy. Scinful first finds the mid point of each light bins, then with Verbinski's curve, convert the light units to proton, carbon and alpha equivalent energies. However, the light outputs are given in terms of $\frac{dN}{dL}$, but the energy outputs are actually dN about energy E. Thus, the output must be processed further to actually give the quantity $\frac{dN}{dE}$. A sample output is shown in Figure 2-22.

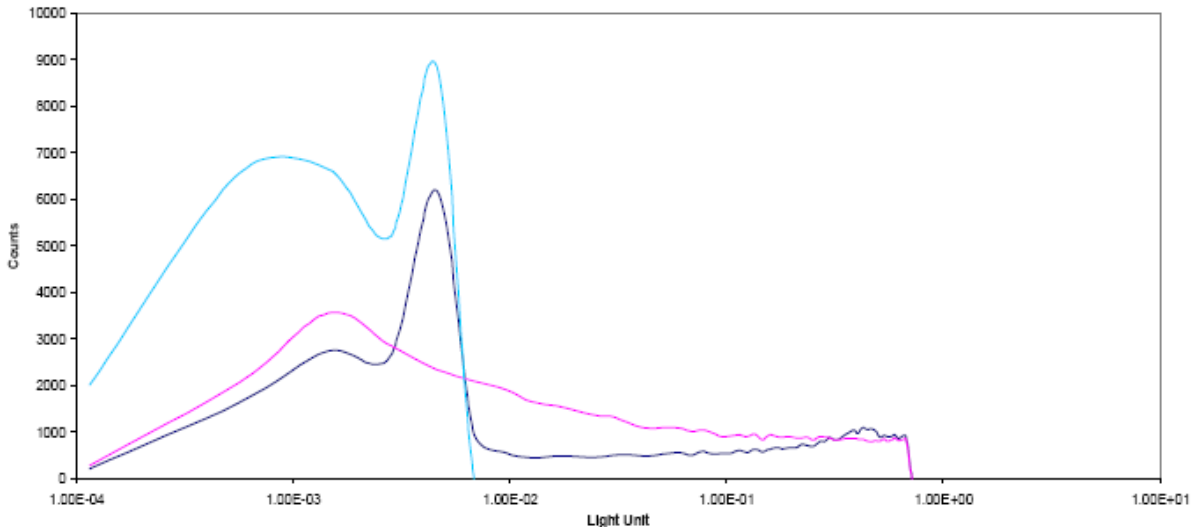

Figure 2-22-Sample Scinful output with different components.

2.8.8 Obtaining Response Function from Scinful output

To convert to the quantity $\frac{dN}{dE}$ from scinful output $\frac{dN}{dL}$, one must first find the relation $\frac{dL}{dE}$. In order to obtain $\frac{dL}{dE}$, Verbinski's curve may be used (Figure 2-23). A power function of the form

$$L = 0.1563E^{1.4318} \qquad 2.32$$

may be fitted for the proton energy. The alpha and the carbon energies are not fitted because the proton energy is by far the most important quantity on the basis of unfolding.

The quantity $\frac{dL}{dE}$ is simply the derivative of Equation (2.32), where

$$\frac{dL}{dE} = .2247E^{.4378} \qquad 2.33$$

The Scinful output $\frac{dN}{dL}$ may then be converted to $M(E)$, a function of energy E_n, through the relation

$$M(E) = \frac{dN}{dL}\frac{dL}{dE}dE \qquad 2.34$$

where $\frac{dL}{dE}$ is simply from Equation (2.33) and dE is the energy bin width of the quantity $\frac{dN}{dE}$.

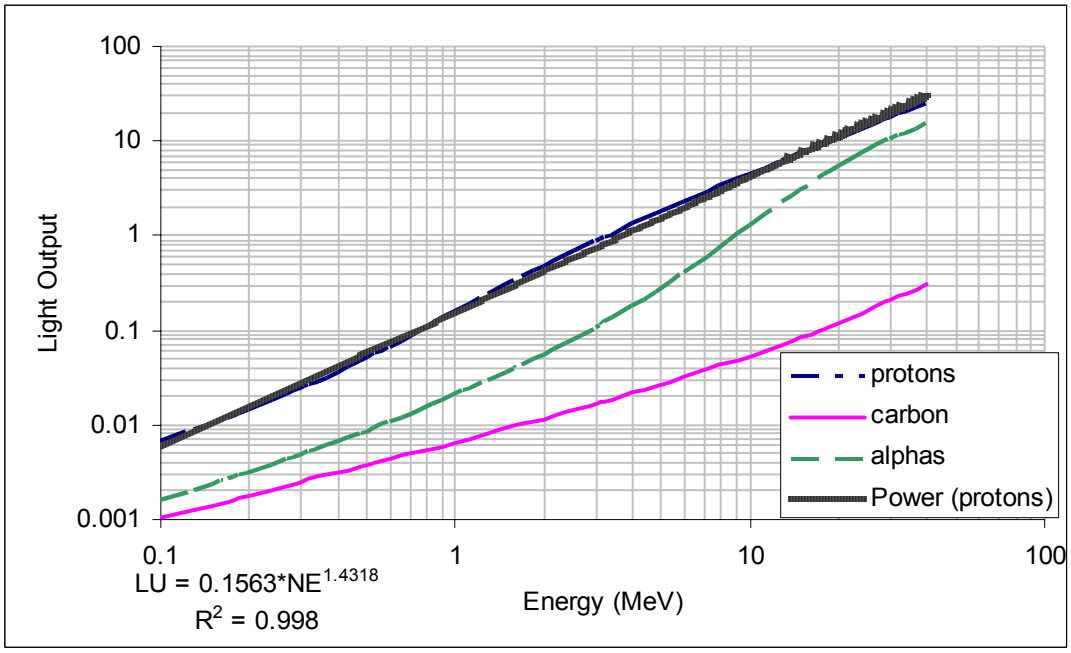

Figure 2-23-Verbinski's Curve fitted with a power function

Relating Equation (2.26) for a mono-energetic neutron source, the Scinful output (after energy conversion) can be related to the mono-energetic source energy spectrum ϕ_0 through

$$M(E)dE = k(E, E_n)\phi_0 dE \qquad 2.35$$

Where the scinful output $M(E)dE$ is the mono-energetic flux smeared by the detector response $k(E, E_n)$.

2.9 Response Surface and Unfolding

The measured spectrum is related to the source spectrum through the relationship

$$M(E) = \int_0^{E\max} dE_n k(E, E_n)\phi(E_n) \qquad 2.36$$

And for a mono-energetic source with energy E and energy spectrum ϕ_0, Equation (2.36) reduces to

$$M(E)dE = k(E, E_n)\phi_0 dE \qquad 2.37$$

Then, with several mono-energetic neutron sources of different energy, a response surface may be constructed (Figure 2-24). Scinful, as described, may be used to obtain the measured spectrum $M(E)dE$ depending on input.

The response surface allows for the construction of a new response function with existing responses. Suppose an unknown distributed neutron source spectrum is obtained through measurement, after normalization, the spectrum essentially consists of a distribution of response functions. The convoluted response is basically a combination of various existing mono-energetic response functions combined with a different weighting factor for

each. Another consideration to unfolding stems from the fact that the quantity measured in a measured spectrum from instrumentation is not the quantity $M(E)$ but the quantity $\frac{dM(E)}{dE}$. The quantity $\frac{dM(E)}{dE}$ may also be expressed as $\int_{E_i}^{E_{i+1}} M(E)dE$, effectively a differential slice. Then, let the source spectrum range from E_j to E_k, Equation (2.37) may be integrated and rewritten as

$$M_i = \int_{E_i}^{E_{i+1}} M(E)dE = \int_{E_i}^{E_{i+1}} dE \int_{E_j}^{E_k} dE_n k(E, E_n)\phi(E_n) \qquad 2.38$$

With the individual mono-energetic measured spectra known and the response functions found (With Scinful or other programs), Equation (2.38) may be solved iteratively using numerical techniques. To aid in the unfolding process, computer codes such as FERD and SAND-II are often used. In the end, a source spectrum $\phi(E_n)$ is obtained. From the $\phi(E_n)$ then, parameters such as detector resolution, efficiency, and noise may then be found and study upon ([1], [2]).

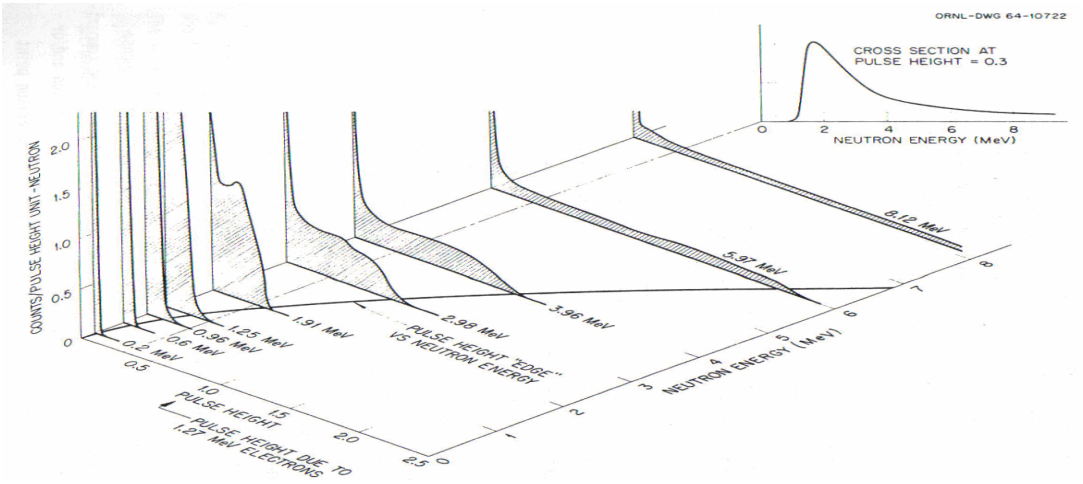

Figure 2-24-An example of a response surface for a NE213 scintillation detector.

2.10 FERD Unfolding

As stated, the measured spectrum is related to the source spectrum through the relationship

$$M(E) = \int_0^{E\max} dE_n k(E, E_n)\phi(E_n) \qquad 2.39$$

where $k(E, E_n)$ is the response function of the detector system at energy E. Then, to obtain the source spectrum $\phi(E_n)$, the measured spectrum would have to be unfolded. To do so, FERD may be used. However, instead of solving for the source spectrum $\phi(E_n)$, FERD actually solve for the quantity S_k, where

$$S_k = \int_0^{E_{\max}} W_k(E)\phi(E)dE \qquad 2.40$$

In this case, the quantity $W_k(E)$ is called the window function. S_k may be any quantity in relation to the source spectrum $\phi(E_n)$, depending on the dimension of $W_k(E)$. For example if $W_k(E)$ is a dose factor, then S_k is the dose rate. If $W_k(E)$ is the detector response, then S_k is the measured spectrum. In this case, the window function $W_k(E)$ approximates the response of ideal instruments, and then S_k is the source spectrum taken with an ideal instrument ([23]).

The inputs required for FERD are the foreground measured spectrum (Figure 2-25), the response function, and the window function (Shown in Appendix B). The foreground measured spectrum is simply measured data that is binned with a certain number of bins. The user then supplies the calibration parameters: the calibration channel, the light unit at the calibration channel and the zero light unit channel.

```
Calibration Channel: 0  Light at CC: 0.095961   Zero Channel: 0
FORMAT = (7x, 8I8)
      1    4624    2507    1647    1077     813     686     513     401
      9     350     299     227     216     161     156     106     107
     17      99      86      75      64      61      35      31      43
     25      32      31      21      25      16       6      18      10
     33       3       8       4       7       5       4       4       6
     41       5       3       1       3       1       1       3       3
     49       2       2       1       0       0       0       0       0
     57       2       2       1       1       0       0       0       2
```

Figure 2-25-Example Foreground Input File.

Besides the foreground input, the user also supplies a response file. Embedded in the response file are the response function and a guassian detector resolution function. The resolution function allows for the detector resolution to be simulated in the unfolding. Also, the user is given the option to supply the FWHM data of the detector to allow FERD to calculate the resolution function instead of supplying the resolution function itself. Furthermore, information pertinent to the resolution function and the response function are required. Needed information include the light unit bin (correspond to the row in the response matrix), the bin width, energy bin (correspond to the column in the response matrix). An example response file is given in Appendix B following the report. In general, the response file requires nine blocks of data, and they are as follow:

1) Control parameter-Where users can change program flow and parameters such as the generation of a log file and the use of FWHM data vs. the window matrix.
2) Integral output-The energy bins which FERD uses for the integral output.
3) Pulse-height bins-The pulse-height bins, in light units, which correspond to the row in the response matrix in block 9.
4) Pulse-height bin width-Bin width corresponding to the bins in block 3.
5) Energy bins-The energy bins, in MeV, which correspond to the column of the window matrix in block 8 and the response matrix in block 9.

6) Window row energy-Energies, in MeV, correspond to the row of the window matrix in block 8.

7) Gaussian FWHM-Full width at half max data for the detector. May be used in place of the window matrix, depending on the switch in block 1.

8) Window Matrix-Window matrix of the system. May be used in place of the Gaussian FWHM, depending on the switch in block 1.

9) Response matrix-The response surface of the detector used.

FERD generates an output file, of which the user can specify the name of, following the unfolding calculation. The output file consists of 2 sections, the differential flux and the integrated flux. The complete output file is not shown, but a sample output is plotted on Figure 2-26.

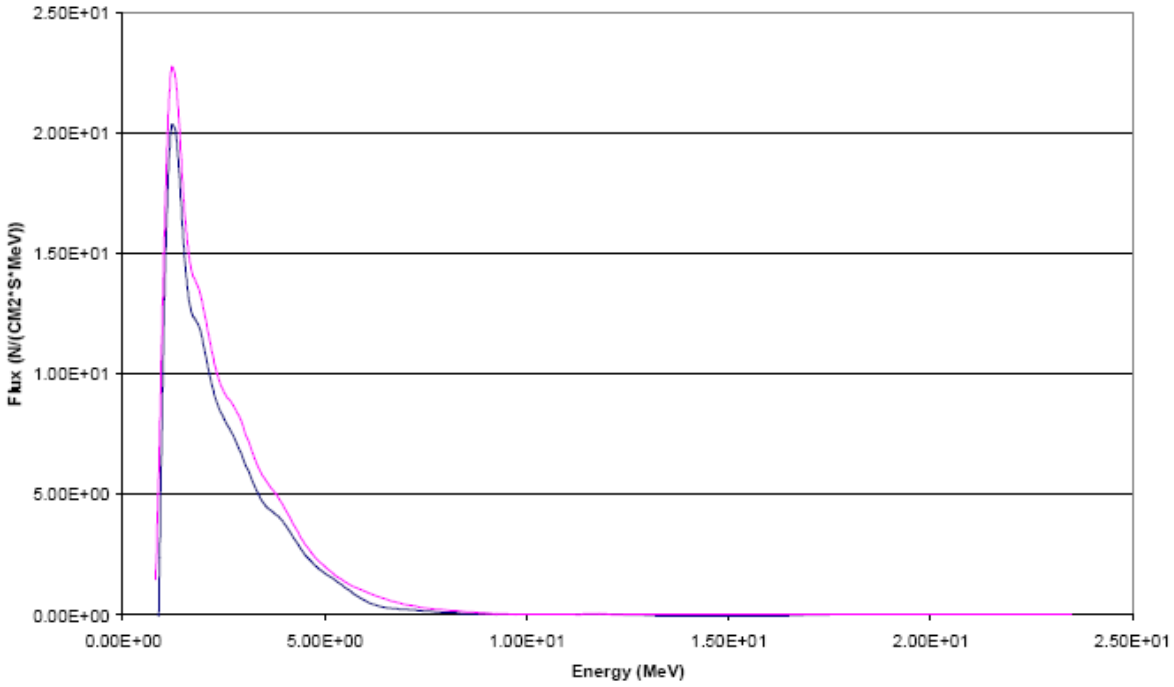

Figure 2-26-FERD's differential output for 64 bin, 50 ohm terminated Cf252 spectrum.

Chapter 3 NE213 Scintillator Experimental Response

The objective of this work is to verify the accuracy of computational response functions from Scinful. To do so, the response functions obtained from Scinful may be verified with experimental results. This approach requires a suitable experimental facility that is capable of producing mono-energetic neutrons. However, accelerators with time-of-flight capability have to be used for this approach. Another approach to verify the Scinful's response functions is to simply unfold a known neutron spectrum using Scinful's response functions and compare the results to the known spectrum. To do so, FERD-PC unfolding code may be used. The second approach is much less equipment/facility intensive and the only required information is the neutron spectrum along with a Na-22 calibration spectrum. The spectra may be taken with a variety of laboratory equipment set-up and neutron sources; in this case a simple digitizer set-up is used with a Cf252 source. The neutron spectrum needs to be separated from its gamma components with a good PSD technique to be unfolded. The amoeba fitting routine is demonstrated as a capable PSD technique and is used to separate the neutron components from the gamma components. Furthermore, the termination effect from the pre-amplifier on the overall PSD performance of the system was also examined.

3.1 Scinful Verification via Unfolding

3.1.1 Experimental Set-Up

The setup shown in Figure 3-1 was used during the spring of 2007 at the NISC (Nonproliferation and International Security Center) building. The pre-amplifier is described

in greater detail in Figure 3-2 and in Appendix C. The fast sampling 8-bit digitizer, Acqiris, was used to digitize the data. The system is capable of recording pulse-shape with a frequency of 1 GHz, making it a very attractive option for performing post data collection pulse shape analysis. In the current set-up, the signal from the detector was first fed into a non-inverting pre-amp. The pre-amp was then fed into four channels of the Acqiris system. The four channels each have a different gain setting, and thus with using the four channels, maximum dynamic range may be obtained. The pre-amp also was fed into a timing SCA, where a lower level discriminator may be set for triggering the Acqiris.

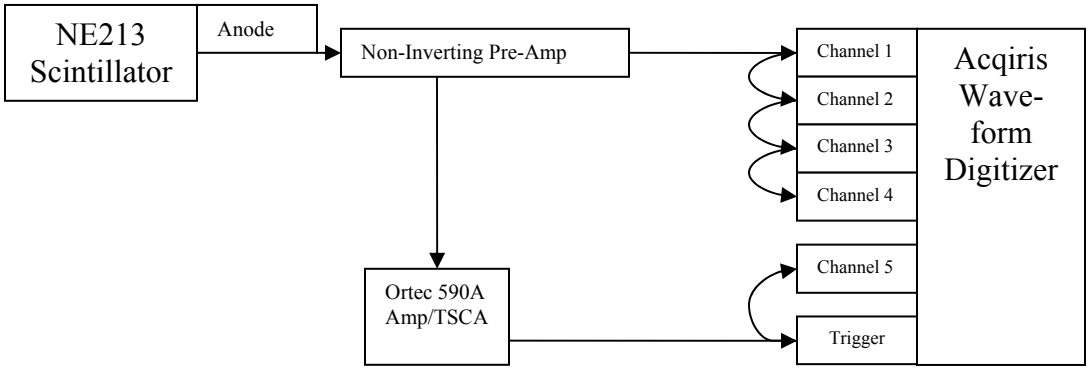

Figure 3-1-Laboratory experimental set-up used for Cf252 spectrum measurements in spring 2007.

Neutron pulse height spectra of Cf252 and gamma spectra of Na-22 were taken with the above system. Furthermore, the fall time PSD technique with amoeba fitting routine was tested and used with the above set-up; different termination resistors were also used in the non-inverting pre-amplifier to investigate their effects on the PSD capability of the system. The best terminator's result would then be used to perform FERD unfolding to verify the validity of Scinful response functions.

A 50 ohm, 500 ohm and a 1000 ohm resistor were tested. The termination resistance creates a high pass filter when combined with the capacitance from the PMT base, which

alters the attenuation of the signal. An important note is that the attenuation change is different depending on the frequency of the signal itself. A high pass filter has less attenuation on the high frequency signals and more attenuation on the low frequency signals. A larger termination resistance translates to a lower cut-off frequency according to $f = \frac{1}{2\pi RC}$, with termination resistance R and device capitance C. In addition, the pre-amplifier's time constant, given by RC, also affects the pulse shape.

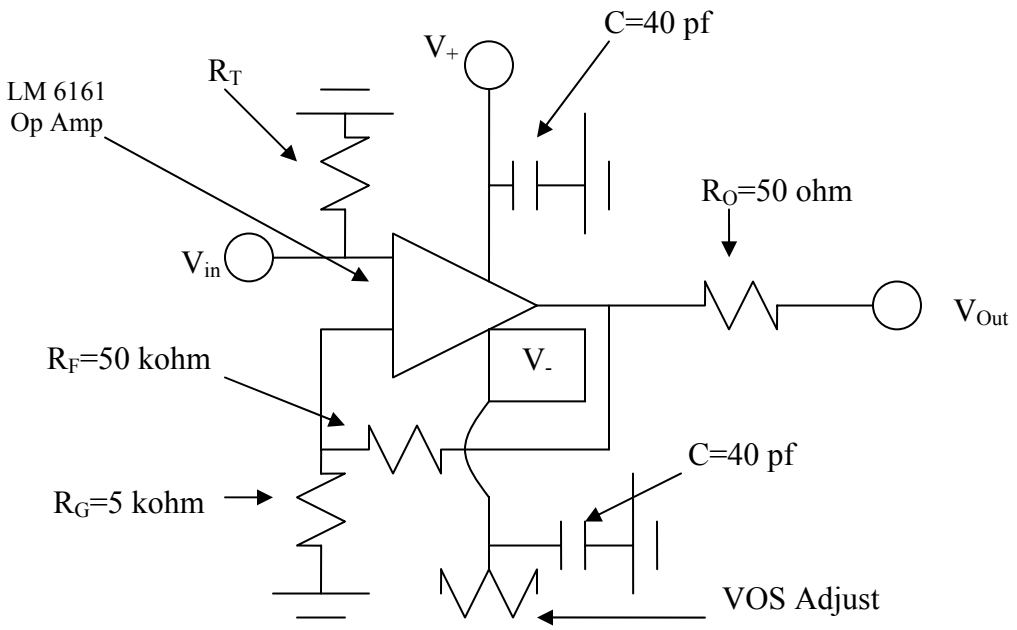

Figure 3-2-Non-inverting pre-amp used with Spring 2007 set-up, where R_T is the termination resistor.

3.1.2 Data Operation

After the collection of data, data analyses were performed. The data was collected in binary file, each pulse was recorded in bits format. In this initial run, data were collected in batches called acquisition, and each acquisition file contains the 4 channels along with trigger with each containing a number of detector pulses. Data was then operated with Matlab in the following fashion:

1. An acquisition file was chosen, the binary data were converted to readable, ASCII data.
2. The data heading information were collected for each channel, and the corresponding trigger channel. The data headings were only recorded once per acquisition file.
3. A single pulse was then read in bits (magnitude ranging from -128 to 127), along with the time stamp of the pulse.
4. Each channel was examined and the lowest, non-saturated channel was chosen to be operated upon for the reminder of the operation (Figure 3-3 and Figure 3-4). The other channels and their corresponding parameters were not considered.

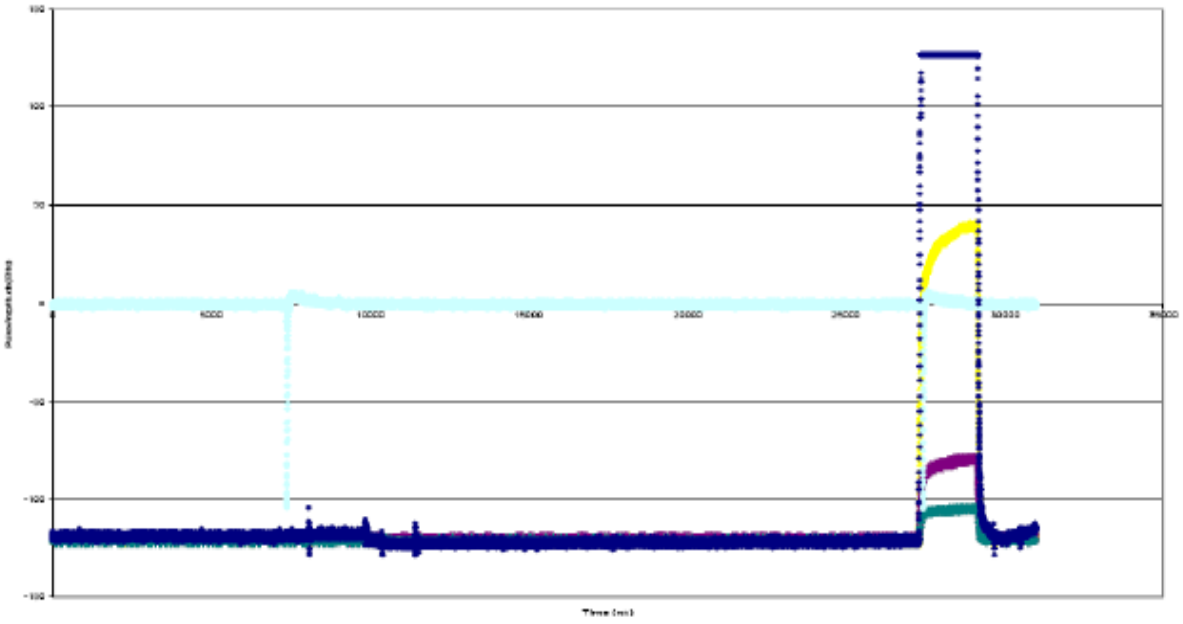

Figure 3-3-Sample pulse recorded by the Acqiris system. The blue pulse (Ch1) is saturated.

5. The baseline of the pulse was then determined. The baseline is the average of the first 50 (arbitrarily chosen) points of the pulse.

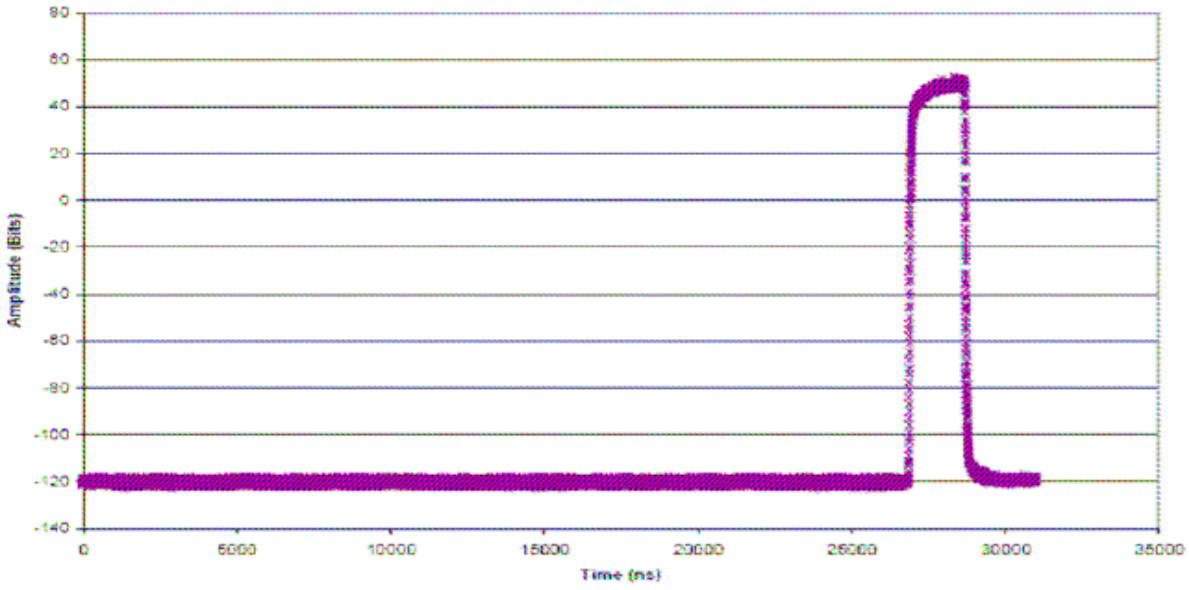

Figure 3-4-Sample unsaturated processed Acqiris pulse.

6. The beginning and the end of the pulse were then found using the median filter technique. The median filter checked for the fluctuation of the median of an arbitrary sub-collection of the data (5 data points). In some cases, the pulse failed to terminate to baseline and a gradual decrease was observed instead. The special cases were also checked for with a simple subtraction scheme and were compared with the median filter result.
7. The waveform in bits is transformed into voltage.
8. A height length and a fall time were specified. The height length dictates the length of time the actual pulse is summed to obtain the height number, with 1500 ns chosen for this operation. The fall time is the length of time the pulse falls, a specified period of 90% of the maximum to 10% of maximum was chosen.
9. The pulse was then checked against the height length to ensure the pulse lasted sufficiently long. If the pulse satisfied the length criteria, the height number and the

fall time as defined above were found. If the pulse failed to satisfy the length criteria, the height number and the fall time were set to an arbitrary number (-100) to signify the failure.

10. With the fall time and height numbers obtained, a PSD spectrum was constructed. From the PSD spectrum, fits were fitted to separate the gamma and the neutron signals via amoeba. The PSD spectrum is generated by plotting the fall time and height number. Gamma signals, with their faster rise time, correspond to the upper half of the PSD spectrum.
11. The same process was used for the Cf252 spectra for all three of the termination resistor settings (50 ohm, 500 ohm, 1000 ohm).
12. The Na-22 spectra were constructed from the height number alone and no PSD were performed on those spectra.

3.1.3 System Calibration and Light Unit Conversion

In the below figures (Figure 3-5 to Figure 3-7), the PSD parameter, fall time, is plotted against a height number. In this case, the height number is defined to be the summed magnitude of the pulse. Since the height number is unique to each detector depending on the gain, a corresponding Na22 spectrum (Figure 3-8 to Figure 3-10) was taken to calibrate the height number to light unit. One light unit conversion is defined to be 1.13 times the half height location of the 1275 keV Na-22 peak.

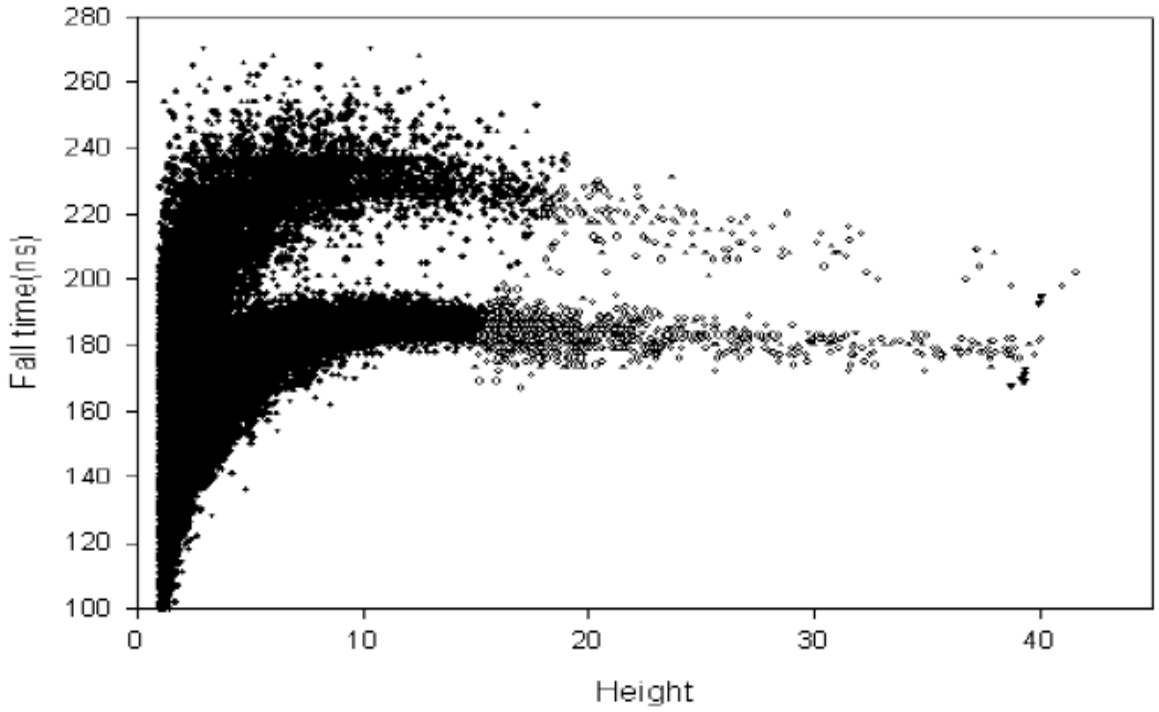

Figure 3-5-50 ohm termination fall time PSD plot.

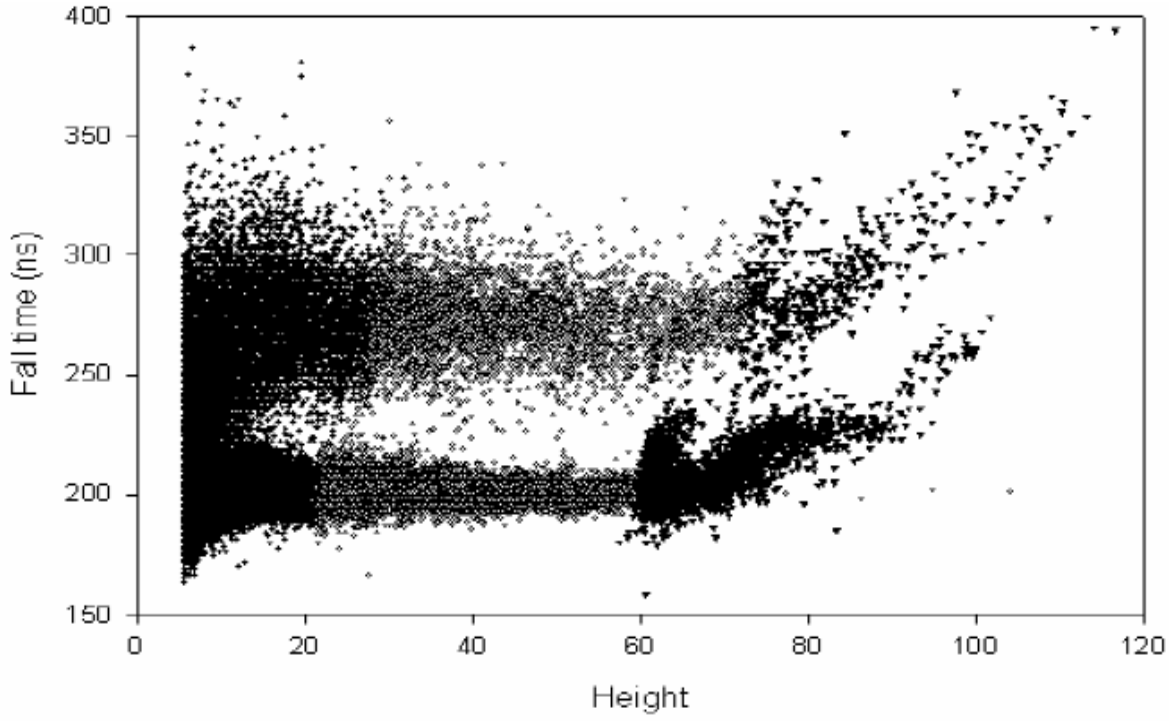

Figure 3-6-500 ohm termination fall time PSD plot.

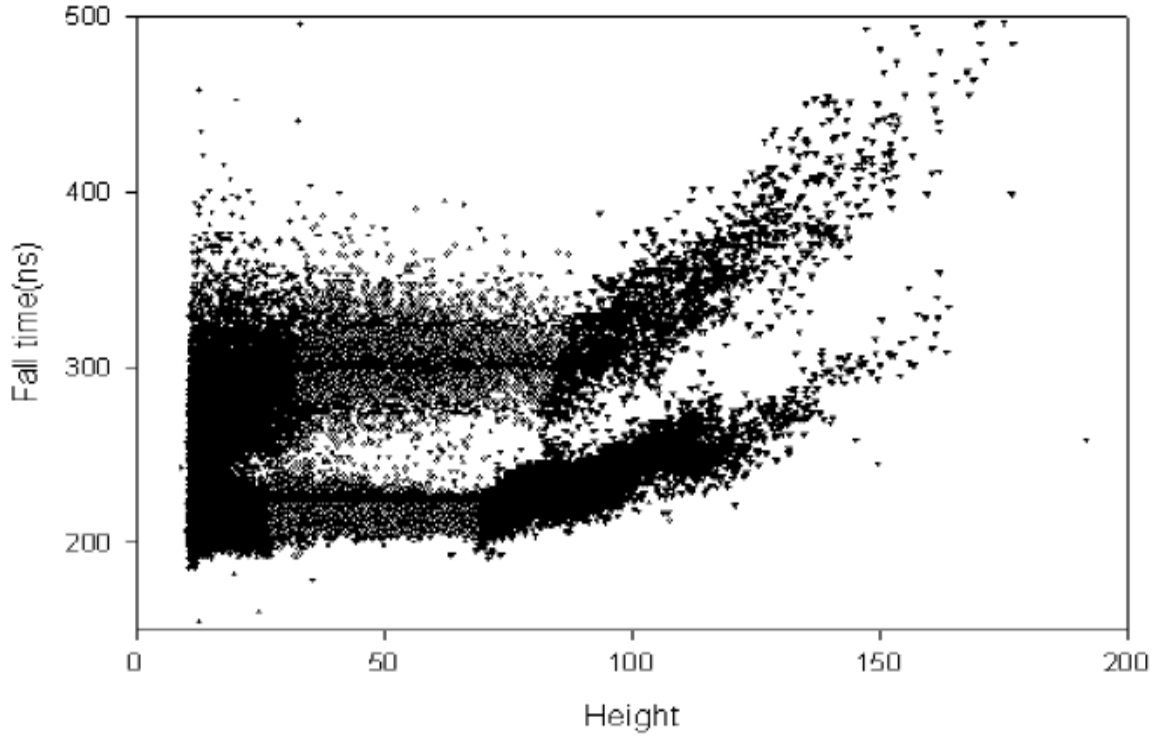

Figure 3-7-1000 ohm termination fall time PSD plot.

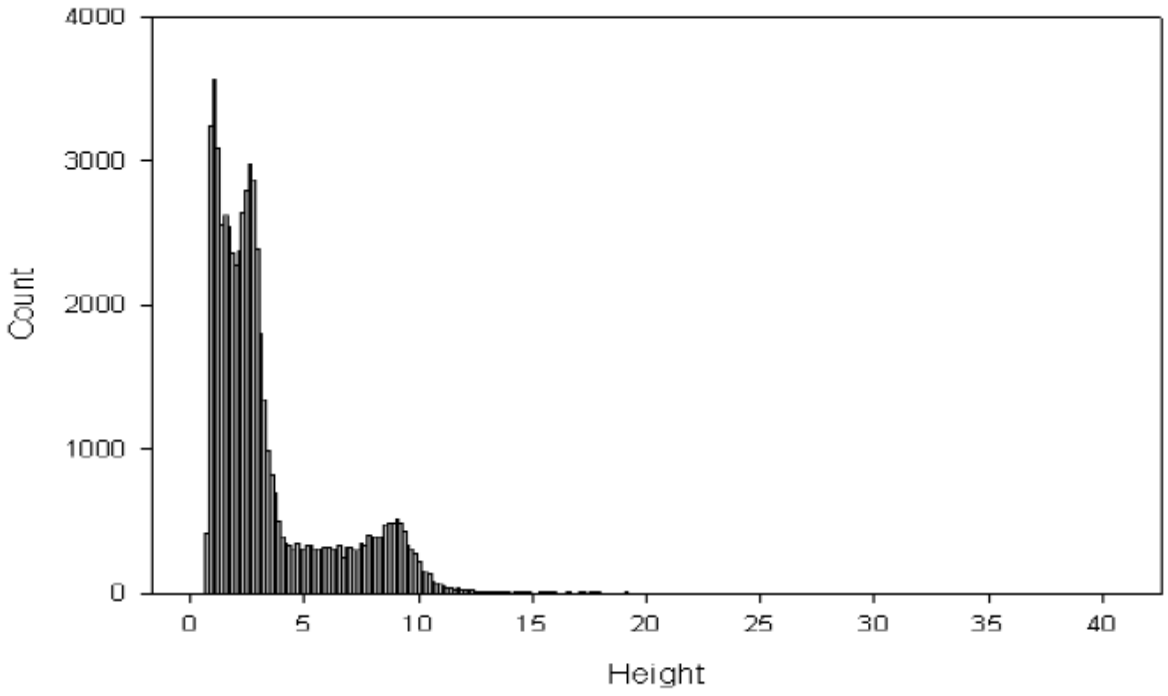

Figure 3-8-Na22 spectrum taken with 50 ohm termination.

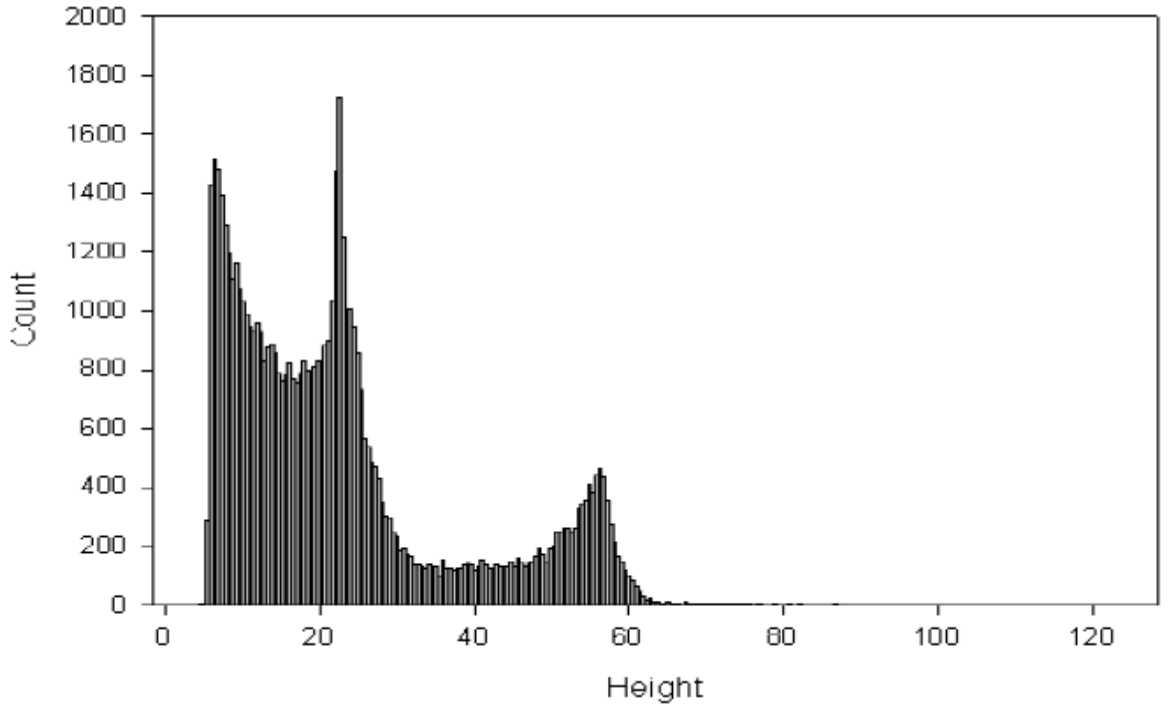

Figure 3-9-Na22 spectrum taken with 500 ohm termination.

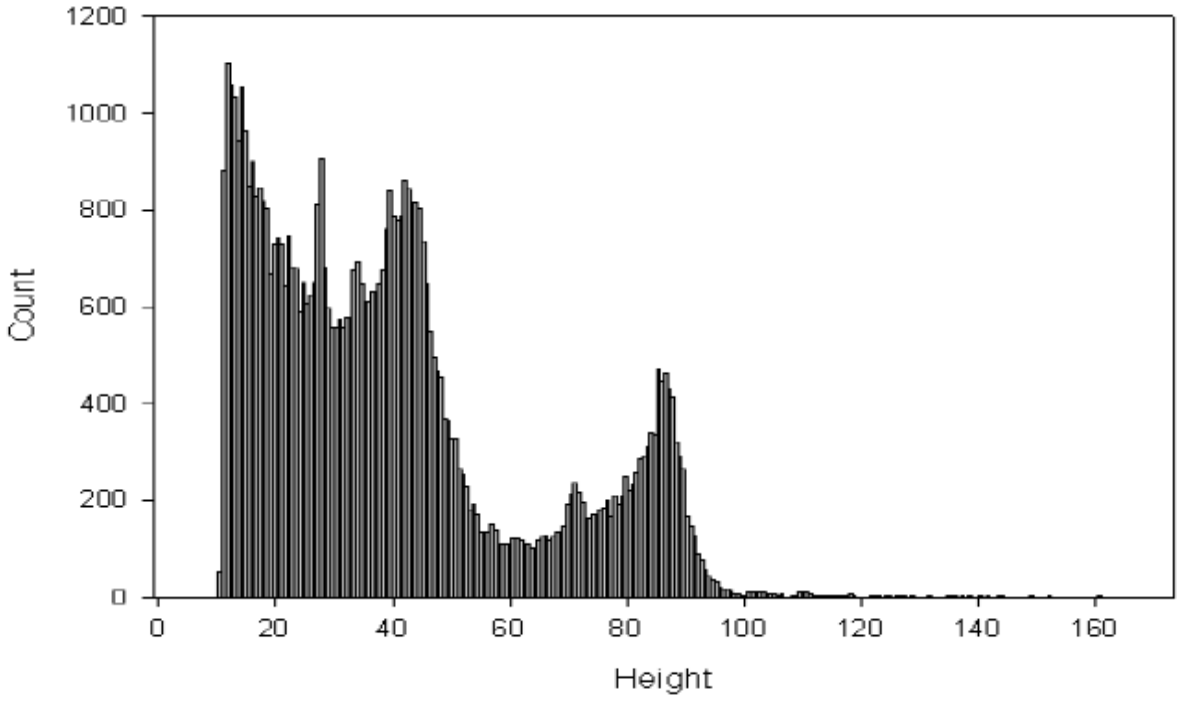

Figure 3-10-Na22 spectrum taken with 1000 ohm termination.

With the Na22 spectra, the calibration conversion may be easily found visually. The results are as follow in Table 3-1:

Table 3-1-Na22 light unit calibration results.

	50 ohm	500 ohm	1000 ohm
Height Number per Light Unit	10.42	65.54	101.70

With the light unit calibration, Figure 3-5-Figure 3-7 may be transformed to standard light unit PSD plots. With light units obtained, a lower physical limit may be imposed on the PSD through a light-energy conversion using Verbinski's results (Figure 2-3). The conversion and the lower limits areshown in Figure 3-11-Figure 3-13.

Table 3-2-Lower PSD limit.

	Approximate Observed Light Unit Limit	Converted Energy Limit (MeV)
50 ohm	0.47	2
500 ohm	0.24	1.3
1000 ohm	0.24	1.3

Table 3-2 shows the limit imposed by PSD caused by indistinguishable gamma/neutron region. The accuracy of PSD results below the limit is questionable. Furthermore, the non-linearity of the PSD results are evident from Figure 3-11 to Figure 3-13. Thus a traditional figure of merit (Discussed in Figure of Merit Section) can not be readily implemented for these cases; a modified figure of merit is used instead (Discussed in Modified Figure of Merit Section). However, since both FOMs are description of the overall PSD capability of the system, all of the common data points (above a common threshold: typically defined by the lowest commonly available point) should be taken into account in

their calculation. The lower limits quoted above serve only as the limit of the PSD accuracy and not as a starting point for the FOM calculation. Amoeba fitting routine is used to calculate the best fits for the calculation of FOM*.

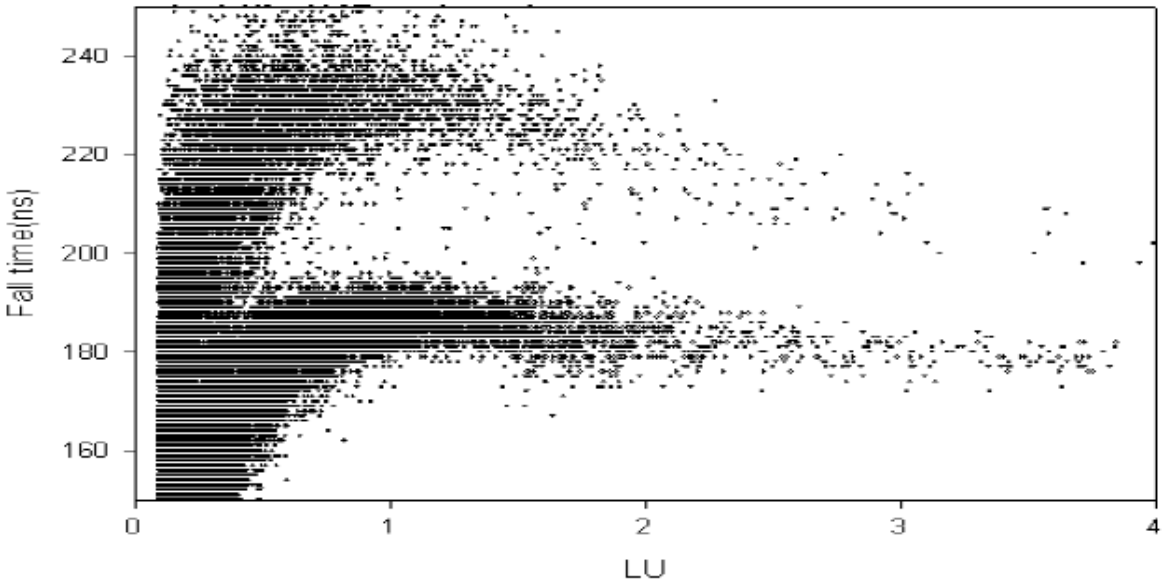

Figure 3-11-50 ohm light unit PSD plot.

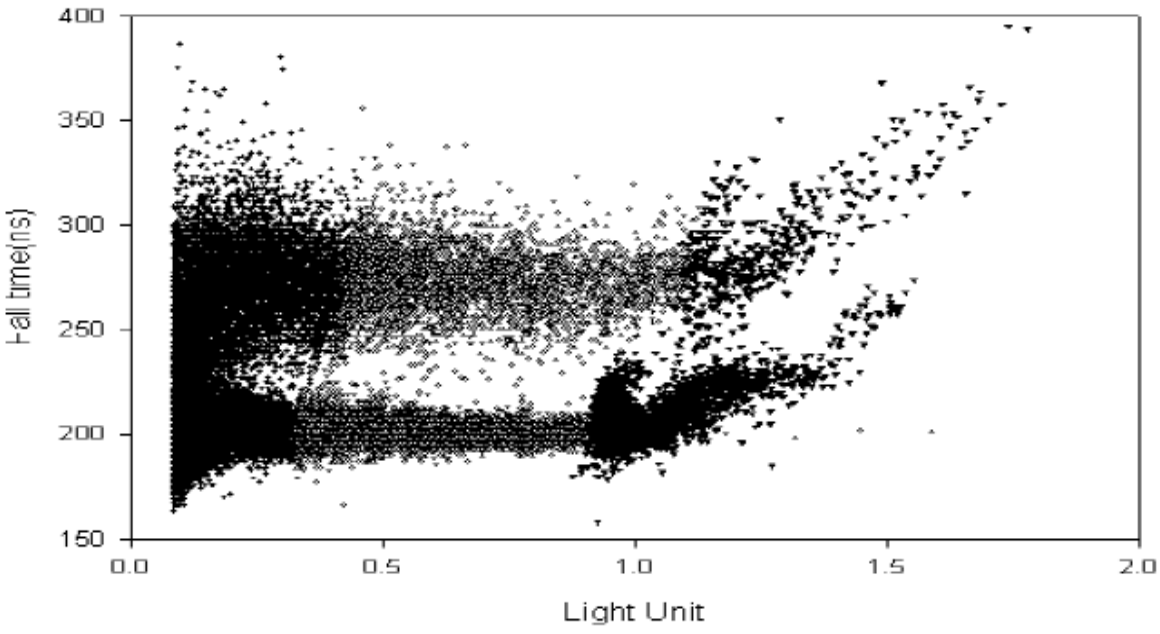

Figure 3-12-500 ohm light unit PSD plot.

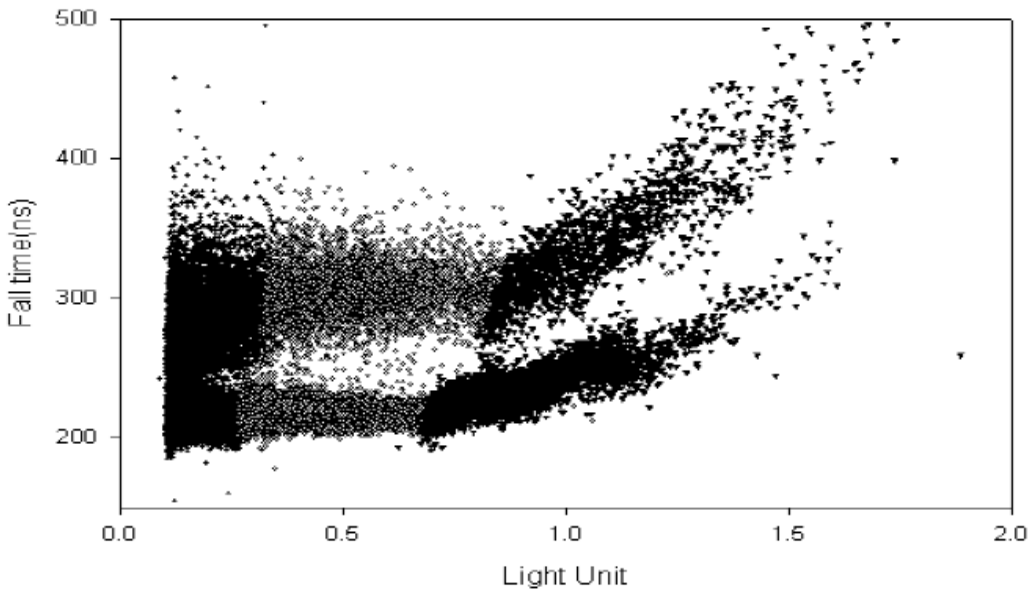

Figure 3-13-1000 ohm light unit PSD plot.

3.1.4 Amoeba Results-500 ohm and 1000 ohm Case

The 500 ohm and the 1000 ohm cases were fitted with Amoeba and the results are shown in Table 3-3, Figure 3-14 and Figure 3-15. The function that simplex minimizes in this case is the simple regression:

$$f = \sum (X_i - X(h))^2 \qquad 3.1$$

Where X_i is the individual date point and $X(h)$ is the fitted function of height (h).

As evident from Figure 3-11-Figure 3-13, there are three distinct regions in the PSD plots: the upper neutron, lower gamma and the middle separation regions. As such, three cubic equations are used and referenced in the amoeba routine, and they are as follows:

$$\gamma(h) = a_\gamma + bh + ch^2 + dh^3 \qquad 3.2$$

$$S(h) = a_\gamma + a_S + bh + ch^2 + dh^3 \qquad 3.3$$

$$N(h) = a_\gamma + a_N + bh + ch^2 + dh^3 \qquad 3.4$$

In the equations above, $a_\gamma, a_S, a_N, b, c, d$ are free parameters and amoeba is free to adjust them. A note of interest is that the three regions are assumed to be the same shape, thus the only difference between the equations are the intercept terms a_s, a_γ and a_N.

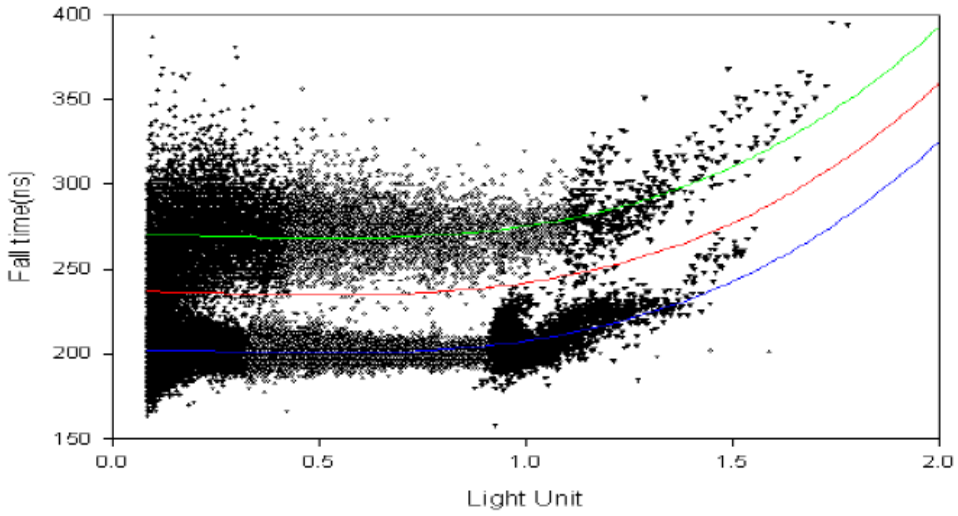

Figure 3-14-Amoeba solution to the 500 ohm PSD. Green line is the neutron mid-line function, red the separation function and blue the gamma mid-line function.

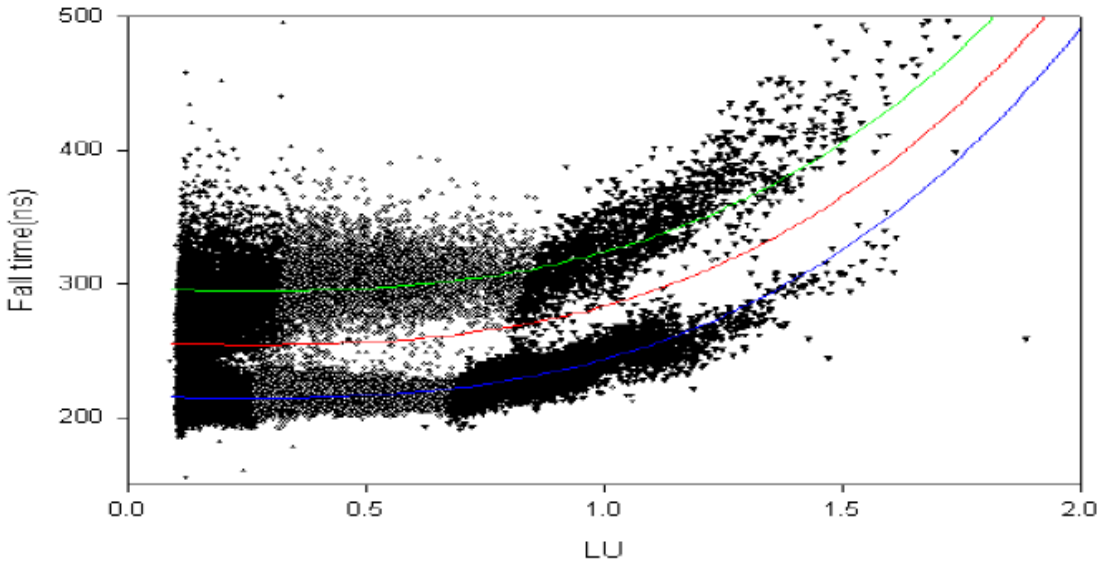

Figure 3-15-Amoeba solution to the 1000 ohm PSD. Green line is the neutron mid-line function, red the separation function and blue the gamma mid-line function.

Table 3-3-Numerical Amoeba results for 500 and 1000 ohm case.

	a_γ	a_N	a_S	b	c	d
500 ohm	202.5	67.55	34.36	0.1347	-20.51	25.56
1000 ohm	215.6	80.30	39.99	-5.607	-4.402	38.04

3.1.5 Amoeba Results-50 ohm Case

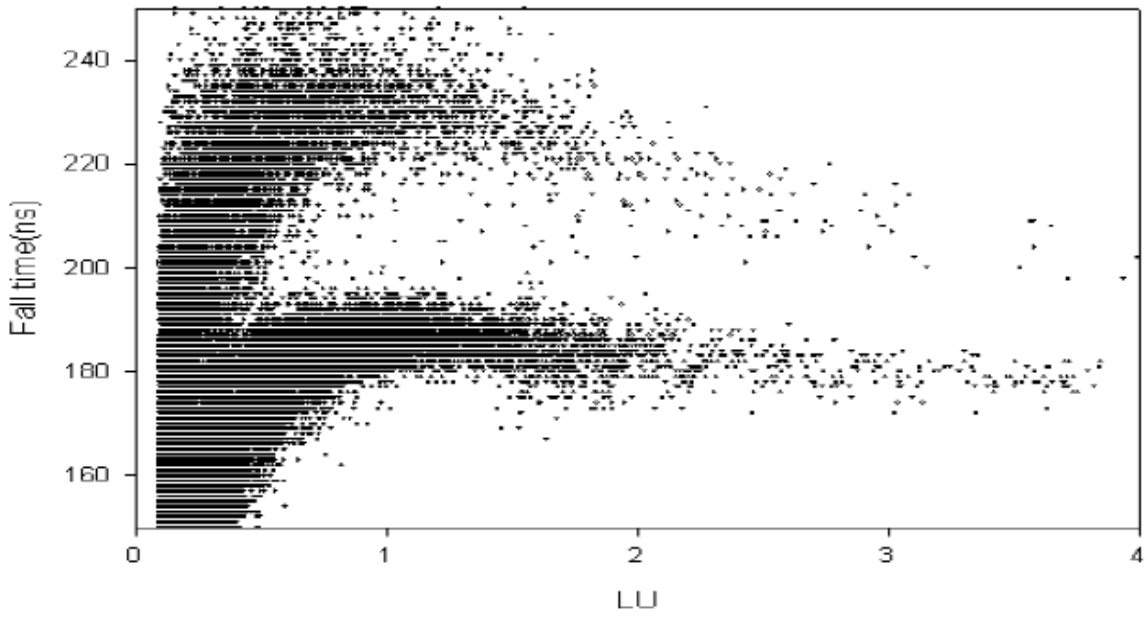

Figure 3-16-50 ohm PSD plot.

Although the amoeba method works well for the 500 and 1000 ohm cases presented above, it does not work well for the 50 ohm PSD plot as shown in Figure 3-16. Part of the reason is that the rise in Figure 3-16 resembles a square wave, thus either an infinite degree polynomial or an infinite series would have to be used to properly model the plot. A solution to properly model the 50 ohm PSD plot is to use a modified spline function.

In this case, the spline function consists of a cubic function and a linear function as follows:

$$X(h) = a_x + b(h - h_0) + c(h - h_0)^2 + d(h - h_0)^3, h < L \quad 3.5$$

$$X(h) = mh + k_x, h \geq L \quad 3.6$$

Equation (3.5) and (3.6) above exist for the neutron region, the gamma region and the separation region, and they differ by the constants a_N and a_S as in the 500 and 1000 ohm case. The added complication is that Equation (3.5) should be used if h is less than L and Equation (3.6) if h is greater than L. Of note from the above equations is that only h_0, L and m are additional parameters, k is predetermined by the condition that $X(h)$ is continuous everywhere in its domain. Thus k is obtained by setting Equation (3.5) and Equation (3.6) equal at L. Furthermore, h_0 is not necessary, but it allows for better initial value estimates with its inclusion. As m is a free parameter determined by amoeba, the derivatives of Equation (3.5) and (3.6) at the interface L are not fixed. To ensure a smooth function, however, a condition should be put into amoeba to penalize an unequal derivation at the interface L. With the added parameters and conditions, the same procedure as that of the 500 and 1000 ohm case is actually used, and the following table and figure show the result for the 50 ohm case (Table 3-4 and Figure 3-17).

Table 3-4-Numerical Amoeba results for 50 ohm case.

	a_γ	a_N	a_S	b	c	d
50 ohm	187.24	36.46	18.41	-6.850	-21.95	77.92
	h_0	L	m	k_γ	k_N	k_S
50 ohm	0.9616	0.9040	-3.939	181.3	223.8	205.7

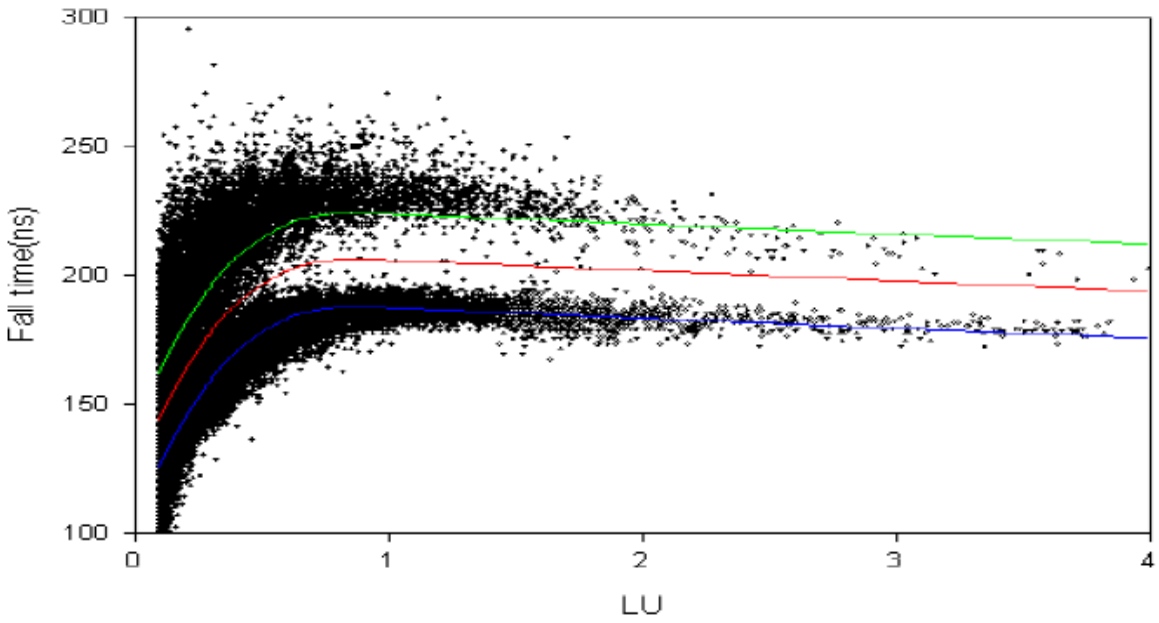

Figure 3-17-Amoeba results for 50 ohm PSD.

3.1.6 FOM* Results

The FOM* derived in the Modified Figure of Merit section is

$$\text{FOM*} = \frac{\int n(h) - \gamma(h)dh}{\int dh} \Big/ (\sigma(\gamma) + \sigma(n)) \qquad 3.7$$

The numerator is the separation distance between the neutron and the gamma best fit and the denominator is the combined spread of the neutron and the gamma data points in respect to their best fit function.

With the amoeba results, the FOM* may then be calculated using Equation (3.7). The results below (Table 3-5) present the numerator and the two terms of the denominator explicitly along with the calculated FOM* to demonstrate the physical significance of the terms when compared with the amoeba result figures shown in the previous sections.

Table 3-5-50, 500 and 1000 ohm terminator FOM* results.

Terms	Physical Meaning	50 ohm	500 ohm	1000 ohm
$\frac{\int n(h)-\gamma(h)dh}{\int dh}$	Normalized Separation	142.344	129.640	161.911
$\sigma(n)$	Neutron Standard Deviation	71.500	69.919	109.301
$\sigma(\gamma)$	Gamma Standard Deviation	56.485	49.711	67.445
FOM*	Figure of Merit	1.112	1.083	0.916

As shown in Table 3-5 above, the 50 ohm and the 500 ohm cases have sufficiently close FOM* value and are the best terminator settings for PSD with the current set-up using the fall time PSD method. However, with cable reflections and device impedances taken into account in more elaborate experiments, the 50 ohm resistor will perform better than the 500 ohm resistor (Common cables and devices are of 50 ohm impedence). As such, the 50 ohm termination resistor is used to unfold a Cf252 spectrum to verify Scinful's response functions' validity. Also of interest are the lower PSD limits listed in Table 3-2, even though the 50 ohm termination resistor has the highest FOM*, which symbolizes the best PSD capability, its PSD limit is actually the highest. Thus, on average, the 50 ohm termination resistor performs better than the other resistors, at energy between 1.3 MeV to 2 MeV, the other resistors should perform better since the 50 ohm resistor's PSD accuracy at that energy range is questionable.

3.1.7 Scinful Response Function

To properly unfold a neutron spectrum using FERD, the user must supply the response function of the detector and the raw neutron spectrum from the source. To generate the response functions, mono-energetic responses from Scinful were used. Specifically, mono-energetic simulations were ran with the following energies (in MeV):

2.347E+01, 2.256E+01, 2.157E+01, 2.055E+01, 1.949E+01, 1.852E+01, 1.753E+01, 1.653E+01, 1.562E+01, 1.479E+01, 1.402E+01, 1.320E+01, 1.239E+01, 1.175E+01, 1.124E+01, 1.077E+01, 1.025E+01, 9.741E+00, 9.261E+00, 8.757E+00, 8.236E+00, 7.736E+00, 7.235E+00, 6.839E+00, 6.555E+00, 6.254E+00, 5.938E+00, 5.645E+00, 5.345E+00, 5.042E+00, 4.752E+00, 4.453E+00, 4.152E+00, 3.906E+00, 3.707E+00, 3.500E+00, 3.296E+00, 3.097E+00, 2.898E+00, 2.702E+00, 2.498E+00, 2.296E+00, 2.099E+00, 1.932E+00, 1.812E+00, 1.709E+00, 1.609E+00, 1.510E+00, 1.412E+00, 1.309E+00, 1.204E+00, 1.106E+00, 1.006E+00, 9.069E-01, 8.113E-01.

The response functions were generated and converted to the FERD specified format for input. Two of the response functions are plotted below (Figure 3-18 and Figure 3-19):

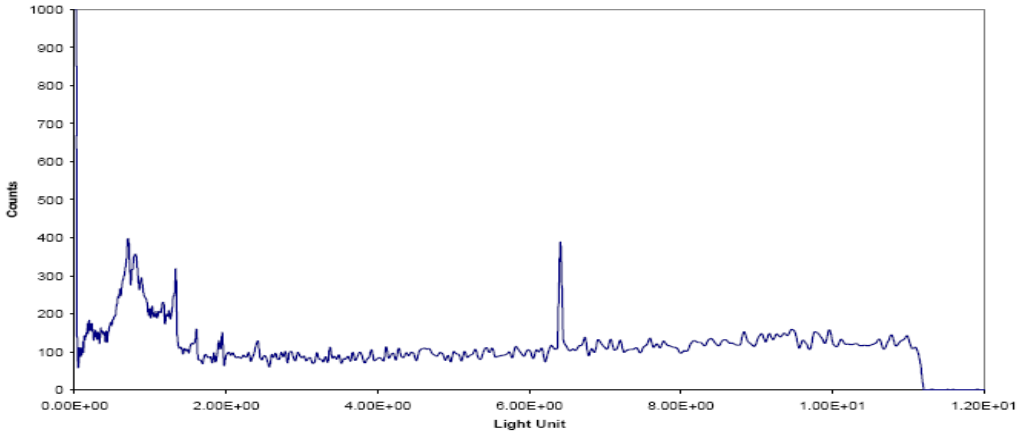

Figure 3-18-Sample Scinful response function for 20.55 MeV mono-energetic neutron source with 3x3 NE213 detector.

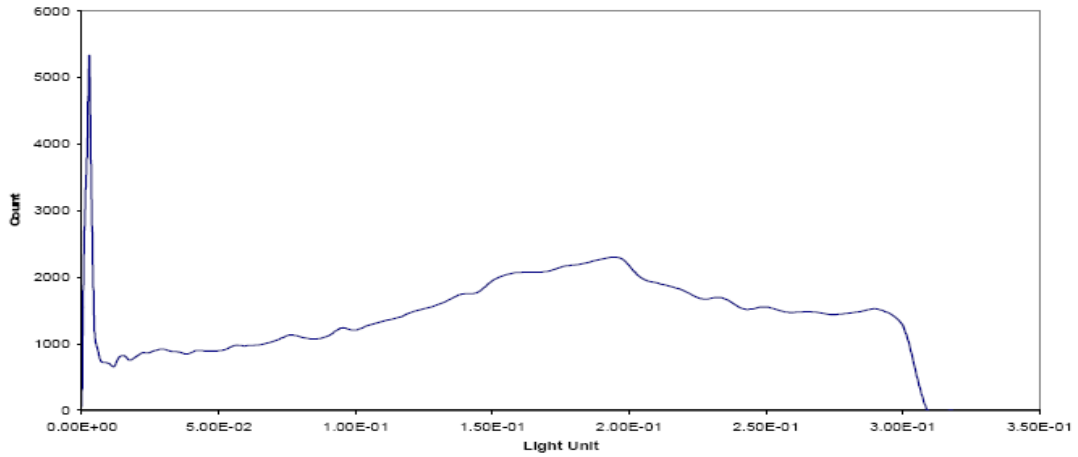

Figure 3-19-Sample Scinful response function for 1.51 MeV mono-energetic neutron source with 3x3 NE213 detector.

3.1.8 FERD Unfolding

With Amoeba performing PSD, neutron spectra may be extracted from a Cf252 spectrum. Specifically, for a 50 ohm termination resistor, neutron data are data points which fall above Equation (3.5) and (3.6) (Values listed in Table 3-4). The neutron spectrum (Figure 3-20) may then be generated by binning the light unit of each neutron point into a histogram (Figure 3-21).

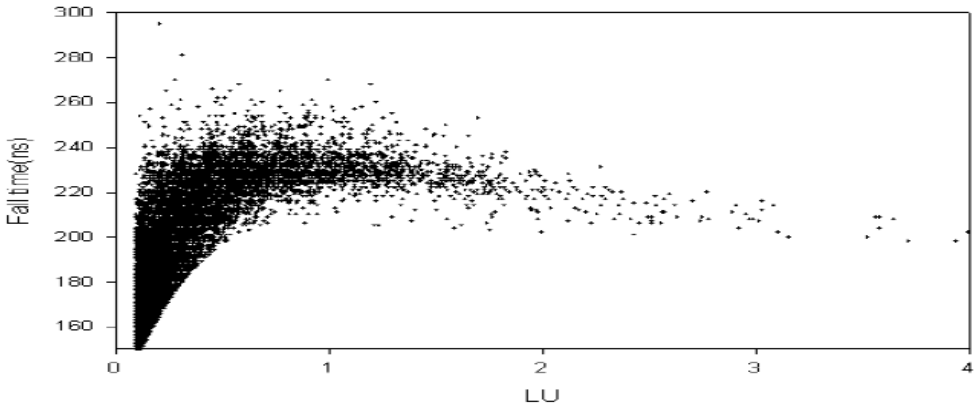

Figure 3-20-PSD Plot of 50 ohm termination neutron data.

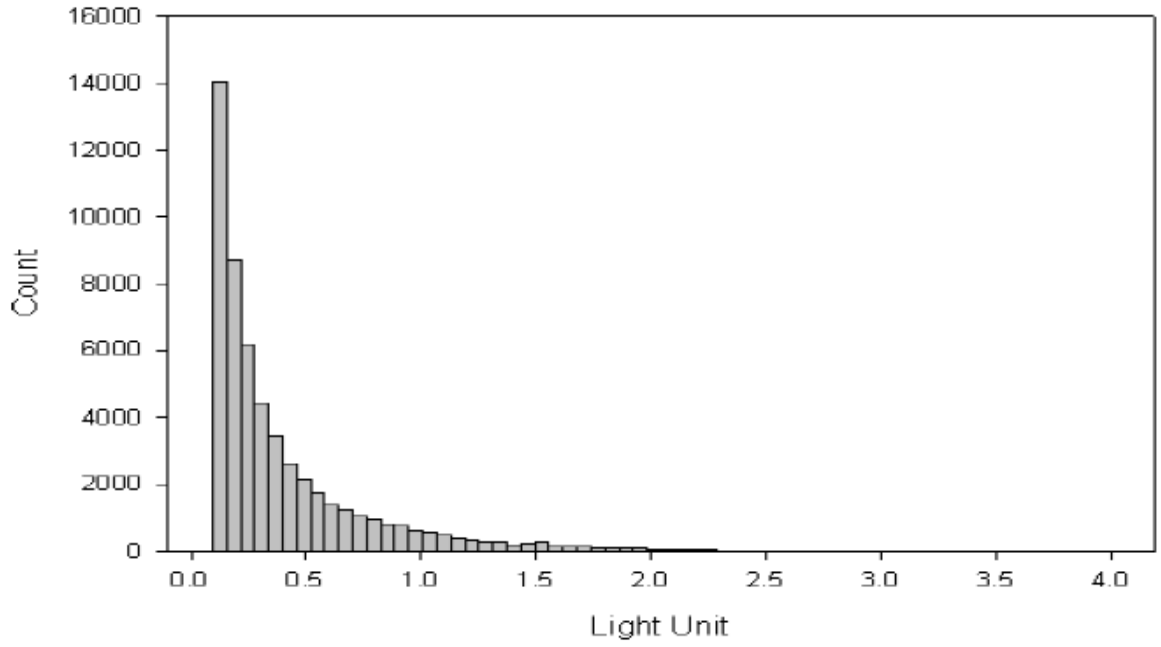

Figure 3-21-Cf252 neutron Spectrum for 50 ohm termination.

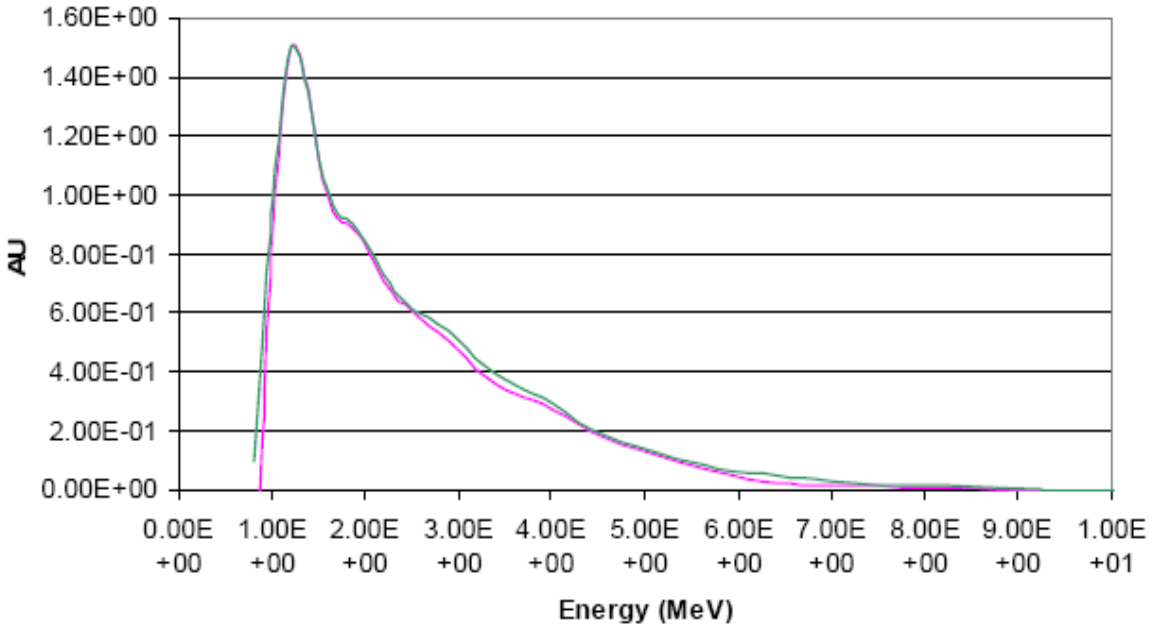

Figure 3-22-Ferd unfolded Cf252 spectrum for 50 ohm termination. The red curve and the green curve corresponds to upper and lower flux, respectively.

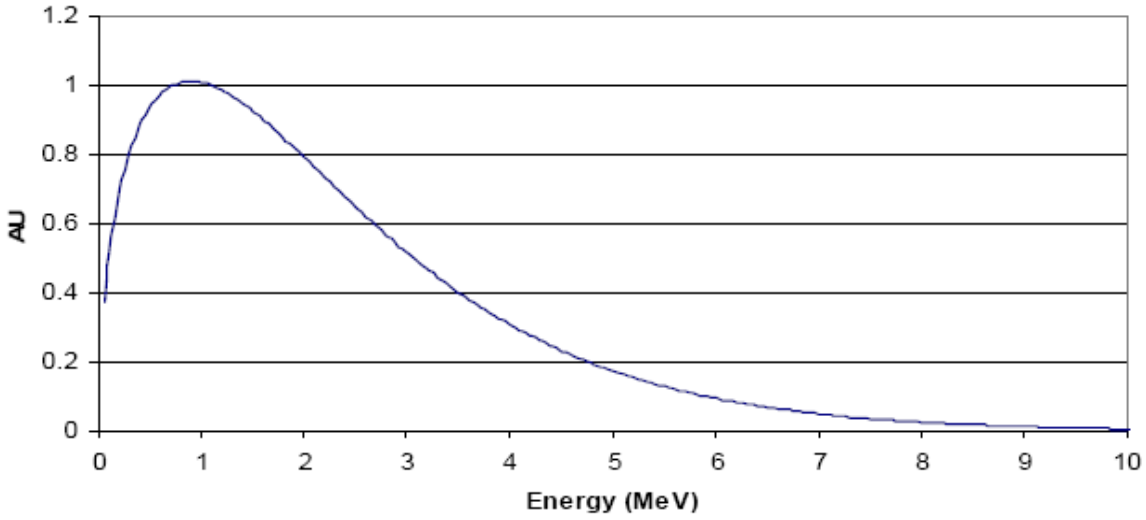

Figure 3-23-Calculated Cf252 spectrum.

Figure 3-22 shown shows the unfolded Cf252 spectrum taken with a 50 ohm termination resistor. The unit of the Y-axis is in arbitrary unit, since for the current comparison only the contour of the plots is compared. An actual Cf252 spectrum (Figure 3-23) may be generated using a Watts spectrum with the constant a=1.025 and b=2.926 with the following equation ([24]):

$$f(E) = C * \exp(-\frac{E}{a})\sinh(bE)^{\frac{1}{2}} \qquad 3.8$$

The constant C is a proportionality constant and E is the energy.

Figure 3-23 shows the calculated spectrum calculated with Equation (3.8). Figure 3-24 is the combined spectrum of Figure 3-22 and Figure 3-23. As evident in Figure 3-24, the calculated Cf252 spectrum and the unfolded spectrum agrees very well above 2 MeV. The unfolded spectrum drops off around 1.1 MeV due to the lower LLD setting. Furthermore, between the 1.1 MeV and 2 MeV range, the unfolded spectrum contains a peak not evident from the calculated spectrum. The peak originates from excess gamma signal in

the neutron spectrum. As shown in Table 3-2, the lower limit of the 50 ohm termination is around 2 MeV. Below 2 MeV, the gamma and the neutron signals are indistinguishable. Thus, it is highly probable that the peak from 1.1 to 2 MeV originated from the physical PSD limit of the 50 ohm termination scheme. However, with the agreement between the unfolded and the calculated spectra ranging from 2 to 8 MeV, the Scinful's response function's accuracy in that range is established with this method.

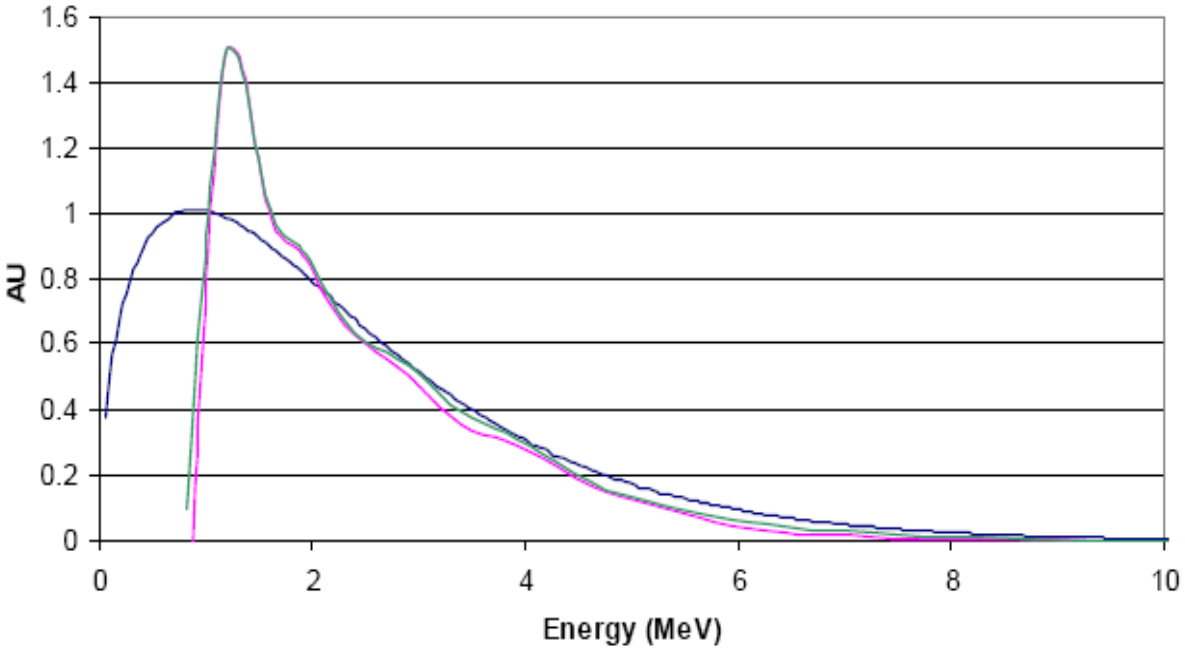

Figure 3-24-Comparison of calculated Cf252 spectrum with the FERD unfolded spectrum. The blue curve is calculated and the green and red curves are the unfolded fluxes.

Since the 50 ohm unfolded spectrum does not match the accepted Cf252 spectrum, the 500 ohm termination case is also tested. The 500 ohm neutron spectrum (Figure 3-25 and Figure 3-26) is extracted with Amoeba with the values listed in

Table 3-3. The extracted spectra are as follow:

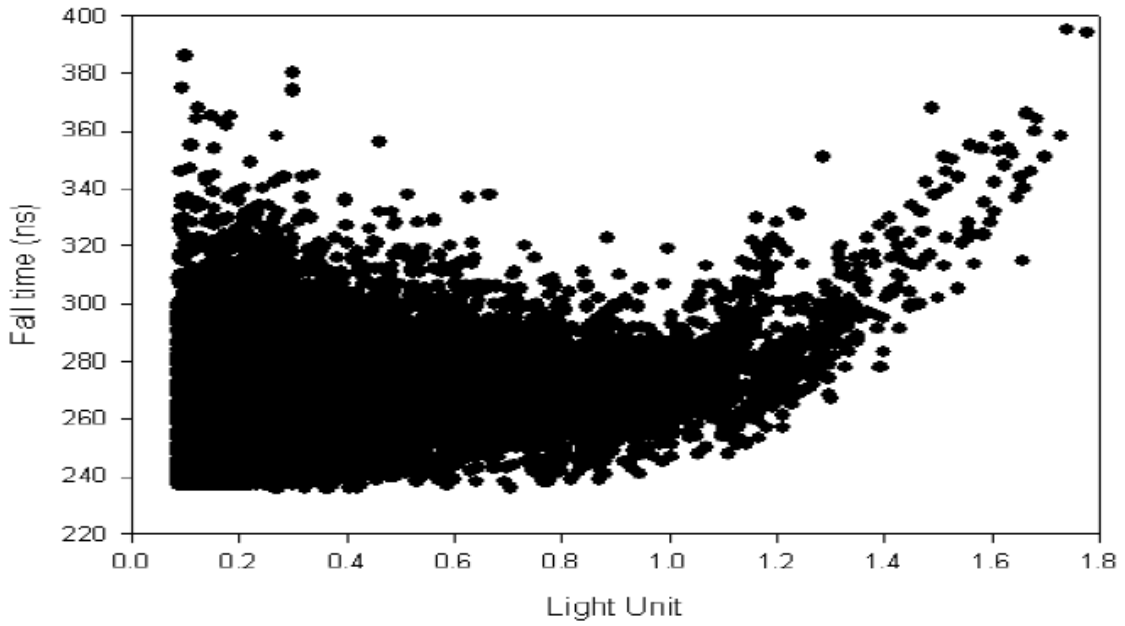

Figure 3-25-Cf252 500 ohm PSD neutron spectrum.

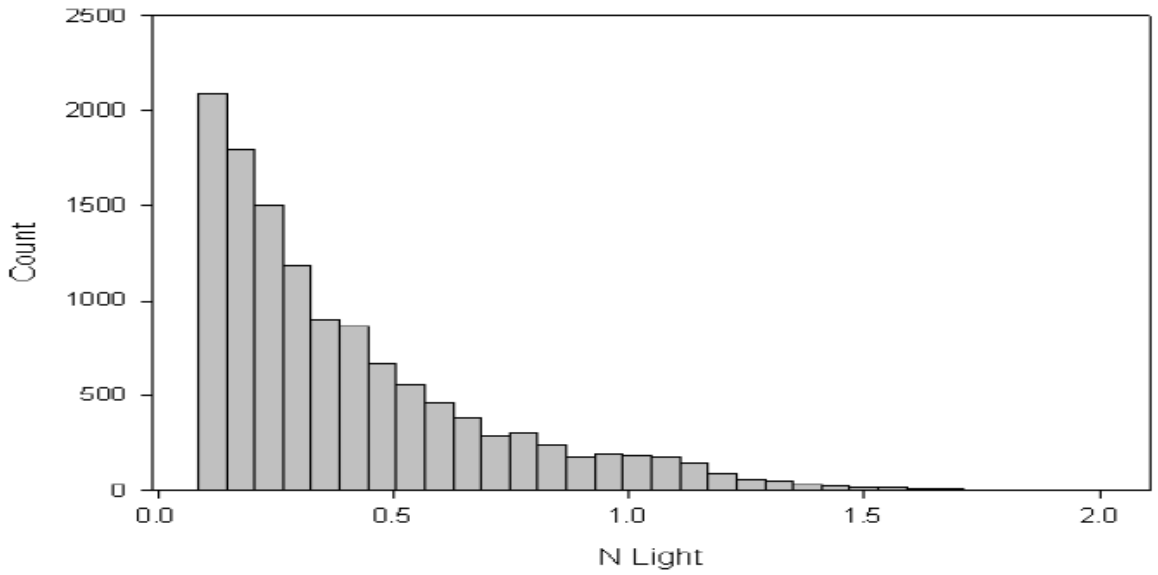

Figure 3-26-Cf252 500 ohm termination neutron spectrum.

With Figure 3-25 and Figure 3-26, the Cf252 spectrum is unfolded with FERD using the same response function used for the 50 ohm unfolding.

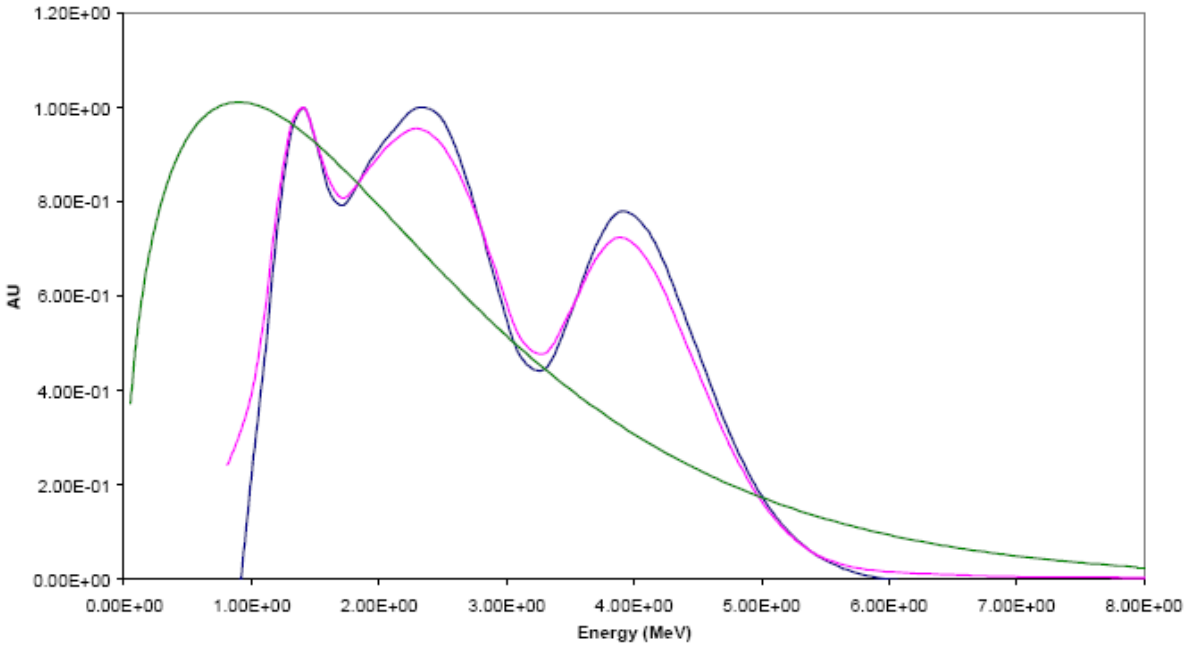

Figure 3-27-500 ohm termination Cf252 neutron unfolded compared with calculated spectrum.

Figure 3-27 shows the unfolded 500 ohm Cf252 neutron spectrum in comparison with the calculated spectrum using Equation (3.8). As can be seen, the agreement between the unfolded and the calculated spectrum is loose. The general trend seems to agree, but fluctuations can be observed from the unfolded spectrum. The fluctuations are likely caused by the low number of data points available for unfolding at higher energies. Furthermore, the same drop off at 1 MeV may be observed as that of the 50 ohm case due to the same LLD setting. The extra peak at 2 MeV is also not observed in the 500 ohm case, which may be contributed to the higher PSD limit for this case (Table 3-2). Since the 500 ohm and the 1000 ohm cases have similar PSD characteristics (See Table 3-2 and Table 3-5), one would expect similarities between their unfolded spectra if the above claims are correct. The extracted neutron spectra are shown in Figure 3-28 and Figure 3-29, and the result of the comparison is shown in Figure 3-30.

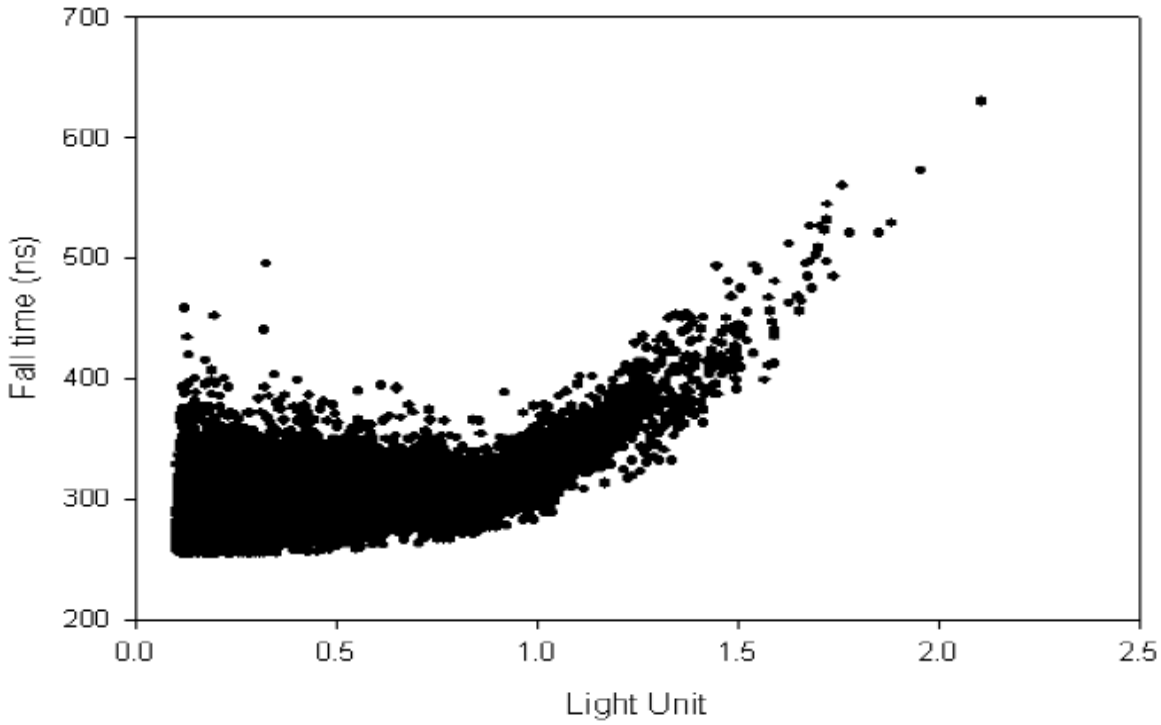

Figure 3-28-Cf252 1000 ohm PSD neutron spectrum.

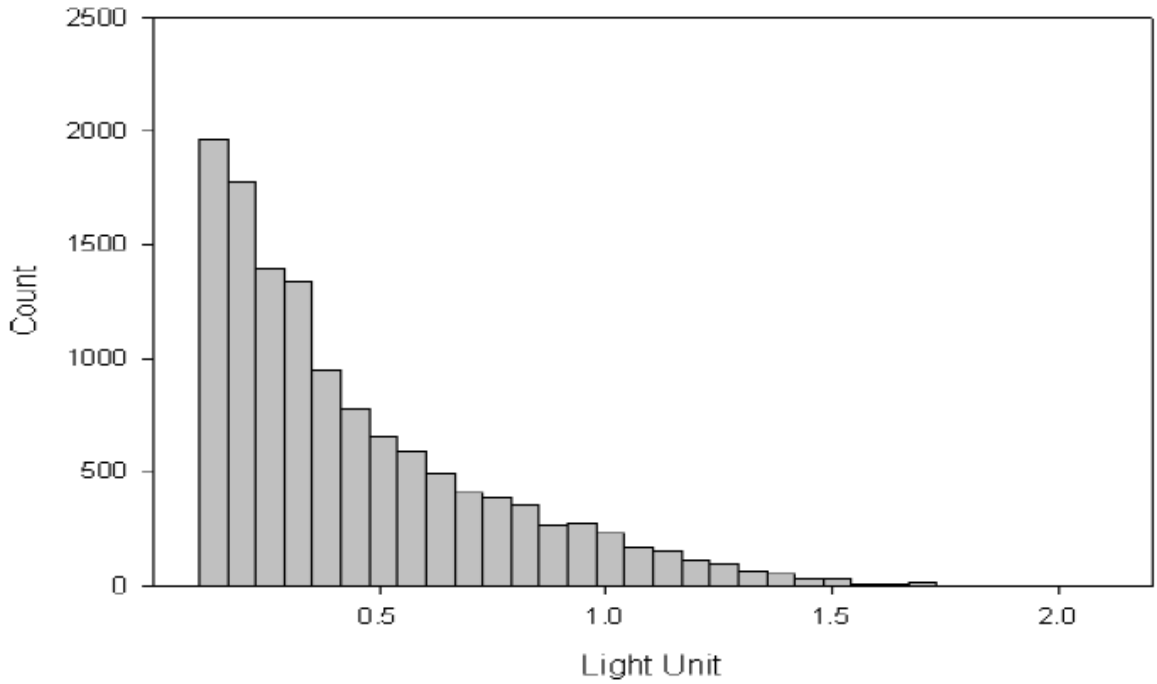

Figure 3-29-Cf252 1000 ohm termination neutron spectrum.

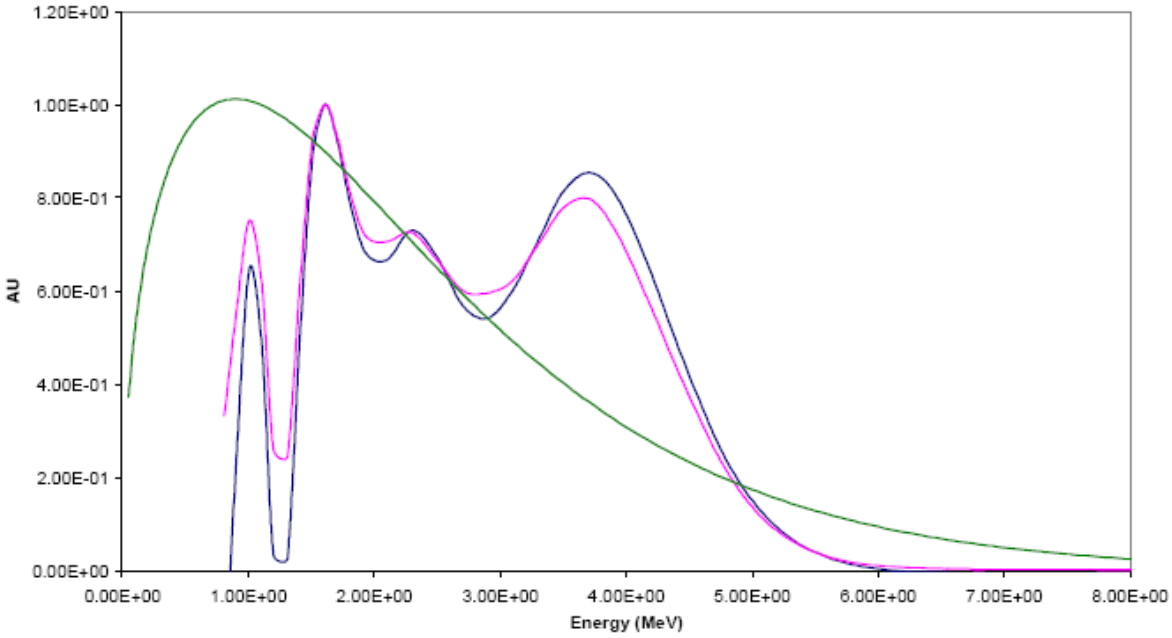

Figure 3-30-1000 ohm termination Cf252 neutron unfolded compared with calculated spectrum.

As can be seen in Figure 3-30, the unfolded 1000 ohm termination spectrum is has similar shape as that of the 500 ohm case. The general trend of the unfolded spectrum agrees with the calculated spectrum, however, huge fluctuation exists. The fluctuation is likely caused by low number of data points, the same for the 500 ohm case. The same LLD drop off at 1 MeV is observed when compared with the 500 ohm case. The higher PD limit compared to the 50 case (Table 3-2) also explains the lack of the 2 MeV peak seen in the 50 ohm case.

Chapter 4 Conclusions

NE213 response functions were verified in this work. Cf252 and Na22 spectra were taken to directly compare with FERD's unfolded spectra in Los Alamos National Laboratory. FERD is a computer code designed to unfold neutron spectra. Cf252 was chosen because its spectrum is well known. Meanwhile, three different termination resistors settings on the preamplifier were explored and tested to investigate their effects on pulse shape discrimination (PSD) and the overall unfolded spectrum. With the different resistors, a new figure of merit (FOM) scheme was developed to quantify the results.

Furthermore, Amoeba simplex fitting was used to implement the new FOM. Amoeba is a non-linear fitting routine and was found to be an effective tool in performing PSD for non-linear systems (Figure 3-14, Figure 3-15, and Figure 3-17). With the amoeba fitting, the 50 ohm termination was found to have the highest FOM, thus the best PSD performing setting (Table 3-5), even though its physical PSD limit was the highest (Table 3-2). The 50 ohm unfolded spectrum measures well against the calculated spectrum for energy range above 2 MeV (Figure 3-24). However, for energy between 1 MeV and 2 MeV, a peak was observed. The peak is likely due to misdiagnosing of gamma data as neutron data due to the high physical PSD limit of the 50 ohm termination setting. Furthermore, a drop-off at 1 MeV is observed due to the lower level discrimination setting of the single channel analyzer used. 500 ohm and the 1000 ohm terminations were tested afterwards. However, conclusive outcomes were not obtained due to statistical fluctuation caused by the low number of data point at high energy bins.

Overall, with the 50 ohm termination case, the unfolded Cf252 energy spectrum between 2 to 10 MeV was extracted with an amoeba augmented PSD scheme, and the results compared favorably with a calculated spectum (Figure 3-24). However, the unfolded Cf252 spectrum beyond the stated 2-10 MeV range did not compare well with the calculated spectrum or is simply unavailable due to the source used.

Bibliography

[1] Knoll, Glenn F. Radiation Detection and Measurement. New York City, NY: John Wiley & Sons, Inc, 1999.

[2] Tsoulfanidis, Nicholas. Measurement and Detection of Radiation. Washington, DC: Taylor and Francis, 1995.

[3] Mayo, Robert M. Introduction to Nuclear Concepts for Engineers. La Grande Park, Il: American Nuclear Society, 1998.

[4] Kuchnir, F., and F. Lynch. "Time-dependence of Scintillators and the Effect on PSD." IEEE Trans. Nucl. Sci. 3.15 (1968): 107-113.

[5] Burrus, W. R., and V. V. Verbinski. "Fast-Neutron Spectroscopy with Thick Organic Scintillators." Nuclear Instruments and Methods 67 (1969): 181-196.

[6] Kinbara, S., and T. Kumahara. "A General Purpose Pulse Shape Discriminating Circuit." Nuclear Instruments and Methods 70 (1969): 173-182.

[7] Ranucci, Gioacchino, Augusto Goretti, and Paolo Lombardi. "Pulse-shape Discrimination of Liquid Scintillators." Nuclear Instrments and Methods in Physics Research A 412 (1998): 374-386.

[8] Ranucci, Gioacchino. "An Analytical Approach to the Evaluation of the Pulse Shape Discrimination Properties of Scintillators." Nuclear Instrments and Methods in Physics Research A 354 (1995): 389-399.

[9] Cao, Zhong, and L. F. Miller. "Evaluation of Pulse Shape Discrimination Performance of Scintillation Materials and PSD Methods by Using Statistical Models." Nuclear Instruments and Methods in Physics Research A 416 (1998): 32-44.

[10] Verbinski, V. V. et al. "Calibration of an Organic Scintillator for Neutron Spectrometry." Nuclear Instruments and Methods 65 (1968): 8-25.

[11] Sellin, P. J., G. Jaffar, and S. D. Jastanish. "Performance of Digital Algorithms for N/γ Pulse Shape Discrimination Using a Liquid Scintillation Detector." 2003 IEEE Nuclear Science Symposium. Conference Record 2 (2004): 1057-1060.

[12] Wolski, D. et al. "Comparison of n-γ Discrimination by Zero-Crossing and Digital Charge Comparison Methods." Nuclear Instruments and Methods in Physics Research A 360 (1995): 584-592.

[13] Cerny, J. et al. "Study of Neutron Response and N-γ Discrimination by Charge Comparison Method for Small Liquid Scintillation Detector." Nuclear Instruments and Methods in Physics Research A 527 (2004): 512-518.

[14] Marrone at al. "Pulse Shape Analysis of Liquid Scintillators for Neutron Studies." Nuclear Instruments and Measurements A 2490 (2002): 299-307.

[15] Li, Andy O., Smith-Nelson, Mark, Hawari, Ayman I., et al. "Termination Effect on Pulse Shape Discrimination." 2007 IEEE Nuclear Science Symposium Conference Record (2007): 1373-1377.

[16] James, F.. "Minuit Tutorial, Function Minimization." Proceedings of the CERN Computing and Data Processing School (1972).

[17] Matthews. Module for Nelder-Mead Search for a Minimum.. 29 May 2007 <http://math.fullerton.edu/mathews/n2003/NelderMeadMod.html>.

[18] Lee, J. H., and C. S. Lee. "Response Function of NE213 Scintillator for 0.5-6 MeV Neutrons Measured by an Improved Pulse Shape Discrimination." Nuclear Instruments and Methods in Physics Research A 405 (1998): 147-154.

[19] Meigo, S.. "Measurements of the Response Function and the Detection Efficiency of an NE213 Scintillator for Neutrons Between 20 and 65 MeV." Nuclear Instruments and Methods in Physics Research A 401 (1997): 365-378.

[20] Oak Ridge National Laboratory. Scinful. Oak Ridge, TN. 1988.

[21] Oak Ridge National Laboratory. Scinful Source Codes. Oak Ridge, TN. 1988.

[22] Brookhaven National Laboratory. ENDF-201, ENDF/B-VI Summary Documentation. Brookhaven, NY. 1991.

[23] Oak Ridge National Laboratory. A User's Manual for the FERDO and FERD Unfolding Codes. Oak Ridge, TN. 1983.

[24] X-5 Monte Carlo Team. "Appendix H-Fission Spectra Constants and Flux-to-Dose Factors." MCNP-A General Monte Carlo N-Particle Transport Code, V. 5. Los Alamos, NM: Los Alamos National Laboratory, 2003. H-3.

Appendices

Appendix A Amoeba Code

This appendix includes the code used for amoeba implementation.

```
#include <fstream>
#include <ostream>
#include <iostream>
#include <string>
#include <stdio.h>
#include <stdlib.h>
#include <math.h>
#include <valarray>
#include <algorithm>

const int para=6;
const int loop_num=100;
const double tolerance=0.0001;

double aa[para]={0};
int output_counter=1;
int tolerance_counter=0;

using namespace std;


void clear_matrix(double n_matrix[][para], double chi_matrix[], int
high_chi_position, double bad_chi_matrix[],double & bad_chi)
{

      for (int i=0; i<para; i++)
      {
            bad_chi_matrix[i]=n_matrix[high_chi_position][i];
            n_matrix[high_chi_position][i]=0;
      }

      bad_chi=chi_matrix[high_chi_position];
      chi_matrix[high_chi_position]=0;

}

void midpoint(double n_matrix[][para], double chi_matrix[], int
high_chi_position, double mid_matrix[], double bad_chi_matrix[],double
bad_chi)
{
      double sum[para]={0};

      for (int i=0;i<para;i++)
      {
            for (int j=0;j<para+1;j++)
            {
                  sum[i]+=n_matrix[j][i];
            }
      }
```

```
for (int i=0;i<para;i++)
      {
            mid_matrix[i]=sum[i]/para;
      }

      for (int i=0; i<para; i++)
      {
            n_matrix[high_chi_position][i]=bad_chi_matrix[i];
      }

      chi_matrix[high_chi_position]=bad_chi;

}

void reflection(double bad_chi_matrix[], double mid_matrix[], double
reflection_matrix[], double expansion_matrix[])
{
      for (int i=0;i<para;i++)
      {
            reflection_matrix[i]=mid_matrix[i]+(mid_matrix[i]-
bad_chi_matrix[i]);


      expansion_matrix[i]=reflection_matrix[i]+(reflection_matrix[i]-
mid_matrix[i]);
      }


}
void contraction(double bad_chi_matrix[], double mid_matrix[], double
reflection_matrix[], double contraction_matrix1[], double
contraction_matrix2[])
{
      for (int i=0;i<para;i++)
      {

      contraction_matrix1[i]=mid_matrix[i]+0.5*(reflection_matrix[i]-
mid_matrix[i]);

            contraction_matrix2[i]=bad_chi_matrix[i]+0.5*(mid_matrix[i]-
bad_chi_matrix[i]);
      }


}

void shrinkage(double n_matrix[][para], double chi_matrix[])
{
      double best_chi;
      int best_chi_position;

      best_chi=*min_element(chi_matrix,chi_matrix+para+1);

      for (int ii=0; ii<para+1; ii++)
      {
```

```
            if (chi_matrix[ii]==best_chi)
            {
                  best_chi_position=ii;
            }
      }//loop for 7 times to find the poisition of the best chi-value

      for (int i=0;i<para+1;i++)
      {
            if (i!=best_chi_position)
            {
                  for (int j=0;j<para;j++)
                  {

      n_matrix[i][j]=(n_matrix[i][j]+n_matrix[best_chi_position][j])*0.5;


                  }
            }
      }
}

void output(double n_matrix[][para], double chi_matrix[], int
high_chi_position)
{

      double chi_difference=(*max_element(chi_matrix,chi_matrix+para+1)-
*min_element(chi_matrix,chi_matrix+para+1));

      ofstream outfile2;
      outfile2.open("Test.txt", std::ios::out|std::ios::app);


      outfile2<<"Iteration: "<<output_counter<<"    ||Highest Chi
Position: "<<high_chi_position+1<<endl;

            for (int i=0;i<para+1;i++)
            {
                  for (int zzzz=0;zzzz<para; zzzz++)
                  {
                        outfile2.width(12);
                        outfile2<<n_matrix[i][zzzz]<<" ";

                  }
                  outfile2<<"|| ";
                  outfile2.width(12);
                  outfile2.precision(6);
                  outfile2<<chi_matrix[i]<<endl;
            }

            outfile2<<endl<<"-----------------------------------"<<endl;

            outfile2.close();
```

```
            if (output_counter%loop_num==0)
            {


                  cout<<endl<<"Tolerance Counter= "<<tolerance_counter<<"
||    Highest Chi Difference: "<<chi_difference<<endl;
                  for (int i=0;i<para+1;i++)
                  {
                        for (int zzzz=0;zzzz<para; zzzz++)
                        {
                              cout.width(8);
                              cout<<n_matrix[i][zzzz]<<" ";

                        }
                        cout<<"|| ";
                        cout.width(8);
                        cout.precision(6);
                        cout<<chi_matrix[i]<<endl;
                  }

                  cout<<endl<<"-----------------------------------"<<endl;
            }

            output_counter+=1;
}

double Sep_function(double height)
{
      double sep;

      sep=aa[2]+aa[0]+aa[3]*height+aa[4]*pow(height,2)+aa[5]*pow(height,3)
;

      return(sep);
}

double Gam_function(double height)
{
      double gam;

      gam=aa[0]+aa[3]*height+aa[4]*pow(height,2)+aa[5]*pow(height,3);

      return(gam);
}

double Neu_function(double height)
{
      double neu;

      neu=aa[1]+aa[0]+aa[3]*height+aa[4]*pow(height,2)+aa[5]*pow(height,3)
;

      return(neu);
}
```

```
int highest_chi(double chi_matrix[], double & high_chi)
{


      high_chi=*max_element(chi_matrix,chi_matrix+para+1);

      int high_chi_position=99;

      for (int ii=0; ii<para+1; ii++)
      {
            if (chi_matrix[ii]==high_chi)
            {
                  high_chi_position=ii;
            }
      }//loop for 7 times to find the poisition of the highest chi-value

      return (high_chi_position);
}

void insertion(double n_matrix[][para], int high_chi_position, double
insertee[], double aa[])
{
      for(int i=0;i<para;i++)
      {
            n_matrix[high_chi_position][i]=insertee[i];
            aa[i]=insertee[i];
      }
}


void chi_calculation(double falltime[], double height[], int count, double
chi_matrix[], int row_number)
{

      double funct_value=9;

      chi_matrix[row_number]=0;

            for (int k=0; k<=count; k++)//do it for each data point
            {
                  if (falltime[k]>Sep_function(height[k]))
                  {
                        //neutron if falltime>function
                        funct_value=Neu_function(height[k]);
                  }
                  else
                  {
                        //gamma if falltime<=function
                        funct_value=Gam_function(height[k]);
                  }

                  chi_matrix[row_number]+=(pow((falltime[k]-
funct_value),2)/falltime[k]);
            }//each data point loop
```

```
            chi_matrix[row_number]=chi_matrix[row_number]/count;
}
void initialization(double n_matrix[][para], double chi_matrix[], double
new_n_matrix[][para], double new_chi_matrix[])
{
            for (int i=0;i<para+1;i++)
            {
                  for (int j=0;j<para;j++)
                  {
                        new_n_matrix[i][j]=n_matrix[i][j];
                  }
                  new_chi_matrix[i]=chi_matrix[i];
            }
}

void reinitialization(double n_matrix[][para], double chi_matrix[])
{
      double low_chi=*min_element(chi_matrix,chi_matrix+para+1);
      int low_chi_position;

      for (int ii=0; ii<para+1; ii++)
      {
            if (chi_matrix[ii]==low_chi)
            {
                  low_chi_position=ii;
            }
      }//loop for 7 times to find the poisition of the highest chi-value

      for (int i=0;i<para;i++)
      {
            aa[i]=n_matrix[low_chi_position][i];
      }

      for (int i=0;i<para+1;i++)
      {
            for (int j=0;j<para;j++)
            {
                  n_matrix[i][j]=aa[j];

                  if (i==para)
                  {
                        n_matrix[j+1][j]=n_matrix[j+1][j]*1.02;
                  }
            }
      }


}
void main()
{

      aa[0]=500;
      aa[1]=1000;
      aa[2]=500;
```

```
aa[3]=-0.1508;
aa[4]=1.594;
aa[5]=2.12;



int high_chi_position;
int old_high_chi_position;
int reflected_high_chi_position;
int expanded_high_chi_position;
int contraction_high_chi_position;
int contraction_high_chi_position1;
int contraction_high_chi_position2;

double high_chi;
double bad_chi;
double old_high_chi;
double reflected_high_chi;
double expanded_high_chi;
double contraction_high_chi;
double contraction_high_chi1;
double contraction_high_chi2;

double n_matrix[para+1][para]={0};
double expansion_n_matrix[para+1][para]={0};
double reflected_n_matrix[para+1][para]={0};
double contraction_n_matrix[para+1][para]={0};
double contraction_n_matrix1[para+1][para]={0};
double contraction_n_matrix2[para+1][para]={0};
double chi_matrix[para+1]={0};
double reflected_chi_matrix[para+1]={0};
double expansion_chi_matrix[para+1]={0};
double contraction_chi_matrix[para+1]={0};
double contraction_chi_matrix1[para+1]={0};
double contraction_chi_matrix2[para+1]={0};
double mid_matrix[para]={0};
double bad_chi_matrix[para]={0};
double reflection_matrix[para]={0};
double expansion_matrix[para]={0};
double contraction_matrix[para]={0};
double contraction_matrix1[para]={0};
double contraction_matrix2[para]={0};

double *height;
double *falltime;

height= new double[300000];
falltime= new double[300000];

int count=0;

ofstream outfile111;
outfile111.open("test.txt", std::ios::out|std::ios::trunc);
outfile111.close();
```

```
	ifstream infile;
	infile.open("input.txt");
	if (!infile.is_open())
	{
		cout<<"Could not open file.\n";

	}

	while (infile.good())
	{
		if (count%1000==0)
		{
			cout<<count<<endl;
		}
		infile>>height[count]>>falltime[count];
		count++;
	}

	count=count-1;//do for (int i=0;i<=count;i++)

	infile.close();

	for (int i=0;i<para+1;i++)
	{
		for (int j=0;j<para;j++)
		{
			n_matrix[i][j]=aa[j];

			if (i==para)
			{
				n_matrix[j+1][j]=n_matrix[j+1][j]*1.10;
			}
		}
	}
//-----------------------------------------------------------------
//-----------------------------------------------------------------


do
{

for (int yyyy=0;yyyy<loop_num;yyyy++)
{

	for (int i=0; i<para+1; i++)
	{
		for (int j=0; j<para; j++)
		{
			aa[j]=n_matrix[i][j];
		}//setting the poly coefficients to the matrix set

		chi_calculation(falltime, height, count, chi_matrix, i);

	}//each simplex vertex loop
```

```
            high_chi_position=highest_chi(chi_matrix, high_chi);

            old_high_chi=high_chi;
            old_high_chi_position=high_chi_position;

//          output(n_matrix, chi_matrix, high_chi_position);
            clear_matrix(n_matrix, chi_matrix, high_chi_position,
bad_chi_matrix, bad_chi);

            midpoint(n_matrix, chi_matrix, high_chi_position, mid_matrix,
bad_chi_matrix, bad_chi);
//          output(n_matrix, chi_matrix, high_chi_position);
            reflection(bad_chi_matrix, mid_matrix, reflection_matrix,
expansion_matrix);


            initialization(n_matrix, chi_matrix, reflected_n_matrix,
reflected_chi_matrix);
            insertion(reflected_n_matrix, high_chi_position,
reflection_matrix, aa);
            chi_calculation(falltime, height, count, reflected_chi_matrix,
old_high_chi_position);
            reflected_high_chi_position=highest_chi(reflected_chi_matrix,
high_chi);
            reflected_high_chi=high_chi;

      //    output(n_matrix, chi_matrix, high_chi_position);
      //    output(reflected_n_matrix, reflected_chi_matrix,
high_chi_position);
            if (output_counter%10==0)
            {
                  cout<<"Iteration: "<<output_counter<<endl;
            }


            if
(chi_matrix[old_high_chi_position]>reflected_chi_matrix[old_high_chi_posit
ion])
            {

                  initialization(n_matrix, chi_matrix, expansion_n_matrix,
expansion_chi_matrix);
                  insertion(expansion_n_matrix, old_high_chi_position,
expansion_matrix, aa);
                  chi_calculation(falltime, height, count,
expansion_chi_matrix, old_high_chi_position);

      expanded_high_chi_position=highest_chi(expansion_chi_matrix,
high_chi);
                  expanded_high_chi=high_chi;

            //    output(n_matrix, chi_matrix, old_high_chi_position);
            //    output(expansion_n_matrix, expansion_chi_matrix,
expanded_high_chi_position);
```

```
                    if
(reflected_chi_matrix[old_high_chi_position]>=expansion_chi_matrix[old_hig
h_chi_position])
                    {
                          initialization(expansion_n_matrix,
expansion_chi_matrix, n_matrix, chi_matrix);
                          high_chi_position=expanded_high_chi_position;
                    }
                    else
                    {
                          initialization(reflected_n_matrix,
reflected_chi_matrix, n_matrix, chi_matrix);
                          high_chi_position=reflected_high_chi_position;
                    }

                    //output(n_matrix, chi_matrix, high_chi_position);
              }
              else
              {
                    initialization(n_matrix, chi_matrix,
contraction_n_matrix1, contraction_chi_matrix1);
                    initialization(n_matrix, chi_matrix,
contraction_n_matrix2, contraction_chi_matrix2);
                    contraction(bad_chi_matrix, mid_matrix,
reflection_matrix, contraction_matrix1, contraction_matrix2);
                    insertion(contraction_n_matrix1, old_high_chi_position,
contraction_matrix1, aa);
                    insertion(contraction_n_matrix2, old_high_chi_position,
contraction_matrix2, aa);
                    chi_calculation(falltime, height, count,
contraction_chi_matrix1, old_high_chi_position);

      contraction_high_chi_position1=highest_chi(contraction_chi_matrix1,
high_chi);
                    contraction_high_chi1=high_chi;
                    chi_calculation(falltime, height, count,
contraction_chi_matrix2, old_high_chi_position);

      contraction_high_chi_position2=highest_chi(contraction_chi_matrix2,
high_chi);
                    contraction_high_chi2=high_chi;

                    if
(contraction_chi_matrix1[old_high_chi_position]>contraction_chi_matrix2[ol
d_high_chi_position])
                    {
                          initialization(contraction_n_matrix2,
contraction_chi_matrix2, contraction_n_matrix, contraction_chi_matrix);

      contraction_high_chi_position=contraction_high_chi_position2;
                          contraction_high_chi=contraction_high_chi2;
                    }
                    else
                    {
```

```
                        initialization(contraction_n_matrix1,
contraction_chi_matrix1, contraction_n_matrix, contraction_chi_matrix);

      contraction_high_chi_position=contraction_high_chi_position1;
                        contraction_high_chi=contraction_high_chi1;
                  }

                  if
(contraction_chi_matrix[old_high_chi_position]>=chi_matrix[old_high_chi_po
sition])
                  {
                        shrinkage(n_matrix, chi_matrix);
                  }
                  else
                  {
                        initialization(contraction_n_matrix,
contraction_chi_matrix, n_matrix, chi_matrix);
                        high_chi_position=contraction_high_chi_position;
                  }


            }

            if (output_counter%loop_num==0)
            {
                  if ((*max_element(chi_matrix,chi_matrix+para+1)-
*min_element(chi_matrix,chi_matrix+para+1))<tolerance)
                  {
                        tolerance_counter+=1;
                  }
            }

            output(n_matrix, chi_matrix, high_chi_position);


}



//reinitialization(n_matrix, chi_matrix);
}while((tolerance_counter<=2));//do loop
}
```

Appendix B FERD-PC Response File Input

Below is an example of a sample response file input for FERD-PC.

NE-213 NEUTRON RESPONSE - FILE #110

(1) CONTROL PARAMETERS FOR FERD-PC:

```
A)  1          : 0/1 = No effect / Prompt user for different response file
B)  0          : 0/1 = No effect / Create unformated response file
C)  0          : 0/1 = No effect / Use unformated response file
D)  0          : 0/1 = No effect / Create log file of unfolding process
E)  1          : 0/1 = No effect / Write response matrix to log file
F)  0          : 0/1 = No effect / Normalize data to a power level (kW)
G)  0          : 0/1 = No effect / Use prebinned data file for input
H)  0          : 0/1 = No effect / Output binned data to file
I)  0          : 0/1 = No effect / Output results to punch style file
J)  0          : 0/1 = No effect / Output synthetic window resolutions
K)  1          : 0/1 = Use windows from blk (8) / FWHM from blk (7)
L)  68         : Number of pulse-height bins (rows in response matrix)
M)  55         : Number of energy bins (col's in response & window matrix)
N)  55         : Number of window vectors (rows in window matrix)
O)  1.000      : Parameter TAU used for weighting the biased estimation
P)  1.000      : Detector normalization factor (multiplier)
Q)  RESPONSE.UNF : Default file name for unformatted response file
R)  1.000      : Normalization parameter for block 7 (FWHM)
```

(2) ENERGY INTERVALS USED IN INTEGRATED OUTPUT IN MeV (6X,2F8.0)

```
   LOW     HIGH
   -----   -----
   0.811   1.000
   1.000   1.200
   1.200   1.600
   1.600   2.000
   2.000   3.000
   3.000   4.000
   4.000   6.000
   6.000   8.000
   8.000   10.00
   10.00   12.00
   12.00   16.00
   1.500   15.00
```

(3) PULSE HEIGHT BINS FOR MATRIX IN LIGHT UNITS (5X,8F9.0)

```
   1.075E-1 1.225E-1 1.375E-1 1.525E-1 1.675E-1 1.825E-1 2.050E-1 2.350E-1
   2.650E-1 2.950E-1 3.250E-1 3.550E-1 3.850E-1 4.150E-1 4.550E-1 5.050E-1
   5.550E-1 6.050E-1 6.550E-1 7.050E-1 7.550E-1 8.050E-1 8.550E-1 9.050E-1
   9.750E-1 1.065E+0 1.155E+0 1.245E+0 1.335E+0 1.425E+0 1.515E+0 1.605E+0
   1.695E+0 1.785E+0 1.915E+0 2.085E+0 2.255E+0 2.425E+0 2.595E+0 2.765E+0
```

2.935E+0 3.105E+0 3.275E+0 3.445E+0 3.685E+0 3.995E+0 4.305E+0 4.615E+0
4.925E+0 5.235E+0 5.545E+0 5.855E+0 6.165E+0 6.475E+0 6.910E+0 7.470E+0
8.030E+0 8.590E+0 9.150E+0 9.710E+0 1.027E+1 1.083E+1 1.139E+1 1.195E+1
1.251E+1 1.307E+1 1.363E+1 1.419E+1

(4) PULSE HEIGHT BINNING WIDTH IN LIGHT UNITS (5X,8F9.0)

0.0150 0.0150 0.0150 0.0150 0.0150 0.0150 0.0300 0.0300
0.0300 0.0300 0.0300 0.0300 0.0300 0.0300 0.0500 0.0500
0.0500 0.0500 0.0500 0.0500 0.0500 0.0500 0.0500 0.0500
0.0900 0.0900 0.0900 0.0900 0.0900 0.0900 0.0900 0.0900
0.0900 0.0900 0.1700 0.1700 0.1700 0.1700 0.1700 0.1700
0.1700 0.1700 0.1700 0.1700 0.3100 0.3100 0.3100 0.3100
0.3100 0.3100 0.3100 0.3100 0.3100 0.3100 0.5600 0.5600
0.5600 0.5600 0.5600 0.5600 0.5600 0.5600 0.5600 0.5600
0.5600 0.5600 0.5600 0.5600

(5) ENERGY BINS FOR RESPONSE AND WINDOW MATRIX IN MeV (5X,7F10.0)

2.347E+01 2.256E+01 2.157E+01 2.055E+01 1.949E+01 1.852E+01 1.753E+01
1.653E+01 1.562E+01 1.479E+01 1.402E+01 1.320E+01 1.239E+01 1.175E+01
1.124E+01 1.077E+01 1.025E+01 9.741E+00 9.261E+00 8.757E+00 8.236E+00
7.736E+00 7.235E+00 6.839E+00 6.555E+00 6.254E+00 5.938E+00 5.645E+00
5.345E+00 5.042E+00 4.752E+00 4.453E+00 4.152E+00 3.906E+00 3.707E+00
3.500E+00 3.296E+00 3.097E+00 2.898E+00 2.702E+00 2.498E+00 2.296E+00
2.099E+00 1.932E+00 1.812E+00 1.709E+00 1.609E+00 1.510E+00 1.412E+00
1.309E+00 1.204E+00 1.106E+00 1.006E+00 9.069E-01 8.113E-01

(6) ROW ENERGIES FOR WINDOW MATRIX IN MeV (5X,7F10.0)

2.347E+01 2.256E+01 2.157E+01 2.055E+01 1.949E+01 1.852E+01 1.753E+01
1.653E+01 1.562E+01 1.479E+01 1.402E+01 1.320E+01 1.239E+01 1.175E+01
1.124E+01 1.077E+01 1.025E+01 9.741E+00 9.261E+00 8.757E+00 8.236E+00
7.736E+00 7.235E+00 6.839E+00 6.555E+00 6.254E+00 5.938E+00 5.645E+00
5.345E+00 5.042E+00 4.752E+00 4.453E+00 4.152E+00 3.906E+00 3.707E+00
3.500E+00 3.296E+00 3.097E+00 2.898E+00 2.702E+00 2.498E+00 2.296E+00
2.099E+00 1.932E+00 1.812E+00 1.709E+00 1.609E+00 1.510E+00 1.412E+00
1.309E+00 1.204E+00 1.106E+00 1.006E+00 9.069E-01 8.113E-01

(7) GAUSSIAN FWHM (%) USED TO CALCULATE WINDOWS (5X,7F10.0)

20.862 20.905 20.956 21.017 21.081 21.145 21.218
21.306 21.393 21.478 21.569 21.676 21.792 21.900
21.999 22.090 22.197 22.318 22.442 22.587 22.752
22.932 23.136 23.317 23.460 23.622 23.810 24.000
24.217 24.458 24.716 25.015 25.352 25.665 25.939
26.263 26.615 26.989 27.416 27.896 28.454 29.096
29.819 30.533 31.110 31.665 32.262 32.922 33.643
34.504 35.497 36.559 37.833 39.304 41.000

(8) WINDOW MATRIX (1X,2I3,1X,7F10.0)

1 1 2.3984E-1 2.0650E-1 1.2491E-1 5.1376E-2 1.3701E-2 2.8638E-3 4.0817E-4

1 8 3.9812E-5 3.4974E-6 2.9309E-7 0.0000E+0 0.0000E+0 0.0000E+0 0.0000E+0
2 1 2.1190E-1 2.4899E-1 2.0572E-1 1.1336E-1 3.9715E-2 1.0365E-2 1.8032E-3
2 8 2.0918E-4 2.0997E-5 1.9471E-6 1.6869E-7 0.0000E+0 0.0000E+0 0.0000E+0
3 1 1.2084E-1 2.1104E-1 2.5979E-1 2.0836E-1 1.0381E-1 3.6144E-2 8.1605E-3
3 8 1.1902E-3 1.4280E-4 1.5199E-5 1.4649E-6 9.1991E-8 0.0000E+0 0.0000E+0
4 1 3.7533E-2 1.0639E-1 2.1353E-1 2.7189E-1 2.0944E-1 1.0441E-1 3.2697E-2
4 8 6.3746E-3 9.6161E-4 1.2249E-4 1.3603E-5 9.6756E-7 0.0000E+0 0.0000E+0
5 1 4.9047E-3 2.5447E-2 9.4164E-2 2.1422E-1 2.8581E-1 2.2450E-1 1.0664E-1
5 8 3.0170E-2 6.1214E-3 9.8644E-4 1.3222E-4 1.1131E-5 6.8819E-7 0.0000E+0
6 1 2.9571E-4 2.9822E-3 2.1660E-2 9.3618E-2 2.2988E-1 2.9987E-1 2.2734E-1
6 8 9.7968E-2 2.7871E-2 5.8890E-3 9.8306E-4 1.0108E-4 7.3595E-6 7.1445E-7
6 15 9.4380E-8 0.0000E+0 0.0000E+0 0.0000E+0 0.0000E+0 0.0000E+0 0.0000E+0
7 1 5.0237E-6 1.1444E-4 1.9041E-3 1.8155E-2 9.4812E-2 2.3228E-1 3.1571E-1
7 8 2.3083E-1 1.0073E-1 3.0083E-2 6.6659E-3 8.9042E-4 8.0621E-5 9.0371E-6
7 15 1.3149E-6 1.9266E-7 0.0000E+0 0.0000E+0 0.0000E+0 0.0000E+0 0.0000E+0
8 1 0.0000E+0 1.0177E-6 4.6772E-5 1.1796E-3 1.5632E-2 8.3622E-2 2.3514E-1
8 8 3.3343E-1 2.4969E-1 1.1581E-1 3.6930E-2 6.9341E-3 8.3791E-4 1.1409E-4
8 15 1.8978E-5 3.0938E-6 3.4739E-7 0.0000E+0 0.0000E+0 0.0000E+0 0.0000E+0
9 1 0.0000E+0 0.0000E+0 3.8088E-7 2.8226E-5 1.0528E-3 1.3453E-2 8.5339E-2
9 8 2.5486E-1 3.5142E-1 2.6900E-1 1.3016E-1 3.6230E-2 6.1371E-3 1.0528E-3
9 15 2.0578E-4 3.8236E-5 4.8645E-6 5.2759E-7 0.0000E+0 0.0000E+0 0.0000E+0
10 1 0.0000E+0 0.0000E+0 0.0000E+0 2.4077E-7 2.8117E-5 9.4113E-4 1.4722E-2
10 8 1.0076E-1 2.7503E-1 3.6968E-1 2.8660E-1 1.2486E-1 3.1176E-2 6.9928E-3
10 15 1.6519E-3 3.5858E-4 5.3043E-5 6.5247E-6 7.3762E-7 0.0000E+0 0.0000E+0
11 1 0.0000E+0 0.0000E+0 0.0000E+0 0.0000E+0 2.7106E-7 2.6474E-5 1.1334E-3
11 8 1.9632E-2 1.1547E-1 2.9323E-1 3.8833E-1 2.8239E-1 1.1029E-1 3.3807E-2
11 15 9.9794E-3 2.6061E-3 4.6231E-4 6.6375E-5 8.5001E-6 7.7656E-7 0.0000E+0
12 1 0.0000E+0 0.0000E+0 0.0000E+0 0.0000E+0 0.0000E+0 1.2852E-7 2.0160E-5
12 8 1.1610E-3 1.8507E-2 1.0770E-1 2.8754E-1 4.1041E-1 2.9003E-1 1.3491E-1
12 15 5.3749E-2 1.8039E-2 4.1047E-3 7.3044E-4 1.1156E-4 1.1931E-5 8.9195E-7
13 8 1.6409E-5 8.8293E-4 1.4187E-2 8.9686E-2 2.9450E-1 4.3492E-1 3.4096E-1
13 15 1.9820E-1 9.1435E-2 2.8610E-2 6.7210E-3 1.2932E-3 1.7066E-4 1.5315E-5
13 22 1.1183E-6 0.0000E+0 0.0000E+0 0.0000E+0 0.0000E+0 0.0000E+0 0.0000E+0
14 8 1.4693E-7 2.5336E-5 1.0799E-3 1.5673E-2 1.1532E-1 3.4907E-1 4.5635E-1
14 15 3.8494E-1 2.4345E-1 1.0471E-1 3.2545E-2 7.9251E-3 1.3000E-3 1.4147E-4
14 22 1.2054E-5 7.3620E-7 0.0000E+0 0.0000E+0 0.0000E+0 0.0000E+0 0.0000E+0
15 8 0.0000E+0 5.9291E-7 6.2870E-5 1.9877E-3 3.1220E-2 1.8606E-1 3.9498E-1
15 15 4.7492E-1 4.0611E-1 2.3714E-1 9.6638E-2 2.9608E-2 6.0168E-3 7.9369E-4
15 22 7.9122E-5 5.5031E-6 5.2029E-7 0.0000E+0 0.0000E+0 0.0000E+0 0.0000E+0
16 8 0.0000E+0 0.0000E+0 2.0969E-6 1.5218E-4 5.3772E-3 6.6222E-2 2.3666E-1
16 15 4.1681E-1 4.9359E-1 4.0131E-1 2.1948E-1 8.6388E-2 2.2203E-2 3.6220E-3
16 22 4.3006E-4 3.4639E-5 3.6041E-6 6.1347E-7 0.0000E+0 0.0000E+0 0.0000E+0
17 8 0.0000E+0 0.0000E+0 0.0000E+0 3.5244E-6 3.5468E-4 1.1176E-2 7.8522E-2
17 15 2.2727E-1 4.1160E-1 5.1612E-1 4.1552E-1 2.2764E-1 7.9911E-2 1.7319E-2
17 22 2.6043E-3 2.5640E-4 3.0483E-5 5.6308E-6 8.1132E-7 0.0000E+0 0.0000E+0
18 8 0.0000E+0 0.0000E+0 0.0000E+0 0.0000E+0 9.3240E-6 8.6916E-4 1.3361E-2
18 15 6.8870E-2 2.0465E-1 4.2597E-1 5.4016E-1 4.3732E-1 2.2237E-1 6.7741E-2
18 22 1.3559E-2 1.7083E-3 2.3990E-4 4.9176E-5 7.8015E-6 9.4437E-7 0.0000E+0
19 8 0.0000E+0 0.0000E+0 0.0000E+0 0.0000E+0 0.0000E+0 3.0731E-5 1.1315E-3
19 15 1.1122E-2 5.7575E-2 2.1185E-1 4.4844E-1 5.6502E-1 4.3795E-1 1.9699E-1
19 22 5.4840E-2 9.2087E-3 1.5739E-3 3.6529E-4 6.5108E-5 8.7575E-6 1.1398E-6
20 8 0.0000E+0 0.0000E+0 0.0000E+0 0.0000E+0 0.0000E+0 2.6686E-7 2.9215E-5
20 15 6.4366E-4 6.6813E-3 5.0304E-2 2.0320E-1 4.4813E-1 5.9369E-1 4.3957E-1
20 22 1.8718E-1 4.5662E-2 1.0103E-2 2.7654E-3 5.7637E-4 8.9525E-5 1.3069E-5

20 29 1.4963E-6 0.0000E+0 0.0000E+0 0.0000E+0 0.0000E+0 0.0000E+0 0.0000E+0
21 15 9.1613E-6 2.2729E-4 4.2046E-3 3.8321E-2 1.7144E-1 4.4833E-1 6.2666E-1
21 22 4.6035E-1 1.8204E-1 5.6411E-2 1.9186E-2 4.9231E-3 9.2806E-4 1.5851E-4
21 29 2.0839E-5 2.1428E-6 1.9649E-7 0.0000E+0 0.0000E+0 0.0000E+0 0.0000E+0
22 15 0.0000E+0 2.0794E-6 1.1030E-4 2.6159E-3 2.6949E-2 1.5763E-1 4.6920E-1
22 22 6.6193E-1 4.6856E-1 2.1868E-1 9.7055E-2 3.2199E-2 7.7309E-3 1.6108E-3
22 29 2.5307E-4 3.0351E-5 3.1464E-6 2.3858E-7 0.0000E+0 0.0000E+0 0.0000E+0
23 15 0.0000E+0 0.0000E+0 5.5245E-7 4.2583E-5 1.2300E-3 1.9526E-2 1.4902E-1
23 22 4.7589E-1 7.0153E-1 5.5049E-1 3.4321E-1 1.5844E-1 5.2060E-2 1.4077E-2
23 29 2.8023E-3 4.1382E-4 5.0849E-5 4.4590E-6 2.9098E-7 0.0000E+0 0.0000E+0
24 15 0.0000E+0 0.0000E+0 0.0000E+0 4.3274E-7 3.3650E-5 1.3975E-3 2.6496E-2
24 22 1.8698E-1 5.6375E-1 7.3639E-1 6.4185E-1 4.1106E-1 1.8471E-1 6.4912E-2
24 29 1.6432E-2 3.0055E-3 4.4112E-4 4.5190E-5 3.3518E-6 3.1798E-7 0.0000E+0
25 15 0.0000E+0 0.0000E+0 0.0000E+0 0.0000E+0 1.1405E-6 1.0596E-4 4.3121E-3
25 22 5.9320E-2 3.2734E-1 6.5874E-1 7.6363E-1 6.4684E-1 3.8019E-1 1.6751E-1
25 29 5.2244E-2 1.1524E-2 1.9793E-3 2.3312E-4 1.9442E-5 1.9951E-6 2.6893E-7
26 15 0.0000E+0 0.0000E+0 0.0000E+0 0.0000E+0 0.0000E+0 3.1567E-6 3.2636E-4
26 22 1.0159E-2 1.1767E-1 4.0298E-1 6.6406E-1 7.9490E-1 6.5197E-1 3.8069E-1
26 29 1.5416E-1 4.3046E-2 9.0241E-3 1.2706E-3 1.2337E-4 1.4043E-5 2.0308E-6
26 36 2.2997E-7 0.0000E+0 0.0000E+0 0.0000E+0 0.0000E+0 0.0000E+0 0.0000E+0
27 15 0.0000E+0 0.0000E+0 0.0000E+0 0.0000E+0 0.0000E+0 0.0000E+0 8.8917E-6
27 22 7.5267E-4 2.1680E-2 1.4299E-1 3.6397E-1 6.6895E-1 8.3057E-1 6.8957E-1
27 29 3.8761E-1 1.4580E-1 3.9397E-2 6.9788E-3 8.2619E-4 1.0791E-4 1.7163E-5
27 36 2.1131E-6 0.0000E+0 0.0000E+0 0.0000E+0 0.0000E+0 0.0000E+0 0.0000E+0
28 22 2.8595E-5 2.2212E-3 2.9965E-2 1.2277E-1 3.6119E-1 7.0778E-1 8.6675E-1
28 29 7.0088E-1 3.6745E-1 1.3198E-1 3.0304E-2 4.4989E-3 6.8890E-4 1.2250E-4
28 36 1.6666E-5 1.9148E-6 0.0000E+0 0.0000E+0 0.0000E+0 0.0000E+0 0.0000E+0
29 22 3.4512E-7 8.8398E-5 2.8266E-3 2.0588E-2 1.0711E-1 3.6545E-1 7.1886E-1
29 29 9.0722E-1 7.1551E-1 3.6545E-1 1.1594E-1 2.2881E-2 4.2895E-3 8.8065E-4
29 36 1.3652E-4 1.7504E-5 1.9183E-6 0.0000E+0 0.0000E+0 0.0000E+0 0.0000E+0
30 22 0.0000E+0 1.0687E-6 9.6301E-5 1.4016E-3 1.4501E-2 9.6721E-2 3.3799E-1
30 29 7.3310E-1 9.5225E-1 7.4938E-1 3.5444E-1 9.9719E-2 2.4109E-2 5.9404E-3
30 36 1.0890E-3 1.6113E-4 1.9882E-5 1.9577E-6 0.0000E+0 0.0000E+0 0.0000E+0
31 22 0.0000E+0 0.0000E+0 1.1467E-6 3.6830E-5 8.3753E-4 1.2064E-2 8.1714E-2
31 29 3.3137E-1 7.6775E-1 9.9982E-1 7.5507E-1 3.2279E-1 1.0563E-1 3.2399E-2
31 36 7.2784E-3 1.2841E-3 1.8375E-4 2.0504E-5 1.8544E-6 0.0000E+0 0.0000E+0
32 22 0.0000E+0 0.0000E+0 0.0000E+0 0.0000E+0 1.2720E-5 4.7756E-4 7.3858E-3
32 29 6.5528E-2 3.1396E-1 7.7156E-1 1.0542E+0 7.6833E-1 3.7087E-1 1.5103E-1
32 36 4.4235E-2 9.8416E-3 1.7169E-3 2.2717E-4 2.3648E-5 1.6881E-6 0.0000E+0
33 22 0.0000E+0 0.0000E+0 0.0000E+0 0.0000E+0 0.0000E+0 4.2743E-6 1.8295E-4
33 29 4.2724E-3 5.0401E-2 2.7302E-1 7.8283E-1 1.1156E+0 8.8055E-1 5.1434E-1
33 36 2.1166E-1 6.3569E-2 1.4370E-2 2.3834E-3 3.0007E-4 2.5232E-5 1.5774E-6
34 22 0.0000E+0 0.0000E+0 0.0000E+0 0.0000E+0 0.0000E+0 0.0000E+0 2.5519E-6
34 29 1.5554E-4 4.4937E-3 5.3546E-2 3.2250E-1 9.0243E-1 1.1714E+0 9.8758E-1
34 36 5.7557E-1 2.3554E-1 6.9722E-2 1.4669E-2 2.2631E-3 2.2755E-4 1.6432E-5
34 43 9.0242E-7 0.0000E+0 0.0000E+0 0.0000E+0 0.0000E+0 0.0000E+0 0.0000E+0
35 29 4.2393E-6 2.8860E-4 7.3236E-3 9.0030E-2 4.8289E-1 1.0144E+0 1.2212E+0
35 36 9.9909E-1 5.5344E-1 2.1362E-1 5.6891E-2 1.0754E-2 1.2958E-3 1.0855E-4
35 43 6.6902E-6 4.7407E-7 0.0000E+0 0.0000E+0 0.0000E+0 0.0000E+0 0.0000E+0
36 29 0.0000E+0 6.4827E-6 4.1303E-4 1.2135E-2 1.4447E-1 5.4868E-1 1.0255E+0
36 36 1.2775E+0 1.0320E+0 5.5555E-1 1.9925E-1 4.8796E-2 7.4256E-3 7.5593E-4
36 43 5.4420E-5 4.2826E-6 5.7767E-7 0.0000E+0 0.0000E+0 0.0000E+0 0.0000E+0
37 29 0.0000E+0 0.0000E+0 8.7853E-6 7.1429E-4 2.1639E-2 1.6479E-1 5.1722E-1
37 36 1.0590E+0 1.3386E+0 1.0711E+0 5.4876E-1 1.8367E-1 3.7134E-2 4.8064E-3

37 43 4.2041E-4 3.7848E-5 5.5271E-6 9.3146E-7 0.0000E+0 0.0000E+0 0.0000E+0
38 29 0.0000E+0 0.0000E+0 0.0000E+0 1.5701E-5 1.4134E-3 2.4273E-2 1.3982E-1
38 36 5.1320E-1 1.0990E+0 1.4049E+0 1.0990E+0 5.3392E-1 1.5184E-1 2.6291E-2
38 43 2.9201E-3 3.1091E-4 5.0222E-5 9.1086E-6 1.5309E-6 0.0000E+0 0.0000E+0
39 29 0.0000E+0 0.0000E+0 0.0000E+0 0.0000E+0 3.0403E-5 1.3848E-3 1.6559E-2
39 36 1.2290E-1 4.9838E-1 1.1263E+0 1.4780E+0 1.1355E+0 4.9295E-1 1.2290E-1
39 43 1.8491E-2 2.4461E-3 4.5142E-4 9.0405E-5 1.6506E-5 2.6777E-6 0.0000E+0
40 29 0.0000E+0 0.0000E+0 0.0000E+0 0.0000E+0 0.0000E+0 2.4664E-5 7.0437E-4
40 36 1.2127E-2 1.0571E-1 4.7409E-1 1.1623E+0 1.5579E+0 1.1343E+0 4.4329E-1
40 43 9.7373E-2 1.6948E-2 3.7108E-3 8.4566E-4 1.7235E-4 3.0710E-5 4.8062E-6
40 50 5.8433E-7 0.0000E+0 0.0000E+0 0.0000E+0 0.0000E+0 0.0000E+0 0.0000E+0
41 29 0.0000E+0 0.0000E+0 0.0000E+0 0.0000E+0 0.0000E+0 0.0000E+0 5.9535E-6
41 36 3.0140E-4 7.0241E-3 7.6185E-2 4.1899E-1 1.1563E+0 1.6521E+0 1.1643E+0
41 43 4.2187E-1 1.0593E-1 2.9211E-2 7.9393E-3 1.8832E-3 3.8274E-4 6.6988E-5
41 50 8.9820E-6 9.6046E-7 0.0000E+0 0.0000E+0 0.0000E+0 0.0000E+0 0.0000E+0
42 36 1.3598E-6 1.0692E-4 3.4676E-3 5.2132E-2 3.5485E-1 1.1829E+0 1.7578E+0
42 43 1.2060E+0 4.8572E-1 1.8087E-1 6.1987E-2 1.7996E-2 4.3691E-3 8.9209E-4
42 50 1.3739E-4 1.6505E-5 1.8827E-6 0.0000E+0 0.0000E+0 0.0000E+0 0.0000E+0
43 36 0.0000E+0 0.0000E+0 3.0891E-5 1.6116E-3 3.3651E-2 3.2262E-1 1.2215E+0
43 43 1.8762E+0 1.3783E+0 7.5454E-1 3.4897E-1 1.3187E-1 4.0471E-2 1.0153E-2
43 50 1.8878E-3 2.6684E-4 3.4486E-5 3.4342E-6 0.0000E+0 0.0000E+0 0.0000E+0
44 36 0.0000E+0 0.0000E+0 0.0000E+0 1.7933E-5 1.2398E-3 3.6891E-2 3.8250E-1
44 43 1.4067E+0 1.9907E+0 1.6640E+0 1.0718E+0 5.4315E-1 2.1684E-1 6.8709E-2
44 50 1.5867E-2 2.7134E-3 4.0748E-4 4.6009E-5 4.1440E-6 0.0000E+0 0.0000E+0
45 36 0.0000E+0 0.0000E+0 0.0000E+0 0.0000E+0 4.2542E-5 3.4072E-3 8.5454E-2
45 43 6.7769E-1 1.7118E+0 2.0832E+0 1.8026E+0 1.1878E+0 6.0079E-1 2.3517E-1
45 50 6.6175E-2 1.3490E-2 2.3311E-3 2.9671E-4 2.9399E-5 2.4524E-6 0.0000E+0
46 36 0.0000E+0 0.0000E+0 0.0000E+0 0.0000E+0 1.0034E-6 2.1727E-4 1.3266E-2
46 43 2.2870E-1 1.0398E+0 1.8548E+0 2.1700E+0 1.8716E+0 1.2079E+0 5.8850E-1
46 50 2.0348E-1 4.9891E-2 1.0009E-2 1.4500E-3 1.5962E-4 1.4424E-5 0.0000E+0
47 36 0.0000E+0 0.0000E+0 0.0000E+0 0.0000E+0 0.0000E+0 6.8605E-6 1.1459E-3
47 43 4.7655E-2 4.2275E-1 1.1663E+0 1.9262E+0 2.2622E+0 1.9324E+0 1.2122E+0
47 50 5.3227E-1 1.6191E-1 3.8723E-2 6.5425E-3 8.1789E-4 8.1580E-5 0.0000E+0
48 36 0.0000E+0 0.0000E+0 0.0000E+0 0.0000E+0 0.0000E+0 0.0000E+0 4.6768E-5
48 43 5.3971E-3 1.0412E-1 4.7749E-1 1.1799E+0 1.9893E+0 2.3622E+0 1.9962E+0
48 50 1.1634E+0 4.5756E-1 1.3512E-1 2.7508E-2 4.0197E-3 4.5365E-4 0.0000E+0
49 36 0.0000E+0 0.0000E+0 0.0000E+0 0.0000E+0 0.0000E+0 0.0000E+0 7.5487E-7
49 43 2.8717E-4 1.3761E-2 1.1457E-1 4.5460E-1 1.1735E+0 2.0558E+0 2.4720E+0
49 50 2.0165E+0 1.0773E+0 4.0962E-1 1.0442E-1 1.8450E-2 2.4246E-3 0.0000E+0
50 43 4.5594E-6 6.8432E-4 1.2063E-2 8.6954E-2 3.8450E-1 1.1024E+0 2.0755E+0
50 50 2.6000E+0 2.0572E+0 1.0837E+0 3.7001E-1 8.3899E-2 1.3502E-2 0.0000E+0
51 43 0.0000E+0 9.5457E-6 4.2776E-4 6.4871E-3 5.6158E-2 2.9817E-1 9.8473E-1
51 50 2.1154E+0 2.7477E+0 2.1879E+0 1.0843E+0 3.3865E-1 7.0872E-2 0.0000E+0
52 43 0.0000E+0 0.0000E+0 5.3332E-6 1.8993E-4 3.5595E-3 3.8435E-2 2.4292E-1
52 50 9.7454E-1 2.2517E+0 2.9043E+0 2.2282E+0 1.0159E+0 2.9079E-1 0.0000E+0
53 43 0.0000E+0 0.0000E+0 0.0000E+0 1.1755E-6 5.8416E-5 1.5488E-3 2.2301E-2
53 50 1.9808E-1 9.5523E-1 2.2879E+0 3.0854E+0 2.3001E+0 9.9298E-1 0.0000E+0
54 43 0.0000E+0 0.0000E+0 0.0000E+0 0.0000E+0 0.0000E+0 1.3541E-5 5.4937E-4
54 50 1.3291E-2 1.6244E-1 8.5267E-1 2.3570E+0 3.2944E+0 2.4124E+0 0.0000E+0
55 43 0.0000E+0 0.0000E+0 0.0000E+0 0.0000E+0 0.0000E+0 0.0000E+0 2.5814E-6
55 50 2.1661E-4 8.4232E-3 1.1776E-1 8.0021E-1 2.4683E+0 3.5303E+0 0.0000E+0

(9) RESPONSE MATRIX 68 x 55 (2I3,8F9.0)

1 1 1.01e-02 1.25e-02 1.10e-02 1.34e-02 1.67e-02 2.19e-02 2.44e-02 2.47e-02
1 9 2.99e-02 3.06e-02 3.28e-02 4.20e-02 4.04e-02 3.73e-02 3.56e-02 2.28e-02
1 17 2.37e-02 2.43e-02 2.94e-02 2.02e-02 1.90e-02 1.34e-02 2.21e-02 2.60e-02
1 25 2.96e-02 2.18e-02 2.89e-02 2.57e-02 2.05e-02 2.27e-02 2.36e-02 2.10e-02
1 33 2.35e-02 2.17e-02 2.14e-02 2.18e-02 2.52e-02 3.19e-02 2.69e-02 3.37e-02
1 41 3.90e-02 4.06e-02 4.43e-02 5.14e-02 5.56e-02 5.86e-02 6.58e-02 7.30e-02
1 49 8.69e-02 9.99e-02 1.31e-01 1.60e-01 1.54e-01 1.27e-01 9.71e-02 0.00E+00
2 1 1.06e-02 1.18e-02 1.15e-02 1.35e-02 1.55e-02 1.17e-02 2.33e-02 2.33e-02
2 9 3.00e-02 3.02e-02 3.23e-02 3.85e-02 3.29e-02 3.55e-02 2.98e-02 2.11e-02
2 17 2.29e-02 2.22e-02 2.66e-02 2.07e-02 1.82e-02 1.23e-02 2.16e-02 2.53e-02
2 25 2.78e-02 2.10e-02 2.59e-02 2.18e-02 1.87e-02 2.12e-02 2.21e-02 2.06e-02
2 33 2.03e-02 2.15e-02 2.14e-02 2.17e-02 2.36e-02 3.01e-02 2.61e-02 3.40e-02
2 41 3.62e-02 4.02e-02 4.40e-02 4.88e-02 5.35e-02 6.04e-02 6.71e-02 7.79e-02
2 49 9.29e-02 1.13e-01 1.34e-01 1.36e-01 1.17e-01 1.06e-01 0.00e+00 0.00E+00
3 1 1.03e-02 1.22e-02 1.24e-02 1.46e-02 1.55e-02 1.34e-02 2.45e-02 2.51e-02
3 9 2.74e-02 2.90e-02 3.48e-02 3.20e-02 3.47e-02 3.33e-02 2.44e-02 1.96e-02
3 17 2.20e-02 2.20e-02 2.33e-02 1.78e-02 1.61e-02 1.27e-02 2.11e-02 2.44e-02
3 25 2.72e-02 1.84e-02 2.30e-02 2.10e-02 1.82e-02 2.13e-02 2.06e-02 1.99e-02
3 33 2.13e-02 2.03e-02 2.03e-02 1.97e-02 2.31e-02 3.04e-02 2.51e-02 3.14e-02
3 41 3.75e-02 3.94e-02 4.38e-02 5.01e-02 5.77e-02 6.28e-02 7.34e-02 8.40e-02
3 49 9.98e-02 1.17e-01 1.23e-01 1.04e-01 9.77e-02 2.71e-02 0.00e+00 0.00E+00
4 1 1.22e-02 1.20e-02 1.25e-02 1.48e-02 1.71e-02 1.40e-02 2.56e-02 2.67e-02
4 9 2.41e-02 2.84e-02 3.43e-02 3.37e-02 3.47e-02 3.12e-02 2.16e-02 1.85e-02
4 17 2.14e-02 2.18e-02 2.32e-02 1.74e-02 1.56e-02 1.23e-02 1.94e-02 2.34e-02
4 25 2.77e-02 1.62e-02 2.16e-02 2.10e-02 1.85e-02 1.99e-02 1.97e-02 2.00e-02
4 33 2.04e-02 2.03e-02 1.91e-02 1.99e-02 2.19e-02 2.82e-02 2.47e-02 3.19e-02
4 41 3.84e-02 4.17e-02 4.48e-02 5.23e-02 5.88e-02 6.71e-02 7.75e-02 9.26e-02
4 49 1.02e-01 1.18e-01 9.66e-02 9.26e-02 8.05e-02 0.00e+00 0.00e+00 0.00E+00
5 1 1.20e-02 1.28e-02 1.30e-02 1.54e-02 1.60e-02 1.50e-02 2.42e-02 2.64e-02
5 9 2.37e-02 2.98e-02 3.17e-02 3.22e-02 3.08e-02 2.42e-02 1.82e-02 1.62e-02
5 17 1.99e-02 1.98e-02 2.10e-02 1.64e-02 1.50e-02 1.08e-02 2.00e-02 2.41e-02
5 25 2.64e-02 1.77e-02 1.99e-02 1.96e-02 1.95e-02 1.93e-02 1.94e-02 1.77e-02
5 33 2.02e-02 1.83e-02 1.87e-02 1.96e-02 2.21e-02 2.71e-02 2.34e-02 3.07e-02
5 41 3.58e-02 4.05e-02 4.32e-02 5.41e-02 6.13e-02 7.02e-02 8.13e-02 9.33e-02
5 49 1.05e-01 9.46e-02 8.40e-02 8.05e-02 0.00e+00 0.00e+00 0.00e+00 0.00E+00
6 1 1.14e-02 1.07e-02 1.26e-02 1.51e-02 1.45e-02 1.67e-02 2.44e-02 2.20e-02
6 9 2.39e-02 3.08e-02 3.33e-02 3.32e-02 2.70e-02 2.18e-02 1.62e-02 1.53e-02
6 17 1.96e-02 1.85e-02 2.01e-02 1.64e-02 1.42e-02 1.09e-02 1.84e-02 2.15e-02
6 25 2.41e-02 1.53e-02 2.00e-02 1.81e-02 1.65e-02 1.89e-02 1.95e-02 1.77e-02
6 33 1.92e-02 1.84e-02 1.90e-02 1.87e-02 2.08e-02 2.68e-02 2.32e-02 3.20e-02
6 41 3.40e-02 3.94e-02 4.46e-02 5.65e-02 6.50e-02 7.71e-02 8.44e-02 9.48e-02
6 49 9.34e-02 7.90e-02 7.52e-02 4.96e-02 0.00e+00 0.00e+00 0.00e+00 0.00E+00
7 1 2.15e-02 2.07e-02 2.65e-02 2.88e-02 3.02e-02 3.01e-02 4.12e-02 4.53e-02
7 9 4.92e-02 5.80e-02 6.27e-02 6.06e-02 4.68e-02 3.59e-02 2.72e-02 2.66e-02
7 17 3.58e-02 3.68e-02 3.53e-02 3.17e-02 2.97e-02 1.87e-02 3.84e-02 4.31e-02
7 25 4.83e-02 2.82e-02 3.73e-02 3.59e-02 3.55e-02 3.86e-02 3.83e-02 3.54e-02
7 33 3.57e-02 3.81e-02 3.40e-02 3.74e-02 4.37e-02 5.51e-02 4.77e-02 6.45e-02
7 41 7.20e-02 8.21e-02 9.37e-02 1.20e-01 1.41e-01 1.57e-01 1.73e-01 1.66e-01
7 49 1.44e-01 1.39e-01 9.89e-02 0.00e+00 0.00e+00 0.00e+00 0.00e+00 0.00E+00
8 1 2.13e-02 2.12e-02 2.60e-02 2.59e-02 2.62e-02 2.97e-02 3.57e-02 4.68e-02
8 9 4.97e-02 5.24e-02 6.43e-02 4.70e-02 3.92e-02 3.04e-02 2.56e-02 2.45e-02
8 17 3.24e-02 3.43e-02 3.27e-02 2.90e-02 2.66e-02 1.84e-02 3.61e-02 4.05e-02

8 25 4.14e-02 2.62e-02 3.34e-02 3.49e-02 3.15e-02 3.52e-02 3.59e-02 3.34e-02
8 33 3.51e-02 3.51e-02 3.42e-02 3.66e-02 4.32e-02 5.37e-02 4.74e-02 6.20e-02
8 41 7.26e-02 8.53e-02 1.00e-01 1.27e-01 1.41e-01 1.55e-01 1.40e-01 1.24e-01
8 49 1.19e-01 8.68e-02 0.00e+00 0.00e+00 0.00e+00 0.00e+00 0.00e+00 0.00E+00
9 1 1.97e-02 1.79e-02 2.20e-02 2.22e-02 2.78e-02 2.58e-02 3.42e-02 5.39e-02
9 9 4.35e-02 5.02e-02 5.51e-02 3.94e-02 3.30e-02 2.40e-02 2.06e-02 2.34e-02
9 17 3.17e-02 3.13e-02 3.00e-02 2.92e-02 2.45e-02 1.64e-02 3.34e-02 3.69e-02
9 25 3.85e-02 2.44e-02 3.12e-02 3.24e-02 3.03e-02 3.45e-02 3.38e-02 3.31e-02
9 33 3.59e-02 3.47e-02 3.48e-02 3.58e-02 4.16e-02 5.34e-02 4.75e-02 6.08e-02
9 41 7.53e-02 9.04e-02 1.08e-01 1.28e-01 1.36e-01 1.21e-01 1.11e-01 1.05e-01
9 49 8.46e-02 0.00e+00 0.00e+00 0.00e+00 0.00e+00 0.00e+00 0.00e+00 0.00E+00
10 1 1.81e-02 1.88e-02 2.03e-02 2.07e-02 2.65e-02 2.74e-02 3.68e-02 5.81e-02
10 9 4.08e-02 5.36e-02 4.37e-02 3.39e-02 2.74e-02 2.19e-02 2.09e-02 2.21e-02
10 17 2.89e-02 2.72e-02 2.86e-02 2.79e-02 2.48e-02 1.77e-02 3.29e-02 3.69e-02
10 25 3.66e-02 2.30e-02 3.13e-02 3.41e-02 3.12e-02 3.50e-02 3.52e-02 3.18e-02
10 33 3.38e-02 3.68e-02 3.37e-02 3.52e-02 4.15e-02 5.37e-02 4.92e-02 6.78e-02
10 41 7.95e-02 9.97e-02 1.08e-01 1.24e-01 1.09e-01 1.03e-01 1.01e-01 7.88e-02
10 49 0.00e+00 0.00e+00 0.00e+00 0.00e+00 0.00e+00 0.00e+00 0.00e+00 0.00E+00
11 1 1.58e-02 1.79e-02 1.92e-02 1.89e-02 2.58e-02 2.58e-02 3.52e-02 3.79e-02
11 9 3.99e-02 4.85e-02 3.67e-02 2.81e-02 2.23e-02 1.96e-02 1.82e-02 1.97e-02
11 17 2.70e-02 2.71e-02 2.74e-02 2.51e-02 2.08e-02 1.61e-02 3.20e-02 3.28e-02
11 25 3.55e-02 2.09e-02 3.00e-02 3.08e-02 2.94e-02 3.37e-02 3.33e-02 2.91e-02
11 33 3.45e-02 3.51e-02 3.35e-02 3.53e-02 4.13e-02 5.34e-02 4.98e-02 6.61e-02
11 41 8.32e-02 1.00e-01 1.08e-01 1.00e-01 9.36e-02 8.96e-02 7.66e-02 0.00e+00
11 49 0.00e+00 0.00e+00 0.00e+00 0.00e+00 0.00e+00 0.00e+00 0.00e+00 0.00E+00
12 1 1.51e-02 1.87e-02 1.88e-02 2.07e-02 2.53e-02 2.34e-02 3.46e-02 4.10e-02
12 9 4.71e-02 3.87e-02 3.21e-02 2.49e-02 2.02e-02 1.71e-02 1.75e-02 1.82e-02
12 17 2.50e-02 2.61e-02 2.59e-02 2.47e-02 2.18e-02 1.62e-02 3.24e-02 3.35e-02
12 25 3.60e-02 2.00e-02 2.98e-02 3.19e-02 2.86e-02 3.30e-02 3.31e-02 2.87e-02
12 33 3.25e-02 3.18e-02 3.41e-02 3.51e-02 3.94e-02 5.42e-02 4.92e-02 6.87e-02
12 41 8.78e-02 9.85e-02 9.23e-02 8.52e-02 8.43e-02 8.24e-02 0.00e+00 0.00e+00
12 49 0.00e+00 0.00e+00 0.00e+00 0.00e+00 0.00e+00 0.00e+00 0.00e+00 0.00E+00
13 1 1.39e-02 1.59e-02 1.90e-02 1.89e-02 2.43e-02 2.58e-02 3.58e-02 3.74e-02
13 9 4.73e-02 3.33e-02 2.91e-02 2.17e-02 1.81e-02 1.76e-02 1.65e-02 2.03e-02
13 17 2.36e-02 2.27e-02 2.56e-02 2.58e-02 2.08e-02 1.68e-02 2.86e-02 3.46e-02
13 25 3.19e-02 1.88e-02 2.98e-02 2.79e-02 2.88e-02 3.17e-02 3.18e-02 2.97e-02
13 33 3.37e-02 3.33e-02 3.30e-02 3.55e-02 4.08e-02 5.67e-02 5.18e-02 7.27e-02
13 41 8.71e-02 1.02e-01 7.62e-02 8.15e-02 8.11e-02 0.00e+00 0.00e+00 0.00e+00
13 49 0.00e+00 0.00e+00 0.00e+00 0.00e+00 0.00e+00 0.00e+00 0.00e+00 0.00E+00
14 1 1.34e-02 1.63e-02 1.44e-02 1.67e-02 2.62e-02 2.92e-02 4.30e-02 3.61e-02
14 9 3.85e-02 2.83e-02 2.45e-02 1.77e-02 1.69e-02 1.56e-02 1.53e-02 1.82e-02
14 17 2.23e-02 2.19e-02 2.59e-02 2.44e-02 2.02e-02 1.62e-02 2.66e-02 3.15e-02
14 25 2.96e-02 2.00e-02 2.62e-02 2.95e-02 2.68e-02 2.93e-02 3.14e-02 2.90e-02
14 33 3.24e-02 3.29e-02 3.33e-02 3.51e-02 4.19e-02 5.54e-02 4.98e-02 7.22e-02
14 41 8.71e-02 8.31e-02 7.02e-02 7.50e-02 1.23e-02 0.00e+00 0.00e+00 0.00e+00
14 49 0.00e+00 0.00e+00 0.00e+00 0.00e+00 0.00e+00 0.00e+00 0.00e+00 0.00E+00
15 1 2.16e-02 3.34e-02 2.70e-02 3.12e-02 4.51e-02 4.42e-02 8.14e-02 6.22e-02
15 9 4.86e-02 4.08e-02 3.12e-02 2.68e-02 2.60e-02 2.47e-02 2.40e-02 2.82e-02
15 17 3.46e-02 3.40e-02 4.64e-02 3.56e-02 3.56e-02 2.49e-02 4.53e-02 4.85e-02
15 25 4.72e-02 3.20e-02 4.59e-02 4.65e-02 4.61e-02 5.35e-02 5.20e-02 4.90e-02
15 33 5.49e-02 5.53e-02 5.49e-02 5.92e-02 7.11e-02 9.77e-02 8.92e-02 1.23e-01
15 41 1.35e-01 1.15e-01 1.07e-01 4.37e-02 0.00e+00 0.00e+00 0.00e+00 0.00e+00
15 49 0.00e+00 0.00e+00 0.00e+00 0.00e+00 0.00e+00 0.00e+00 0.00e+00 0.00E+00
16 1 2.33e-02 2.48e-02 2.63e-02 3.38e-02 3.68e-02 4.99e-02 9.74e-02 5.50e-02

16 9 3.51e-02 3.30e-02 2.82e-02 2.19e-02 2.31e-02 2.22e-02 2.30e-02 2.65e-02
16 17 3.44e-02 3.57e-02 5.01e-02 3.74e-02 3.31e-02 2.44e-02 4.37e-02 4.84e-02
16 25 4.52e-02 2.88e-02 4.31e-02 4.78e-02 4.47e-02 5.01e-02 5.13e-02 4.82e-02
16 33 5.41e-02 5.64e-02 5.84e-02 6.11e-02 7.38e-02 1.03e-01 8.93e-02 1.19e-01
16 41 1.06e-01 1.05e-01 5.93e-02 0.00e+00 0.00e+00 0.00e+00 0.00e+00 0.00e+00
16 49 0.00e+00 0.00e+00 0.00e+00 0.00e+00 0.00e+00 0.00e+00 0.00e+00 0.00E+00
17 1 2.38e-02 2.71e-02 3.03e-02 3.91e-02 4.24e-02 5.41e-02 5.20e-02 3.94e-02
17 9 3.20e-02 2.69e-02 2.27e-02 2.21e-02 2.21e-02 2.34e-02 2.35e-02 2.48e-02
17 17 3.38e-02 3.81e-02 5.49e-02 3.48e-02 3.32e-02 2.33e-02 4.23e-02 4.66e-02
17 25 4.56e-02 3.06e-02 4.28e-02 4.57e-02 4.61e-02 5.27e-02 5.25e-02 4.95e-02
17 33 5.43e-02 5.66e-02 5.62e-02 6.11e-02 7.67e-02 1.05e-01 8.61e-02 9.49e-02
17 41 9.58e-02 9.78e-02 0.00e+00 0.00e+00 0.00e+00 0.00e+00 0.00e+00 0.00e+00
17 49 0.00e+00 0.00e+00 0.00e+00 0.00e+00 0.00e+00 0.00e+00 0.00e+00 0.00E+00
18 1 2.47e-02 2.75e-02 3.02e-02 4.39e-02 4.53e-02 6.18e-02 4.35e-02 2.92e-02
18 9 2.64e-02 2.10e-02 2.13e-02 2.04e-02 2.19e-02 2.10e-02 2.40e-02 2.31e-02
18 17 3.24e-02 3.82e-02 5.26e-02 3.39e-02 3.23e-02 2.25e-02 3.99e-02 4.65e-02
18 25 4.39e-02 3.15e-02 4.49e-02 4.75e-02 4.38e-02 5.11e-02 5.21e-02 4.93e-02
18 33 5.55e-02 5.93e-02 5.93e-02 6.21e-02 7.59e-02 1.07e-01 7.27e-02 8.70e-02
18 41 9.03e-02 0.00e+00 0.00e+00 0.00e+00 0.00e+00 0.00e+00 0.00e+00 0.00e+00
18 49 0.00e+00 0.00e+00 0.00e+00 0.00e+00 0.00e+00 0.00e+00 0.00e+00 0.00E+00
19 1 2.78e-02 2.52e-02 3.58e-02 4.96e-02 4.88e-02 6.10e-02 4.09e-02 2.57e-02
19 9 2.38e-02 2.06e-02 2.00e-02 2.02e-02 2.03e-02 2.17e-02 2.35e-02 2.54e-02
19 17 3.28e-02 3.76e-02 2.75e-02 3.45e-02 3.27e-02 2.19e-02 3.83e-02 4.50e-02
19 25 4.26e-02 3.11e-02 4.16e-02 4.45e-02 4.63e-02 5.43e-02 5.16e-02 5.02e-02
19 33 5.66e-02 6.22e-02 6.40e-02 6.50e-02 7.89e-02 9.17e-02 6.48e-02 8.16e-02
19 41 5.78e-02 0.00e+00 0.00e+00 0.00e+00 0.00e+00 0.00e+00 0.00e+00 0.00e+00
19 49 0.00e+00 0.00e+00 0.00e+00 0.00e+00 0.00e+00 0.00e+00 0.00e+00 0.00E+00
20 1 2.90e-02 2.94e-02 3.60e-02 5.79e-02 5.03e-02 6.52e-02 3.91e-02 3.30e-02
20 9 1.84e-02 1.81e-02 2.13e-02 2.01e-02 1.97e-02 2.12e-02 2.36e-02 2.46e-02
20 17 3.13e-02 4.03e-02 2.70e-02 3.40e-02 2.99e-02 2.02e-02 3.84e-02 4.71e-02
20 25 4.45e-02 2.95e-02 4.39e-02 4.54e-02 4.59e-02 5.11e-02 5.25e-02 5.20e-02
20 33 5.94e-02 6.39e-02 6.23e-02 6.52e-02 7.05e-02 8.03e-02 5.94e-02 7.57e-02
20 41 0.00e+00 0.00e+00 0.00e+00 0.00e+00 0.00e+00 0.00e+00 0.00e+00 0.00e+00
20 49 0.00e+00 0.00e+00 0.00e+00 0.00e+00 0.00e+00 0.00e+00 0.00e+00 0.00E+00
21 1 2.62e-02 3.13e-02 4.08e-02 4.69e-02 4.84e-02 7.47e-02 2.33e-02 2.08e-02
21 9 1.78e-02 1.79e-02 1.86e-02 1.93e-02 1.90e-02 2.07e-02 1.98e-02 2.50e-02
21 17 3.40e-02 4.15e-02 2.67e-02 3.20e-02 2.88e-02 1.98e-02 3.72e-02 4.23e-02
21 25 4.46e-02 3.01e-02 4.27e-02 4.55e-02 4.40e-02 5.26e-02 5.24e-02 5.23e-02
21 33 5.85e-02 6.28e-02 5.97e-02 6.55e-02 6.07e-02 7.57e-02 5.65e-02 2.11e-02
21 41 0.00e+00 0.00e+00 0.00e+00 0.00e+00 0.00e+00 0.00e+00 0.00e+00 0.00e+00
21 49 0.00e+00 0.00e+00 0.00e+00 0.00e+00 0.00e+00 0.00e+00 0.00e+00 0.00E+00
22 1 2.78e-02 3.28e-02 4.36e-02 5.11e-02 4.25e-02 2.65e-02 1.90e-02 1.76e-02
22 9 1.63e-02 1.83e-02 1.84e-02 1.73e-02 1.77e-02 2.06e-02 2.16e-02 2.39e-02
22 17 3.47e-02 3.57e-02 2.49e-02 3.18e-02 2.68e-02 2.01e-02 3.57e-02 4.35e-02
22 25 4.50e-02 3.09e-02 4.54e-02 4.62e-02 4.61e-02 5.30e-02 5.56e-02 5.19e-02
22 33 6.22e-02 6.31e-02 6.14e-02 5.41e-02 5.48e-02 7.07e-02 4.61e-02 0.00e+00
22 41 0.00e+00 0.00e+00 0.00e+00 0.00e+00 0.00e+00 0.00e+00 0.00e+00 0.00e+00
22 49 0.00e+00 0.00e+00 0.00e+00 0.00e+00 0.00e+00 0.00e+00 0.00e+00 0.00E+00
23 1 3.33e-02 3.67e-02 4.71e-02 4.01e-02 3.76e-02 2.19e-02 1.94e-02 1.61e-02
23 9 1.46e-02 1.64e-02 1.64e-02 1.70e-02 1.75e-02 1.95e-02 1.96e-02 2.34e-02
23 17 3.35e-02 2.52e-02 2.54e-02 2.99e-02 2.67e-02 1.89e-02 3.54e-02 4.21e-02
23 25 4.00e-02 2.81e-02 4.37e-02 4.54e-02 4.43e-02 5.30e-02 5.53e-02 5.35e-02
23 33 6.33e-02 6.36e-02 5.70e-02 4.99e-02 5.49e-02 6.70e-02 0.00e+00 0.00e+00
23 41 0.00e+00 0.00e+00 0.00e+00 0.00e+00 0.00e+00 0.00e+00 0.00e+00 0.00e+00

23 49 0.00e+00 0.00e+00 0.00e+00 0.00e+00 0.00e+00 0.00e+00 0.00e+00 0.00E+00
24 1 3.20e-02 3.84e-02 5.15e-02 3.67e-02 3.63e-02 1.80e-02 1.69e-02 1.48e-02
24 9 1.48e-02 1.52e-02 1.64e-02 1.55e-02 1.72e-02 1.92e-02 2.03e-02 2.32e-02
24 17 3.42e-02 2.58e-02 2.30e-02 3.11e-02 2.57e-02 1.81e-02 3.53e-02 4.23e-02
24 25 4.21e-02 2.94e-02 4.32e-02 4.65e-02 4.54e-02 5.34e-02 5.80e-02 5.67e-02
24 33 6.13e-02 6.27e-02 4.87e-02 4.50e-02 4.98e-02 3.56e-02 0.00e+00 0.00e+00
24 41 0.00e+00 0.00e+00 0.00e+00 0.00e+00 0.00e+00 0.00e+00 0.00e+00 0.00e+00
24 49 0.00e+00 0.00e+00 0.00e+00 0.00e+00 0.00e+00 0.00e+00 0.00e+00 0.00E+00
25 1 5.79e-02 6.86e-02 9.08e-02 5.16e-02 7.00e-02 2.57e-02 2.82e-02 2.33e-02
25 9 2.48e-02 2.74e-02 2.66e-02 2.79e-02 3.08e-02 3.36e-02 3.62e-02 4.10e-02
25 17 6.01e-02 4.56e-02 4.14e-02 4.96e-02 4.22e-02 3.10e-02 6.29e-02 7.34e-02
25 25 7.84e-02 4.98e-02 7.63e-02 8.02e-02 8.43e-02 9.60e-02 1.03e-01 1.04e-01
25 33 1.09e-01 8.97e-02 7.76e-02 7.37e-02 5.98e-02 0.00e+00 0.00e+00 0.00e+00
25 41 0.00e+00 0.00e+00 0.00e+00 0.00e+00 0.00e+00 0.00e+00 0.00e+00 0.00e+00
25 49 0.00e+00 0.00e+00 0.00e+00 0.00e+00 0.00e+00 0.00e+00 0.00e+00 0.00E+00
26 1 5.88e-02 7.22e-02 6.22e-02 4.61e-02 3.87e-02 3.44e-02 3.54e-02 2.19e-02
26 9 2.23e-02 2.47e-02 2.57e-02 2.64e-02 3.16e-02 3.37e-02 3.32e-02 4.20e-02
26 17 4.43e-02 4.00e-02 3.89e-02 4.72e-02 4.10e-02 2.99e-02 6.12e-02 7.59e-02
26 25 7.11e-02 5.11e-02 7.48e-02 8.57e-02 8.27e-02 1.02e-01 1.06e-01 1.06e-01
26 33 8.87e-02 7.66e-02 7.17e-02 5.20e-02 0.00e+00 0.00e+00 0.00e+00 0.00e+00
26 41 0.00e+00 0.00e+00 0.00e+00 0.00e+00 0.00e+00 0.00e+00 0.00e+00 0.00e+00
26 49 0.00e+00 0.00e+00 0.00e+00 0.00e+00 0.00e+00 0.00e+00 0.00e+00 0.00E+00
27 1 6.53e-02 6.12e-02 5.17e-02 4.60e-02 2.90e-02 1.83e-02 1.94e-02 1.94e-02
27 9 2.20e-02 2.40e-02 2.62e-02 2.84e-02 3.02e-02 3.39e-02 3.42e-02 3.72e-02
27 17 4.19e-02 4.04e-02 3.78e-02 4.75e-02 3.93e-02 2.97e-02 6.14e-02 7.38e-02
27 25 7.13e-02 5.36e-02 7.98e-02 8.44e-02 8.67e-02 1.03e-01 1.09e-01 8.67e-02
27 33 7.73e-02 7.12e-02 5.27e-02 0.00e+00 0.00e+00 0.00e+00 0.00e+00 0.00e+00
27 41 0.00e+00 0.00e+00 0.00e+00 0.00e+00 0.00e+00 0.00e+00 0.00e+00 0.00e+00
27 49 0.00e+00 0.00e+00 0.00e+00 0.00e+00 0.00e+00 0.00e+00 0.00e+00 0.00E+00
28 1 5.40e-02 6.79e-02 4.35e-02 4.23e-02 1.98e-02 1.91e-02 2.07e-02 1.82e-02
28 9 2.02e-02 2.18e-02 2.33e-02 2.68e-02 2.92e-02 2.94e-02 3.23e-02 4.12e-02
28 17 4.05e-02 4.04e-02 3.71e-02 4.33e-02 3.93e-02 2.82e-02 6.06e-02 7.22e-02
28 25 7.63e-02 5.41e-02 7.84e-02 8.64e-02 9.22e-02 1.06e-01 9.80e-02 7.68e-02
28 33 7.21e-02 5.93e-02 0.00e+00 0.00e+00 0.00e+00 0.00e+00 0.00e+00 0.00e+00
28 41 0.00e+00 0.00e+00 0.00e+00 0.00e+00 0.00e+00 0.00e+00 0.00e+00 0.00e+00
28 49 0.00e+00 0.00e+00 0.00e+00 0.00e+00 0.00e+00 0.00e+00 0.00e+00 0.00E+00
29 1 5.13e-02 4.72e-02 3.57e-02 4.42e-02 1.72e-02 1.74e-02 1.91e-02 1.91e-02
29 9 2.06e-02 2.06e-02 2.34e-02 2.74e-02 2.84e-02 3.14e-02 3.17e-02 3.26e-02
29 17 3.81e-02 3.50e-02 3.50e-02 4.71e-02 4.03e-02 2.91e-02 6.15e-02 7.58e-02
29 25 7.61e-02 5.51e-02 8.28e-02 9.09e-02 9.41e-02 1.05e-01 8.40e-02 7.05e-02
29 33 6.76e-02 0.00e+00 0.00e+00 0.00e+00 0.00e+00 0.00e+00 0.00e+00 0.00e+00
29 41 0.00e+00 0.00e+00 0.00e+00 0.00e+00 0.00e+00 0.00e+00 0.00e+00 0.00e+00
29 49 0.00e+00 0.00e+00 0.00e+00 0.00e+00 0.00e+00 0.00e+00 0.00e+00 0.00E+00
30 1 4.87e-02 3.57e-02 3.05e-02 2.10e-02 2.03e-02 1.98e-02 1.70e-02 1.83e-02
30 9 1.92e-02 2.02e-02 2.27e-02 2.70e-02 2.81e-02 3.02e-02 3.40e-02 3.40e-02
30 17 4.11e-02 3.57e-02 3.64e-02 4.61e-02 3.89e-02 2.94e-02 6.27e-02 7.75e-02
30 25 8.03e-02 5.65e-02 8.14e-02 9.68e-02 9.29e-02 8.98e-02 7.81e-02 6.94e-02
30 33 0.00e+00 0.00e+00 0.00e+00 0.00e+00 0.00e+00 0.00e+00 0.00e+00 0.00e+00
30 41 0.00e+00 0.00e+00 0.00e+00 0.00e+00 0.00e+00 0.00e+00 0.00e+00 0.00e+00
30 49 0.00e+00 0.00e+00 0.00e+00 0.00e+00 0.00e+00 0.00e+00 0.00e+00 0.00E+00
31 1 4.55e-02 3.64e-02 3.28e-02 2.11e-02 1.72e-02 2.35e-02 1.78e-02 1.73e-02
31 9 1.85e-02 2.03e-02 2.20e-02 2.53e-02 2.93e-02 3.09e-02 3.18e-02 3.23e-02
31 17 3.80e-02 3.62e-02 3.84e-02 4.61e-02 3.91e-02 3.08e-02 6.40e-02 7.73e-02
31 25 7.79e-02 5.76e-02 8.29e-02 9.49e-02 8.51e-02 8.32e-02 7.38e-02 5.71e-02

31 33 0.00e+00 0.00e+00 0.00e+00 0.00e+00 0.00e+00 0.00e+00 0.00e+00 0.00e+00
31 41 0.00e+00 0.00e+00 0.00e+00 0.00e+00 0.00e+00 0.00e+00 0.00e+00 0.00e+00
31 49 0.00e+00 0.00e+00 0.00e+00 0.00e+00 0.00e+00 0.00e+00 0.00e+00 0.00E+00
32 1 3.88e-02 3.40e-02 3.70e-02 2.19e-02 1.56e-02 1.60e-02 1.74e-02 1.86e-02
32 9 1.89e-02 1.99e-02 2.27e-02 2.44e-02 2.99e-02 3.12e-02 3.00e-02 3.22e-02
32 17 3.77e-02 3.63e-02 3.65e-02 4.44e-02 3.96e-02 3.13e-02 6.73e-02 8.29e-02
32 25 8.50e-02 5.89e-02 8.92e-02 9.38e-02 7.53e-02 7.97e-02 7.47e-02 0.00e+00
32 33 0.00e+00 0.00e+00 0.00e+00 0.00e+00 0.00e+00 0.00e+00 0.00e+00 0.00e+00
32 41 0.00e+00 0.00e+00 0.00e+00 0.00e+00 0.00e+00 0.00e+00 0.00e+00 0.00e+00
32 49 0.00e+00 0.00e+00 0.00e+00 0.00e+00 0.00e+00 0.00e+00 0.00e+00 0.00E+00
33 1 2.99e-02 2.90e-02 2.72e-02 1.49e-02 1.40e-02 1.57e-02 1.75e-02 1.74e-02
33 9 1.76e-02 1.96e-02 2.09e-02 2.63e-02 2.76e-02 2.75e-02 2.93e-02 3.16e-02
33 17 3.83e-02 3.65e-02 3.61e-02 4.43e-02 4.29e-02 3.09e-02 6.99e-02 8.39e-02
33 25 8.70e-02 5.72e-02 8.85e-02 8.15e-02 7.17e-02 7.46e-02 3.55e-02 0.00e+00
33 33 0.00e+00 0.00e+00 0.00e+00 0.00e+00 0.00e+00 0.00e+00 0.00e+00 0.00e+00
33 41 0.00e+00 0.00e+00 0.00e+00 0.00e+00 0.00e+00 0.00e+00 0.00e+00 0.00e+00
33 49 0.00e+00 0.00e+00 0.00e+00 0.00e+00 0.00e+00 0.00e+00 0.00e+00 0.00E+00
34 1 3.10e-02 2.60e-02 1.83e-02 1.46e-02 1.41e-02 1.47e-02 1.77e-02 1.77e-02
34 9 1.60e-02 1.93e-02 2.30e-02 2.45e-02 2.88e-02 3.07e-02 2.82e-02 3.20e-02
34 17 3.60e-02 3.79e-02 3.50e-02 4.38e-02 4.05e-02 3.18e-02 6.72e-02 8.38e-02
34 25 8.69e-02 6.03e-02 7.91e-02 7.75e-02 7.17e-02 7.25e-02 0.00e+00 0.00e+00
34 33 0.00e+00 0.00e+00 0.00e+00 0.00e+00 0.00e+00 0.00e+00 0.00e+00 0.00e+00
34 41 0.00e+00 0.00e+00 0.00e+00 0.00e+00 0.00e+00 0.00e+00 0.00e+00 0.00e+00
34 49 0.00e+00 0.00e+00 0.00e+00 0.00e+00 0.00e+00 0.00e+00 0.00e+00 0.00E+00
35 1 5.26e-02 5.52e-02 2.86e-02 3.28e-02 3.28e-02 2.93e-02 3.07e-02 3.33e-02
35 9 3.49e-02 3.74e-02 4.56e-02 4.69e-02 5.31e-02 5.20e-02 5.47e-02 5.75e-02
35 17 7.26e-02 6.81e-02 6.79e-02 8.69e-02 7.99e-02 6.17e-02 1.39e-01 1.67e-01
35 25 1.74e-01 1.05e-01 1.35e-01 1.39e-01 1.17e-01 0.00e+00 0.00e+00 0.00e+00
35 33 0.00e+00 0.00e+00 0.00e+00 0.00e+00 0.00e+00 0.00e+00 0.00e+00 0.00e+00
35 41 0.00e+00 0.00e+00 0.00e+00 0.00e+00 0.00e+00 0.00e+00 0.00e+00 0.00e+00
35 49 0.00e+00 0.00e+00 0.00e+00 0.00e+00 0.00e+00 0.00e+00 0.00e+00 0.00E+00
36 1 4.57e-02 3.42e-02 2.98e-02 2.84e-02 2.38e-02 2.89e-02 3.03e-02 2.92e-02
36 9 3.28e-02 3.61e-02 4.34e-02 4.72e-02 5.21e-02 5.39e-02 5.57e-02 5.58e-02
36 17 7.15e-02 6.98e-02 6.77e-02 9.02e-02 8.16e-02 6.60e-02 1.47e-01 1.75e-01
36 25 1.58e-01 9.01e-02 1.30e-01 1.04e-01 0.00e+00 0.00e+00 0.00e+00 0.00e+00
36 33 0.00e+00 0.00e+00 0.00e+00 0.00e+00 0.00e+00 0.00e+00 0.00e+00 0.00e+00
36 41 0.00e+00 0.00e+00 0.00e+00 0.00e+00 0.00e+00 0.00e+00 0.00e+00 0.00e+00
36 49 0.00e+00 0.00e+00 0.00e+00 0.00e+00 0.00e+00 0.00e+00 0.00e+00 0.00E+00
37 1 4.50e-02 2.64e-02 2.44e-02 2.59e-02 2.69e-02 2.70e-02 3.20e-02 3.01e-02
37 9 3.08e-02 3.92e-02 4.41e-02 4.56e-02 5.13e-02 5.09e-02 5.25e-02 5.67e-02
37 17 6.97e-02 6.77e-02 7.13e-02 9.39e-02 8.52e-02 6.53e-02 1.49e-01 1.54e-01
37 25 1.44e-01 8.36e-02 7.92e-02 0.00e+00 0.00e+00 0.00e+00 0.00e+00 0.00e+00
37 33 0.00e+00 0.00e+00 0.00e+00 0.00e+00 0.00e+00 0.00e+00 0.00e+00 0.00e+00
37 41 0.00e+00 0.00e+00 0.00e+00 0.00e+00 0.00e+00 0.00e+00 0.00e+00 0.00e+00
37 49 0.00e+00 0.00e+00 0.00e+00 0.00e+00 0.00e+00 0.00e+00 0.00e+00 0.00E+00
38 1 2.88e-02 2.74e-02 2.77e-02 2.83e-02 2.41e-02 2.54e-02 2.82e-02 2.89e-02
38 9 3.00e-02 3.64e-02 4.21e-02 4.26e-02 4.60e-02 4.75e-02 5.03e-02 5.50e-02
38 17 6.63e-02 6.72e-02 6.72e-02 9.86e-02 8.74e-02 6.56e-02 1.32e-01 1.35e-01
38 25 1.31e-01 4.71e-02 0.00e+00 0.00e+00 0.00e+00 0.00e+00 0.00e+00 0.00e+00
38 33 0.00e+00 0.00e+00 0.00e+00 0.00e+00 0.00e+00 0.00e+00 0.00e+00 0.00e+00
38 41 0.00e+00 0.00e+00 0.00e+00 0.00e+00 0.00e+00 0.00e+00 0.00e+00 0.00e+00
38 49 0.00e+00 0.00e+00 0.00e+00 0.00e+00 0.00e+00 0.00e+00 0.00e+00 0.00E+00
39 1 2.26e-02 2.49e-02 2.36e-02 2.29e-02 2.48e-02 2.51e-02 2.81e-02 2.58e-02
39 9 2.97e-02 3.38e-02 3.95e-02 4.20e-02 4.49e-02 5.20e-02 5.02e-02 5.19e-02

39 17 7.09e-02 6.80e-02 7.37e-02 9.72e-02 8.77e-02 5.94e-02 1.12e-01 1.26e-01
39 25 6.87e-02 0.00e+00 0.00e+00 0.00e+00 0.00e+00 0.00e+00 0.00e+00 0.00e+00
39 33 0.00e+00 0.00e+00 0.00e+00 0.00e+00 0.00e+00 0.00e+00 0.00e+00 0.00e+00
39 41 0.00e+00 0.00e+00 0.00e+00 0.00e+00 0.00e+00 0.00e+00 0.00e+00 0.00e+00
39 49 0.00e+00 0.00e+00 0.00e+00 0.00e+00 0.00e+00 0.00e+00 0.00e+00 0.00E+00
40 1 2.33e-02 2.37e-02 2.44e-02 2.40e-02 2.28e-02 2.57e-02 2.75e-02 2.82e-02
40 9 3.02e-02 3.53e-02 4.11e-02 4.28e-02 4.53e-02 5.10e-02 4.85e-02 5.40e-02
40 17 6.87e-02 7.12e-02 7.33e-02 1.02e-01 9.10e-02 5.49e-02 1.13e-01 5.74e-02
40 25 0.00e+00 0.00e+00 0.00e+00 0.00e+00 0.00e+00 0.00e+00 0.00e+00 0.00e+00
40 33 0.00e+00 0.00e+00 0.00e+00 0.00e+00 0.00e+00 0.00e+00 0.00e+00 0.00e+00
40 41 0.00e+00 0.00e+00 0.00e+00 0.00e+00 0.00e+00 0.00e+00 0.00e+00 0.00e+00
40 49 0.00e+00 0.00e+00 0.00e+00 0.00e+00 0.00e+00 0.00e+00 0.00e+00 0.00E+00
41 1 2.54e-02 2.42e-02 2.33e-02 2.31e-02 2.22e-02 2.42e-02 2.74e-02 2.76e-02
41 9 3.14e-02 3.58e-02 4.02e-02 4.10e-02 4.30e-02 4.61e-02 5.05e-02 5.59e-02
41 17 7.22e-02 7.39e-02 7.42e-02 1.04e-01 8.00e-02 4.71e-02 7.22e-02 0.00e+00
41 25 0.00e+00 0.00e+00 0.00e+00 0.00e+00 0.00e+00 0.00e+00 0.00e+00 0.00e+00
41 33 0.00e+00 0.00e+00 0.00e+00 0.00e+00 0.00e+00 0.00e+00 0.00e+00 0.00e+00
41 41 0.00e+00 0.00e+00 0.00e+00 0.00e+00 0.00e+00 0.00e+00 0.00e+00 0.00e+00
41 49 0.00e+00 0.00e+00 0.00e+00 0.00e+00 0.00e+00 0.00e+00 0.00e+00 0.00E+00
42 1 2.11e-02 2.20e-02 2.32e-02 2.03e-02 2.10e-02 2.42e-02 2.72e-02 2.73e-02
42 9 3.05e-02 3.35e-02 3.97e-02 4.13e-02 4.37e-02 4.76e-02 4.91e-02 5.61e-02
42 17 7.45e-02 7.39e-02 7.78e-02 9.12e-02 7.20e-02 4.72e-02 0.00e+00 0.00e+00
42 25 0.00e+00 0.00e+00 0.00e+00 0.00e+00 0.00e+00 0.00e+00 0.00e+00 0.00e+00
42 33 0.00e+00 0.00e+00 0.00e+00 0.00e+00 0.00e+00 0.00e+00 0.00e+00 0.00e+00
42 41 0.00e+00 0.00e+00 0.00e+00 0.00e+00 0.00e+00 0.00e+00 0.00e+00 0.00e+00
42 49 0.00e+00 0.00e+00 0.00e+00 0.00e+00 0.00e+00 0.00e+00 0.00e+00 0.00E+00
43 1 2.60e-02 2.31e-02 2.13e-02 2.04e-02 2.00e-02 2.35e-02 2.69e-02 2.71e-02
43 9 3.07e-02 3.47e-02 3.65e-02 3.75e-02 4.39e-02 4.45e-02 4.93e-02 5.63e-02
43 17 7.77e-02 7.73e-02 7.64e-02 8.21e-02 6.79e-02 1.45e-02 0.00e+00 0.00e+00
43 25 0.00e+00 0.00e+00 0.00e+00 0.00e+00 0.00e+00 0.00e+00 0.00e+00 0.00e+00
43 33 0.00e+00 0.00e+00 0.00e+00 0.00e+00 0.00e+00 0.00e+00 0.00e+00 0.00e+00
43 41 0.00e+00 0.00e+00 0.00e+00 0.00e+00 0.00e+00 0.00e+00 0.00e+00 0.00e+00
43 49 0.00e+00 0.00e+00 0.00e+00 0.00e+00 0.00e+00 0.00e+00 0.00e+00 0.00E+00
44 1 2.04e-02 2.22e-02 2.10e-02 2.12e-02 2.15e-02 2.37e-02 2.62e-02 2.67e-02
44 9 2.98e-02 3.29e-02 3.44e-02 3.93e-02 4.52e-02 4.85e-02 5.17e-02 6.00e-02
44 17 7.74e-02 8.00e-02 6.68e-02 7.68e-02 6.33e-02 0.00e+00 0.00e+00 0.00e+00
44 25 0.00e+00 0.00e+00 0.00e+00 0.00e+00 0.00e+00 0.00e+00 0.00e+00 0.00e+00
44 33 0.00e+00 0.00e+00 0.00e+00 0.00e+00 0.00e+00 0.00e+00 0.00e+00 0.00e+00
44 41 0.00e+00 0.00e+00 0.00e+00 0.00e+00 0.00e+00 0.00e+00 0.00e+00 0.00e+00
44 49 0.00e+00 0.00e+00 0.00e+00 0.00e+00 0.00e+00 0.00e+00 0.00e+00 0.00E+00
45 1 3.60e-02 3.65e-02 3.90e-02 3.60e-02 3.74e-02 4.39e-02 4.65e-02 4.84e-02
45 9 5.24e-02 5.72e-02 6.67e-02 7.13e-02 7.96e-02 9.47e-02 1.02e-01 1.09e-01
45 17 1.48e-01 1.23e-01 1.14e-01 1.33e-01 1.10e-03 0.00e+00 0.00e+00 0.00e+00
45 25 0.00e+00 0.00e+00 0.00e+00 0.00e+00 0.00e+00 0.00e+00 0.00e+00 0.00e+00
45 33 0.00e+00 0.00e+00 0.00e+00 0.00e+00 0.00e+00 0.00e+00 0.00e+00 0.00e+00
45 41 0.00e+00 0.00e+00 0.00e+00 0.00e+00 0.00e+00 0.00e+00 0.00e+00 0.00e+00
45 49 0.00e+00 0.00e+00 0.00e+00 0.00e+00 0.00e+00 0.00e+00 0.00e+00 0.00E+00
46 1 3.55e-02 3.45e-02 3.43e-02 3.56e-02 3.52e-02 3.90e-02 4.88e-02 4.81e-02
46 9 5.18e-02 5.66e-02 6.83e-02 7.35e-02 8.51e-02 9.94e-02 1.01e-01 1.11e-01
46 17 1.27e-01 1.12e-01 9.34e-02 3.93e-04 0.00e+00 0.00e+00 0.00e+00 0.00e+00
46 25 0.00e+00 0.00e+00 0.00e+00 0.00e+00 0.00e+00 0.00e+00 0.00e+00 0.00e+00
46 33 0.00e+00 0.00e+00 0.00e+00 0.00e+00 0.00e+00 0.00e+00 0.00e+00 0.00e+00
46 41 0.00e+00 0.00e+00 0.00e+00 0.00e+00 0.00e+00 0.00e+00 0.00e+00 0.00e+00
46 49 0.00e+00 0.00e+00 0.00e+00 0.00e+00 0.00e+00 0.00e+00 0.00e+00 0.00E+00

47 1 3.21e-02 3.31e-02 3.33e-02 3.64e-02 3.49e-02 4.15e-02 4.61e-02 4.71e-02
47 9 5.36e-02 5.92e-02 6.39e-02 7.28e-02 8.95e-02 9.94e-02 9.88e-02 9.69e-02
47 17 1.15e-01 8.40e-02 0.00e+00 0.00e+00 0.00e+00 0.00e+00 0.00e+00 0.00e+00
47 25 0.00e+00 0.00e+00 0.00e+00 0.00e+00 0.00e+00 0.00e+00 0.00e+00 0.00e+00
47 33 0.00e+00 0.00e+00 0.00e+00 0.00e+00 0.00e+00 0.00e+00 0.00e+00 0.00e+00
47 41 0.00e+00 0.00e+00 0.00e+00 0.00e+00 0.00e+00 0.00e+00 0.00e+00 0.00e+00
47 49 0.00e+00 0.00e+00 0.00e+00 0.00e+00 0.00e+00 0.00e+00 0.00e+00 0.00E+00
48 1 3.13e-02 3.47e-02 3.52e-02 3.76e-02 3.85e-02 4.08e-02 4.47e-02 4.84e-02
48 9 5.03e-02 5.72e-02 6.78e-02 7.45e-02 9.42e-02 9.53e-02 8.82e-02 9.16e-02
48 17 8.55e-02 0.00e+00 0.00e+00 0.00e+00 0.00e+00 0.00e+00 0.00e+00 0.00e+00
48 25 0.00e+00 0.00e+00 0.00e+00 0.00e+00 0.00e+00 0.00e+00 0.00e+00 0.00e+00
48 33 0.00e+00 0.00e+00 0.00e+00 0.00e+00 0.00e+00 0.00e+00 0.00e+00 0.00e+00
48 41 0.00e+00 0.00e+00 0.00e+00 0.00e+00 0.00e+00 0.00e+00 0.00e+00 0.00e+00
48 49 0.00e+00 0.00e+00 0.00e+00 0.00e+00 0.00e+00 0.00e+00 0.00e+00 0.00E+00
49 1 3.31e-02 3.38e-02 3.47e-02 3.31e-02 3.64e-02 3.95e-02 4.77e-02 4.46e-02
49 9 4.76e-02 5.83e-02 7.27e-02 8.04e-02 8.56e-02 8.31e-02 8.20e-02 6.31e-02
49 17 0.00e+00 0.00e+00 0.00e+00 0.00e+00 0.00e+00 0.00e+00 0.00e+00 0.00e+00
49 25 0.00e+00 0.00e+00 0.00e+00 0.00e+00 0.00e+00 0.00e+00 0.00e+00 0.00e+00
49 33 0.00e+00 0.00e+00 0.00e+00 0.00e+00 0.00e+00 0.00e+00 0.00e+00 0.00e+00
49 41 0.00e+00 0.00e+00 0.00e+00 0.00e+00 0.00e+00 0.00e+00 0.00e+00 0.00e+00
49 49 0.00e+00 0.00e+00 0.00e+00 0.00e+00 0.00e+00 0.00e+00 0.00e+00 0.00E+00
50 1 3.03e-02 3.19e-02 3.31e-02 3.23e-02 3.54e-02 3.94e-02 4.53e-02 4.36e-02
50 9 5.19e-02 6.04e-02 7.10e-02 7.63e-02 7.82e-02 7.68e-02 4.98e-02 0.00e+00
50 17 0.00e+00 0.00e+00 0.00e+00 0.00e+00 0.00e+00 0.00e+00 0.00e+00 0.00e+00
50 25 0.00e+00 0.00e+00 0.00e+00 0.00e+00 0.00e+00 0.00e+00 0.00e+00 0.00e+00
50 33 0.00e+00 0.00e+00 0.00e+00 0.00e+00 0.00e+00 0.00e+00 0.00e+00 0.00e+00
50 41 0.00e+00 0.00e+00 0.00e+00 0.00e+00 0.00e+00 0.00e+00 0.00e+00 0.00e+00
50 49 0.00e+00 0.00e+00 0.00e+00 0.00e+00 0.00e+00 0.00e+00 0.00e+00 0.00E+00
51 1 3.02e-02 3.37e-02 3.52e-02 3.36e-02 3.27e-02 4.18e-02 4.62e-02 4.65e-02
51 9 4.98e-02 6.48e-02 7.98e-02 7.38e-02 7.28e-02 4.77e-02 0.00e+00 0.00e+00
51 17 0.00e+00 0.00e+00 0.00e+00 0.00e+00 0.00e+00 0.00e+00 0.00e+00 0.00e+00
51 25 0.00e+00 0.00e+00 0.00e+00 0.00e+00 0.00e+00 0.00e+00 0.00e+00 0.00e+00
51 33 0.00e+00 0.00e+00 0.00e+00 0.00e+00 0.00e+00 0.00e+00 0.00e+00 0.00e+00
51 41 0.00e+00 0.00e+00 0.00e+00 0.00e+00 0.00e+00 0.00e+00 0.00e+00 0.00e+00
51 49 0.00e+00 0.00e+00 0.00e+00 0.00e+00 0.00e+00 0.00e+00 0.00e+00 0.00E+00
52 1 3.06e-02 3.25e-02 3.17e-02 3.33e-02 3.48e-02 3.93e-02 4.40e-02 4.78e-02
52 9 5.71e-02 6.65e-02 7.48e-02 6.84e-02 6.57e-02 0.00e+00 0.00e+00 0.00e+00
52 17 0.00e+00 0.00e+00 0.00e+00 0.00e+00 0.00e+00 0.00e+00 0.00e+00 0.00e+00
52 25 0.00e+00 0.00e+00 0.00e+00 0.00e+00 0.00e+00 0.00e+00 0.00e+00 0.00e+00
52 33 0.00e+00 0.00e+00 0.00e+00 0.00e+00 0.00e+00 0.00e+00 0.00e+00 0.00e+00
52 41 0.00e+00 0.00e+00 0.00e+00 0.00e+00 0.00e+00 0.00e+00 0.00e+00 0.00e+00
52 49 0.00e+00 0.00e+00 0.00e+00 0.00e+00 0.00e+00 0.00e+00 0.00e+00 0.00E+00
53 1 2.93e-02 2.85e-02 3.33e-02 3.25e-02 3.38e-02 4.20e-02 4.67e-02 4.60e-02
53 9 5.55e-02 6.71e-02 7.05e-02 6.47e-02 0.00e+00 0.00e+00 0.00e+00 0.00e+00
53 17 0.00e+00 0.00e+00 0.00e+00 0.00e+00 0.00e+00 0.00e+00 0.00e+00 0.00e+00
53 25 0.00e+00 0.00e+00 0.00e+00 0.00e+00 0.00e+00 0.00e+00 0.00e+00 0.00e+00
53 33 0.00e+00 0.00e+00 0.00e+00 0.00e+00 0.00e+00 0.00e+00 0.00e+00 0.00e+00
53 41 0.00e+00 0.00e+00 0.00e+00 0.00e+00 0.00e+00 0.00e+00 0.00e+00 0.00e+00
53 49 0.00e+00 0.00e+00 0.00e+00 0.00e+00 0.00e+00 0.00e+00 0.00e+00 0.00E+00
54 1 3.96e-02 4.02e-02 4.59e-02 4.74e-02 4.81e-02 5.52e-02 6.51e-02 6.91e-02
54 9 8.39e-02 9.86e-02 1.15e-01 7.36e-02 3.72e-02 3.20e-02 3.35e-02 4.51e-02
54 17 8.65e-02 9.36e-02 9.19e-02 3.12e-02 5.79e-02 3.39e-02 0.00e+00 0.00e+00
54 25 0.00e+00 0.00e+00 0.00e+00 0.00e+00 0.00e+00 0.00e+00 0.00e+00 0.00e+00
54 33 0.00e+00 0.00e+00 0.00e+00 0.00e+00 0.00e+00 0.00e+00 0.00e+00 0.00e+00

54 41 0.00e+00 0.00e+00 0.00e+00 0.00e+00 0.00e+00 0.00e+00 0.00e+00 0.00e+00
54 49 0.00e+00 0.00e+00 0.00e+00 0.00e+00 0.00e+00 0.00e+00 0.00e+00 0.00E+00
55 1 5.60e-02 5.71e-02 5.82e-02 6.46e-02 6.27e-02 7.35e-02 8.58e-02 9.61e-02
55 9 9.70e-02 1.06e-01 7.19e-02 4.24e-04 1.07e-03 1.31e-03 1.02e-03 1.49e-03
55 17 1.28e-03 1.05e-03 6.30e-04 4.84e-05 0.00e+00 0.00e+00 0.00e+00 0.00e+00
55 25 0.00e+00 0.00e+00 0.00e+00 0.00e+00 0.00e+00 0.00e+00 0.00e+00 0.00e+00
55 33 0.00e+00 0.00e+00 0.00e+00 0.00e+00 0.00e+00 0.00e+00 0.00e+00 0.00e+00
55 41 0.00e+00 0.00e+00 0.00e+00 0.00e+00 0.00e+00 0.00e+00 0.00e+00 0.00e+00
55 49 0.00e+00 0.00e+00 0.00e+00 0.00e+00 0.00e+00 0.00e+00 0.00e+00 0.00E+00
56 1 5.27e-02 5.36e-02 5.78e-02 6.07e-02 6.49e-02 7.90e-02 9.01e-02 8.93e-02
56 9 9.00e-02 4.31e-02 2.77e-04 5.00e-04 5.15e-04 9.28e-04 6.18e-04 4.75e-04
56 17 7.17e-05 0.00e+00 0.00e+00 0.00e+00 0.00e+00 0.00e+00 0.00e+00 0.00e+00
56 25 0.00e+00 0.00e+00 0.00e+00 0.00e+00 0.00e+00 0.00e+00 0.00e+00 0.00e+00
56 33 0.00e+00 0.00e+00 0.00e+00 0.00e+00 0.00e+00 0.00e+00 0.00e+00 0.00e+00
56 41 0.00e+00 0.00e+00 0.00e+00 0.00e+00 0.00e+00 0.00e+00 0.00e+00 0.00e+00
56 49 0.00e+00 0.00e+00 0.00e+00 0.00e+00 0.00e+00 0.00e+00 0.00e+00 0.00E+00
57 1 5.35e-02 5.42e-02 6.10e-02 6.02e-02 6.68e-02 7.90e-02 8.40e-02 8.33e-02
57 9 3.32e-02 6.74e-04 7.81e-04 5.67e-04 3.58e-04 0.00e+00 8.17e-07 0.00e+00
57 17 0.00e+00 0.00e+00 0.00e+00 0.00e+00 0.00e+00 0.00e+00 0.00e+00 0.00e+00
57 25 0.00e+00 0.00e+00 0.00e+00 0.00e+00 0.00e+00 0.00e+00 0.00e+00 0.00e+00
57 33 0.00e+00 0.00e+00 0.00e+00 0.00e+00 0.00e+00 0.00e+00 0.00e+00 0.00e+00
57 41 0.00e+00 0.00e+00 0.00e+00 0.00e+00 0.00e+00 0.00e+00 0.00e+00 0.00e+00
57 49 0.00e+00 0.00e+00 0.00e+00 0.00e+00 0.00e+00 0.00e+00 0.00e+00 0.00E+00
58 1 5.24e-02 5.31e-02 6.00e-02 6.37e-02 7.00e-02 7.32e-02 7.96e-02 3.08e-02
58 9 6.53e-04 2.31e-04 6.98e-04 0.00e+00 2.53e-05 0.00e+00 0.00e+00 0.00e+00
58 17 0.00e+00 0.00e+00 0.00e+00 0.00e+00 0.00e+00 0.00e+00 0.00e+00 0.00e+00
58 25 0.00e+00 0.00e+00 0.00e+00 0.00e+00 0.00e+00 0.00e+00 0.00e+00 0.00e+00
58 33 0.00e+00 0.00e+00 0.00e+00 0.00e+00 0.00e+00 0.00e+00 0.00e+00 0.00e+00
58 41 0.00e+00 0.00e+00 0.00e+00 0.00e+00 0.00e+00 0.00e+00 0.00e+00 0.00e+00
58 49 0.00e+00 0.00e+00 0.00e+00 0.00e+00 0.00e+00 0.00e+00 0.00e+00 0.00E+00
59 1 5.12e-02 5.46e-02 6.02e-02 6.66e-02 6.73e-02 6.99e-02 3.86e-02 4.12e-04
59 9 1.92e-04 3.00e-04 2.67e-04 0.00e+00 0.00e+00 0.00e+00 0.00e+00 0.00e+00
59 17 0.00e+00 0.00e+00 0.00e+00 0.00e+00 0.00e+00 0.00e+00 0.00e+00 0.00e+00
59 25 0.00e+00 0.00e+00 0.00e+00 0.00e+00 0.00e+00 0.00e+00 0.00e+00 0.00e+00
59 33 0.00e+00 0.00e+00 0.00e+00 0.00e+00 0.00e+00 0.00e+00 0.00e+00 0.00e+00
59 41 0.00e+00 0.00e+00 0.00e+00 0.00e+00 0.00e+00 0.00e+00 0.00e+00 0.00e+00
59 49 0.00e+00 0.00e+00 0.00e+00 0.00e+00 0.00e+00 0.00e+00 0.00e+00 0.00E+00
60 1 5.03e-02 5.36e-02 6.15e-02 6.43e-02 6.24e-02 4.37e-02 6.67e-04 3.59e-04
60 9 0.00e+00 3.88e-05 0.00e+00 0.00e+00 0.00e+00 0.00e+00 0.00e+00 0.00e+00
60 17 0.00e+00 0.00e+00 0.00e+00 0.00e+00 0.00e+00 0.00e+00 0.00e+00 0.00e+00
60 25 0.00e+00 0.00e+00 0.00e+00 0.00e+00 0.00e+00 0.00e+00 0.00e+00 0.00e+00
60 33 0.00e+00 0.00e+00 0.00e+00 0.00e+00 0.00e+00 0.00e+00 0.00e+00 0.00e+00
60 41 0.00e+00 0.00e+00 0.00e+00 0.00e+00 0.00e+00 0.00e+00 0.00e+00 0.00e+00
60 49 0.00e+00 0.00e+00 0.00e+00 0.00e+00 0.00e+00 0.00e+00 0.00e+00 0.00E+00
61 1 5.54e-02 5.87e-02 6.09e-02 5.52e-02 4.70e-02 5.26e-04 2.42e-04 4.25e-04
61 9 0.00e+00 0.00e+00 0.00e+00 0.00e+00 0.00e+00 0.00e+00 0.00e+00 0.00e+00
61 17 0.00e+00 0.00e+00 0.00e+00 0.00e+00 0.00e+00 0.00e+00 0.00e+00 0.00e+00
61 25 0.00e+00 0.00e+00 0.00e+00 0.00e+00 0.00e+00 0.00e+00 0.00e+00 0.00e+00
61 33 0.00e+00 0.00e+00 0.00e+00 0.00e+00 0.00e+00 0.00e+00 0.00e+00 0.00e+00
61 41 0.00e+00 0.00e+00 0.00e+00 0.00e+00 0.00e+00 0.00e+00 0.00e+00 0.00e+00
61 49 0.00e+00 0.00e+00 0.00e+00 0.00e+00 0.00e+00 0.00e+00 0.00e+00 0.00E+00
62 1 5.50e-02 5.59e-02 5.41e-02 5.59e-02 3.87e-04 2.52e-04 3.51e-04 0.00e+00
62 9 0.00e+00 0.00e+00 0.00e+00 0.00e+00 0.00e+00 0.00e+00 0.00e+00 0.00e+00
62 17 0.00e+00 0.00e+00 0.00e+00 0.00e+00 0.00e+00 0.00e+00 0.00e+00 0.00e+00

62 25 0.00e+00 0.00e+00 0.00e+00 0.00e+00 0.00e+00 0.00e+00 0.00e+00 0.00e+00
62 33 0.00e+00 0.00e+00 0.00e+00 0.00e+00 0.00e+00 0.00e+00 0.00e+00 0.00e+00
62 41 0.00e+00 0.00e+00 0.00e+00 0.00e+00 0.00e+00 0.00e+00 0.00e+00 0.00e+00
62 49 0.00e+00 0.00e+00 0.00e+00 0.00e+00 0.00e+00 0.00e+00 0.00e+00 0.00E+00
63 1 5.37e-02 5.39e-02 5.23e-02 5.38e-03 1.77e-04 0.00e+00 0.00e+00 0.00e+00
63 9 0.00e+00 0.00e+00 0.00e+00 0.00e+00 0.00e+00 0.00e+00 0.00e+00 0.00e+00
63 17 0.00e+00 0.00e+00 0.00e+00 0.00e+00 0.00e+00 0.00e+00 0.00e+00 0.00e+00
63 25 0.00e+00 0.00e+00 0.00e+00 0.00e+00 0.00e+00 0.00e+00 0.00e+00 0.00e+00
63 33 0.00e+00 0.00e+00 0.00e+00 0.00e+00 0.00e+00 0.00e+00 0.00e+00 0.00e+00
63 41 0.00e+00 0.00e+00 0.00e+00 0.00e+00 0.00e+00 0.00e+00 0.00e+00 0.00e+00
63 49 0.00e+00 0.00e+00 0.00e+00 0.00e+00 0.00e+00 0.00e+00 0.00e+00 0.00E+00
64 1 4.83e-02 5.00e-02 1.62e-02 4.22e-05 0.00e+00 0.00e+00 0.00e+00 0.00e+00
64 9 0.00e+00 0.00e+00 0.00e+00 0.00e+00 0.00e+00 0.00e+00 0.00e+00 0.00e+00
64 17 0.00e+00 0.00e+00 0.00e+00 0.00e+00 0.00e+00 0.00e+00 0.00e+00 0.00e+00
64 25 0.00e+00 0.00e+00 0.00e+00 0.00e+00 0.00e+00 0.00e+00 0.00e+00 0.00e+00
64 33 0.00e+00 0.00e+00 0.00e+00 0.00e+00 0.00e+00 0.00e+00 0.00e+00 0.00e+00
64 41 0.00e+00 0.00e+00 0.00e+00 0.00e+00 0.00e+00 0.00e+00 0.00e+00 0.00e+00
64 49 0.00e+00 0.00e+00 0.00e+00 0.00e+00 0.00e+00 0.00e+00 0.00e+00 0.00E+00
65 1 4.92e-02 2.38e-02 3.43e-04 1.27e-04 0.00e+00 0.00e+00 0.00e+00 0.00e+00
65 9 0.00e+00 0.00e+00 0.00e+00 0.00e+00 0.00e+00 0.00e+00 0.00e+00 0.00e+00
65 17 0.00e+00 0.00e+00 0.00e+00 0.00e+00 0.00e+00 0.00e+00 0.00e+00 0.00e+00
65 25 0.00e+00 0.00e+00 0.00e+00 0.00e+00 0.00e+00 0.00e+00 0.00e+00 0.00e+00
65 33 0.00e+00 0.00e+00 0.00e+00 0.00e+00 0.00e+00 0.00e+00 0.00e+00 0.00e+00
65 41 0.00e+00 0.00e+00 0.00e+00 0.00e+00 0.00e+00 0.00e+00 0.00e+00 0.00e+00
65 49 0.00e+00 0.00e+00 0.00e+00 0.00e+00 0.00e+00 0.00e+00 0.00e+00 0.00E+00
66 1 2.61e-02 3.59e-04 2.63e-04 4.22e-05 0.00e+00 0.00e+00 0.00e+00 0.00e+00
66 9 0.00e+00 0.00e+00 0.00e+00 0.00e+00 0.00e+00 0.00e+00 0.00e+00 0.00e+00
66 17 0.00e+00 0.00e+00 0.00e+00 0.00e+00 0.00e+00 0.00e+00 0.00e+00 0.00e+00
66 25 0.00e+00 0.00e+00 0.00e+00 0.00e+00 0.00e+00 0.00e+00 0.00e+00 0.00e+00
66 33 0.00e+00 0.00e+00 0.00e+00 0.00e+00 0.00e+00 0.00e+00 0.00e+00 0.00e+00
66 41 0.00e+00 0.00e+00 0.00e+00 0.00e+00 0.00e+00 0.00e+00 0.00e+00 0.00e+00
66 49 0.00e+00 0.00e+00 0.00e+00 0.00e+00 0.00e+00 0.00e+00 0.00e+00 0.00E+00
67 1 2.28e-04 1.35e-04 0.00e+00 0.00e+00 0.00e+00 0.00e+00 0.00e+00 0.00e+00
67 9 0.00e+00 0.00e+00 0.00e+00 0.00e+00 0.00e+00 0.00e+00 0.00e+00 0.00e+00
67 17 0.00e+00 0.00e+00 0.00e+00 0.00e+00 0.00e+00 0.00e+00 0.00e+00 0.00e+00
67 25 0.00e+00 0.00e+00 0.00e+00 0.00e+00 0.00e+00 0.00e+00 0.00e+00 0.00e+00
67 33 0.00e+00 0.00e+00 0.00e+00 0.00e+00 0.00e+00 0.00e+00 0.00e+00 0.00e+00
67 41 0.00e+00 0.00e+00 0.00e+00 0.00e+00 0.00e+00 0.00e+00 0.00e+00 0.00e+00
67 49 0.00e+00 0.00e+00 0.00e+00 0.00e+00 0.00e+00 0.00e+00 0.00e+00 0.00E+00
68 1 0.00e+00 0.00e+00 0.00e+00 0.00e+00 0.00e+00 0.00e+00 0.00e+00 0.00e+00
68 9 0.00e+00 0.00e+00 0.00e+00 0.00e+00 0.00e+00 0.00e+00 0.00e+00 0.00e+00
68 17 0.00e+00 0.00e+00 0.00e+00 0.00e+00 0.00e+00 0.00e+00 0.00e+00 0.00e+00
68 25 0.00e+00 0.00e+00 0.00e+00 0.00e+00 0.00e+00 0.00e+00 0.00e+00 0.00e+00
68 33 0.00e+00 0.00e+00 0.00e+00 0.00e+00 0.00e+00 0.00e+00 0.00e+00 0.00e+00
68 41 0.00e+00 0.00e+00 0.00e+00 0.00e+00 0.00e+00 0.00e+00 0.00e+00 0.00e+00
68 49 0.00e+00 0.00e+00 0.00e+00 0.00e+00 0.00e+00 0.00e+00 0.00e+00 0.00E+00
00 0

END

Appendix C Circuitry Analysis

The non-inverting pre-amplifier used in this work (Figure C-1) is analyzed in this section (Ref [1]).

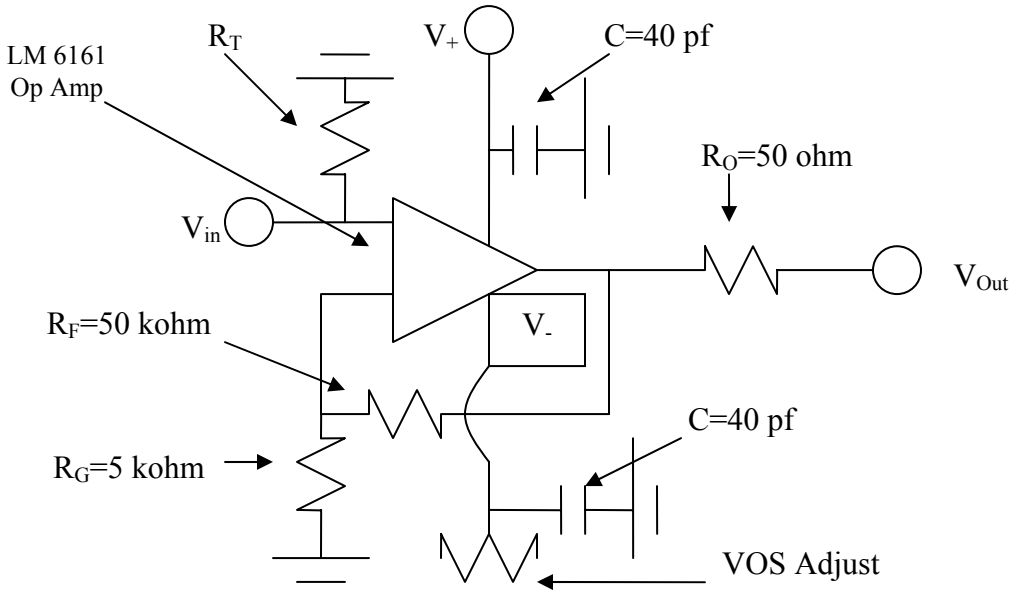

Figure C-1-Non-inverting pre-amp used with Spring 2007 set-up, where R_T is the termination resistor.

Without the power conditioning and the voltage stabilizers, the functionality of the circuit shown above may be broken down into two sections as follows in Figure C-2:

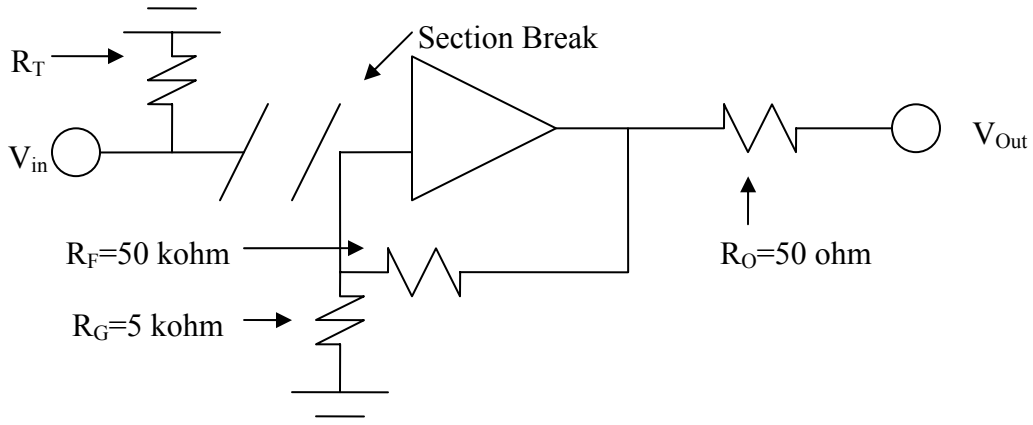

Figure C-2--inverting pre-amp used with Spring 2007 set-up section view.

C.1 Attenuation Network

In the first section, the signal, with the capacitor from the PMT base up in the signal chain, is combined with the termination resistor to create a high pass filter. The voltage across this combination is simply $V_0 - V$ and the current I may be given by

$$I = C\frac{d}{dt}(V_0 - V) = \frac{V}{R} \tag{C.1}$$

R in Equation (C.1) is the termination resistance in this case.

If the time constant $\tau = RC$ is chosen to be large, Equation (C.1) becomes

$$RC\frac{d}{dt}(V_0) \approx RC\frac{d}{dt}(V) \tag{C.2}$$

For a sinusoidal signal input

$$V_0 = V_C \sin(2\pi ft) \tag{C.3}$$

Then the real part of the output has the form

$$V = V_0|A|\sin(2\pi ft + \theta) \tag{C.4}$$

In Equation (C.4), A is a complex argument and is the magnitude is given by

$$|A| = \frac{1}{\sqrt{1 + \left[\frac{(2\pi\tau)}{f}\right]^2}} \tag{C.5}$$

Then, as can be observed, the shape of the output signal does not change much if $f >> 2\pi\tau$. Specifically, high frequency signals will pass through this CR network relatively unchanged, whereas low frequency signals will be attenuated. In the case of this particular set-up, the input capacitance was measured to be 30 pf, given a time constant of 1.5 ns, 15 ns, and a 30 ns time constant for the 50 ohm, 500 ohm, and the 1000 ohm termination resistor. Since the

light decay signal has a 3 ns, a 32 ns, and a 270 ns components, the attenuation network will attenuate the 3 ns and the 32 ns component. The changed pulse shape may or may not improve the PSD performance of the system.

C.2 Non-Inverting Amplifier

The second half of Figure C-2 is simply a non-inverting amplifier (Figure C-3).

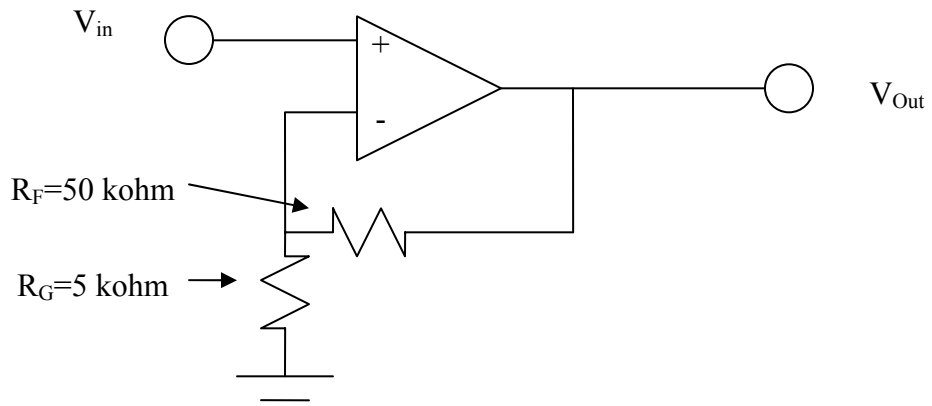

Figure C-3-Schmatics of a generic non-inverting amplifier.

The voltage at the (-) end is simply V_{in} so the voltage in terms of the output and the resistors is simply:

$$V_{in} = V_{out}\left(\frac{R_G}{R_G + R_F}\right) \qquad \text{C.6}$$

In terms of V_{out}:

$$V_{out} = V_{in}\left(\frac{R_F}{R_G} + 1\right) \qquad \text{C.7}$$

The gain of the amplifier is simply $\left(\frac{R_F}{R_G} + 1\right)$. For this system then, a gain of 11 is used.

With the total pre-amplifier, the system first attenuates the input signal. Depending on the termination resistor used, different attenuation of the three components of the input signal may be observed. The attenuated signal then is processed through a non-inverting amplifier to amplify the signal by 11 fold. The signal then continues down the signal chain as depicted in Figure 3-1.